The A in SAFT: developing the contribution of association to the Helmholtz free energy within a Wertheim TPT1 treatment of generic Mie fluids

Simon Dufal, Thomas Lafitte, Andrew J. Haslam, Amparo Galindo, Gary N.I. Clark, Carlos Vega & George Jackson

Taylor & Francis
Taylor & Francis Group

INVITED ARTICLE

The A in SAFT: developing the contribution of association to the Helmholtz free energy within a Wertheim TPT1 treatment of generic Mie fluids

Simon Dufal[a], Thomas Lafitte[b,c], Andrew J. Haslam[a], Amparo Galindo[a,b], Gary N.I. Clark[b,d], Carlos Vega[d] and George Jackson[a,b,*]

[a]Department of Chemical Engineering, Qatar Carbonates and Carbon Storage Research Centre, Imperial College London, South Kensington Campus, London SW7 2AZ, United Kingdom; [b]Department of Chemical Engineering, Centre for Process Systems Engineering, Imperial College London, South Kensington Campus, London SW7 2AZ, United Kingdom; [c]Process Systems Enterprise Ltd, 26-28 Hammersmith Grove, London W6 7HA, United Kingdom; [d]Departamento de Química Física, Facultad de Ciencias Químicas, Universidad Complutense de Madrid, 28040 Madrid, Spain

An accurate representation of molecular association is a vital ingredient of advanced equations of state (EOSs), providing a description of thermodynamic properties of complex fluids where hydrogen bonding plays an important role. The combination of the first-order thermodynamic perturbation theory (TPT1) of Wertheim for associating systems with an accurate description of the structural and thermodynamic properties of the monomer fluid forms the basis of the statistical associating fluid theory (SAFT) family of EOSs. The contribution of association to the free energy in SAFT and related EOSs is very sensitive to the nature of intermolecular potential used to describe the monomers and, crucially, to the accuracy of the representation of the thermodynamic and structural properties. Here we develop an accurate description of the association contribution for use within the recently developed SAFT-VR Mie framework for chain molecules formed from segments interacting through a Mie potential [T. Lafitte, A. Apostolakou, C. Avendaño, A, Galindo, C. S. Adjiman, E. A. Müller, and G. Jackson, J. Chem. Phys. **139**, 154504 (2013)]. As the Mie interaction represents a soft-core potential model, a method similar to that adopted for the Lennard-Jones potential [E. A. Müller and K. E. Gubbins, Ind. Eng. Chem. Res. **34**, 3662 (1995)] is employed to describe the association contribution to the Helmholtz free energy. The radial distribution function (RDF) of the Mie fluid (which is required for the evaluation of the integral at the heart of the association term) is determined for a broad range of thermodynamic conditions (temperatures and densities) using the reference hyper-netted chain (RHNC) integral-equation theory. The numerical data for the association kernel of Mie fluids with different association geometries are then correlated for a range of thermodynamic states to obtain a general expression for the association contribution which can be applied for varying values of the Mie repulsive exponent. The resulting SAFT-VR Mie EOS allows for a much improved description of the vapour-liquid equilibria and single-phase properties of associating fluids such as water, methanol, ammonia, hydrogen sulphide, and their mixtures. A comparison is also made between the theoretical predictions of the degree of association for water and the extent of hydrogen bonding obtained from molecular simulations of the SPC/E and TIP4P/2005 atomistic models.

Keywords: hydrogen bonding; complex associating fluids; statistical mechanics; integral equation theory; perturbation theory

1. Introduction

One of the principal motivations for the development of the statistical associating fluid theory (SAFT) [1,2] in the late 1980s was the need for a rigorous and reliable equation of state (EOS) for the thermodynamic properties and phase equilibria of associating fluids; these systems could not be described in an adequate manner with the more traditional cubic EOSs available at the time. The most important class of associating fluids involves the formation of hydrogen bonds. Since the inception of the idea of hydrogen bonding (HB) as a specific interaction in the early part of the twentieth century, numerous studies have been devoted to understanding the various forms of hydrogen bonds, resulting in a wealth of literature (see, e.g., references [3–6]

and citations therein). This is due to both the specificity of the hydrogen bond, which makes it scientifically intriguing and challenging to describe, and its ubiquitous nature particularly in biological systems. In the early days of quantum mechanics, Lennard-Jones and Pople [7,8] described molecular association in terms of a 'crude' but chemically intuitive representation based on the hybridisation of atomic orbitals into molecular orbitals. In the case of water, the molecule can be pictured as an oxygen atom with two hydroxyl (OH) bonds and two orbitals corresponding to the 'lone pairs' of electrons; the interaction of the slight positive charge at the centre of the OH bond with the negative charge of the lone-pair orbitals leads to a localised, and therefore directional, HB interaction. The precise nature of

---

the hydrogen bond has been the subject of long-standing debate. It is rather surprising that even as recently as 2011 two complementary review articles [5,6] were devoted entirely to the definition of the hydrogen bond; the first of these [5] contains a fascinating historical overview of the subject. In the context of our current contribution, the subtleties of different definitions are not of prime importance; we consider HB simply in terms of the specific interactions exhibited predominantly by molecules with a hydrogen atom directly linked to an electronegative atom, found in compounds such as alcohols, carboxylic acids, amines, thiols, or halides.

The challenging aspects of modelling the effect of HB and association in fluids at the molecular level have also been recognised for a long time. One of the first rigorous treatments of associating fluids within a continuum statistical-mechanical framework was proposed by Hill [9–12] 60 years ago following a description based on physical clusters; there had been some earlier studies with lattice models (see, e.g., references [13] and [14]) but these are not discussed here as our focus is on a continuum representation of the system. Hill's approach has subsequently been reformulated as cluster expansions of the free energy and EOS in terms of the density or the fugacity (activity) of the fluid; representative examples include the work of Andersen and co-workers [15–18], Chandler and Pratt [19], Hirata [20], and Høye and Olaussen [21], to name but a few. Along an alternative vein, simple models of associating fluids have been examined with traditional integral-equation theories, including the work of Ben-Naim [22–25], Carnie and co-workers [26,27], Stell and co-workers [28–32], and Nezbeda and co-workers [33–36]. Of particular relevance to our current work is the seminal theory of Wertheim [37–40] for associating fluids which is based on a highly-convergent cluster expansion in terms of both the density of the monomer (un-associated) species and the overall density. Wertheim put forward an elegant formalism (for molecules modelled as hard cores with directional, off-centre bonding sites) cast both as an integral-equation theory and as a first-order thermodynamic perturbation theory (TPT1); the latter form is particularly convenient for the development of algebraic EOSs for associating fluids [41,42] and is now firmly at the heart of the SAFT family of EOSs [1,2,43–48].

An accurate representation of the structure and thermodynamic properties of the reference monomer fluid is required for the implementation of Wertheim's perturbative approach. In the case of a TPT1 treatment, one assumes that bonding at a given site is independent of bonding at another, and furthermore only single bonding is permitted (a reasonable assumption if the range of the bonding interaction is small compared to the size of the molecular cores [49]); as a consequence, the contribution to the free energy due to site-site association can be determined simply from a knowledge of the pair (two-body) radial distribution function (RDF) of the reference un-associated fluid. The three-body distribu-

tion function is required to extend the perturbation theory to second order (TPT2), allowing for an explicit description of higher-order steric effects on the bonding and hence of the molecular geometry/flexibility [50–56]. A key feature of the Wertheim formalism is that by taking the limit of complete association, one can further develop expressions for the contributions to the free energy due to the formation of fully bonded dimers [57] or flexible molecular chains comprising bonded monomeric segments [42,50,58]. The Wertheim TPT1 treatment therefore provides a route to the separate contributions to the EOS for both reversible association (e.g., resulting from intermolecular HB) and for molecules formed from bonded segments. A consideration of mixtures of associating monomers can also be employed to provide a reliable description of the thermodynamic properties of heteronuclear dimers [59,60], trimers [61,62], and generic molecules formed from segments of different type [55,62–71]; such a formalism has been invaluable in the recent development of group-contribution approaches for heteronuclear molecules based on the SAFT EOS, allowing for the separate chemical moieties to be considered explicitly [72–78].

Wertheim's theoretical framework has now been extended to deal with association into ring-like structures [53,54,79–85], double bonding [85,86], and the effects of cooperative bonding on the energetics of the association interactions [84,87,88]. A number of recent developments have been made to increase the scope and general applicability of Wertheim's approach [89–96], largely motivated by a new found interest in the theory as applied to the description of the effect of association on the properties and phase behaviour of proteins and patchy colloids (e.g., see references [97–108]).

It is clear from the preceding discussion that a rigorous statistical mechanical treatment of all manner of bonding schemes in continuum fluids is now available. However, a sophisticated (and computationally costly) numerical procedure is generally required for its implementation. The aim of our current work is the provision of an algebraic platform for the accurate treatment of associating fluids (at the Wertheim TPT1 level) interacting via the generic Mie (generalised Lennard-Jones) potential. We examine the importance of incorporating an accurate representation of the pair distribution function of the Mie reference fluid in the development of a reliable TPT1 description of the association contribution to the Helmholtz free energy for associating molecules represented as Mie cores with off-centre square-well (SW) bonding sites. The various approximate methodologies commonly employed with the SAFT family of EOSs to obtain tractable expressions for the integrated association strength (which characterises the degree of association and its effect on the free energy and other thermodynamic properties of the fluid) are discussed, and a critical assessment of the respective advantages and disadvantages of each approach is provided. A detailed analysis of the adequacy

of the expressions for the integrated association strength developed at the different levels of approximation is made based on a comparison of the performance of the description of the degree of association and thermodynamic properties. Novel generic algebraic expressions for the integrated association strength of associating fluids are proposed for use with the SAFT EOSs based on the Mie reference system. As a final assessment of our new treatment of the association contribution, the expressions are coupled to a version of the SAFT EOS for interactions of variable range (SAFT-VR) [109,110] which has been developed recently to allow for a generic description of non-associative molecular segment interactions with a Mie potential form (SAFT-VR Mie) [111]. The SAFT-VR Mie EOS with our improved treatment of the association contribution is then used to represent the thermodynamic properties, fluid-phase equilibria, and degree of association of real associating fluids, including water, methanol, ammonia, hydrogen sulphide, and aqueous mixtures. Although the focus of our current work is on the use of the Mie potential as the underlying molecular model, it is important to emphasise that much of the analysis is completely general, and that our methodology will be of direct relevance to fluids described with other intermolecular interactions, such as the ubiquitous Lennard-Jones (LJ) (12-6) potential (which is but a specific form of the Mie interaction).

2. Intermolecular potential model and theory

2.1. *Models of associating fluids*

Any rigorous statistical mechanical treatment of associating fluids should of course be based on a well-defined intermolecular potential model which is appropriate for the representation of the particular interactions between molecules, including HB. The models must be sufficiently simple to accommodate the development of the theory, yet must allow one to capture key aspects of the essential physics to provide a satisfactory description of the thermodynamics of the association.

The earliest models of associating fluids are based on a classical description of the molecular interactions where a Lennard-Jones core (which represents the intermolecular repulsions and London-dispersion attractions) is decorated with a number of distributed point charges (to account for the polarity and the specific directional interactions that give rise to the association). The ever-increasing proliferation of distributed-charge LJ potentials for water (the omnipresent associating molecule) widely employed in direct molecular simulation (including, e.g., the BNS [24,25], ST2 [112,113], SPC [114,115], and TIP [116–120] families of models) are descendants of the intermolecular models proposed early on by Bernal and Fowler [121], Rowlinson [122,123], Pople [8], and Bjerrum [124]. Unfortunately, the development of tractable and, more particularly, analytical,

statistical-mechanical theories of distributed-charge models of this type still remains elusive, and the corresponding theoretical description of the structural and thermodynamic properties is at best only qualitative.

On the other hand, simpler intermolecular models of associating fluids allow one to develop a statistical mechanical platform (e.g., integral-equation or perturbation theories) for an accurate representation of the structural and thermodynamic properties of the systems. These simpler intermolecular potentials not only provide a route to an amenable description of real associating fluids, but also allow one to gain physical insight into the effect of association on the behaviour of the system at a fraction of the computational cost. As may have become apparent from the introductory section, a variety of different prototypical intermolecular potential models have been employed in the development of theories for associating molecules (see the review of Nezbeda [125] for further details). The models introduced by Ben-Naim [23–25] are based on a Lennard-Jonesium molecular core with directional attractive sites characterised by an angular-dependent Gaussian cutoff; this type of model has been used to study the anomalous properties of pure water, including the maximum in the liquid density close to the triple point, the minimum in the isothermal compressibility, and its large heat capacity [126–128]. Related models incorporating association sites with an angular-dependent SW conical cutoff have also been used in a number of studies [18,41,98,129], as have models with an internal SW bonding region which can be used to mimic chemical association [28,29]. Alternatively, one can employ models comprising molecular cores with embedded off-centre (but now spherically symmetrical) SW bonding sites [20,33,37,41,130] where the centre-to-centre distance between the molecular cores and the site-site distances fully define the intermolecular potential. The latter representation of associating molecules is the generic model of choice with the SAFT family of EOSs which are based on the Wertheim TPT1 description of association: the model corresponds to molecules formed from a number of spherical monomeric segments (e.g., represented by hard-sphere (HS), SW, LJ, Yukawa, or Mie potentials), incorporating off-centre SW bonding sites distributed on the monomer cores to mediate the association interactions.

As was mentioned earlier, our current work is motivated by the recent development of versions of the SAFT-VR EOS [111] and its group-contribution cousin the SAFT-γ EOS [77] which are based on the Mie interaction. We develop explicit forms of the Wertheim TPT1 associative contribution to the Helmholtz free energy for molecules formed from segments characterised by the Mie potential decorated with SW HB sites:

$$\Phi = \Phi^{\text{Mie}} + \Phi^{\text{HB}} . \tag{1}$$

The Mie [131] intermolecular potential Φ^{Mie} is a generalised LJ potential [132–136] with adjustable attractive and repulsive exponents that characterise the softness/hardness and the range of the interaction. The form of the pair-interaction energy between two monomeric segments is given as a function of the inter-segment distance r by

$$\Phi^{\text{Mie}}(r) = \mathcal{C}\varepsilon \left[\left(\frac{\sigma}{r} \right)^{\lambda_{\text{r}}} - \left(\frac{\sigma}{r} \right)^{\lambda_{\text{a}}} \right], \qquad (2)$$

where, in line with the common notation, σ is the segment diameter (at which the potential is zero), ε is the depth of the potential well, λ_{r} and λ_{a} are the repulsive and attractive exponents, respectively, and the prefactor $\mathcal{C}$ ensures that the minimum of the interaction is $-\varepsilon$:

$$\mathcal{C} = \frac{\lambda_{\text{r}}}{\lambda_{\text{r}} - \lambda_{\text{a}}} \left(\frac{\lambda_{\text{r}}}{\lambda_{\text{a}}} \right)^{\frac{\lambda_{\text{a}}}{\lambda_{\text{r}} - \lambda_{\text{a}}}}. \qquad (3)$$

The association interaction Φ^{HB} between two segments is represented as a sum of the interactions between the SW sites a on a given segment and the sites b on the other segment with which it associates:

$$\Phi^{\text{HB}} = \sum_{ab} \Phi^{\text{HB}}_{ab}, \qquad (4)$$

where each site-site bonding interaction is given by

$$\Phi^{\text{HB}}_{ab}(r_{ab}) = \begin{cases} -\varepsilon^{\text{HB}}_{ab} & \text{if } r_{ab} \leq r^{\text{c}}_{ab}, \\ 0 & \text{if } r_{ab} > r^{\text{c}}_{ab}, \end{cases} \qquad (5)$$

and r_{ab} is the centre–centre distance between sites a and b, $\varepsilon^{\text{HB}}_{ab}$ is the depth of the association energy well, and r^{c}_{ab} the cutoff range of the SW interaction between sites a and b. To fully characterise the geometry of the intermolecular potential model, the distance r^{d}_{aa} of each association site a from the centre of the corresponding segment is also specified.

The molecular model of water commonly employed in a SAFT description provides a useful illustration of the simplified representation of association interactions [137]: a single spherical molecular core with a number of bonding sites (typically four), as depicted in Figure 1.

The original TPT1 treatment of Wertheim is based on a number of assumptions that can limit its applicability but greatly simplify the theoretical treatment by taking advantage of the steric incompatibility between the molecular cores. The key assumptions are that: two molecules cannot bond to each other at more than one site; each site can bond only with one other site; and ring structures are not considered in the basic treatment. In order to implement the TPT1 description of associating fluids, one requires the RDF of the underlying model potential. A formal procedure for an
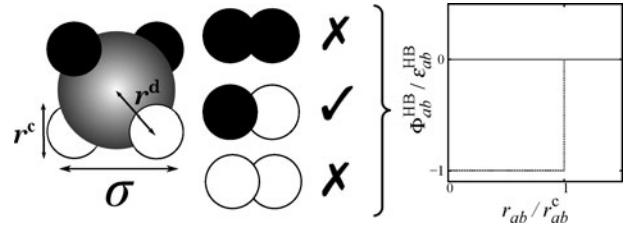

Figure 1. A generic illustration of the prototypical model of water commonly used in a SAFT treatment [137]. This particular example features four off-centre SW sites, two nominally representing the electron lone pairs on the oxygen atom (often referred to as type 'e' sites) and two representing the hydrogen atoms (type 'H' sites); in common with the usual Wertheim TPT1 description, only interactions between unlike sites are allowed. The site-site interaction corresponds to the SW form illustrated on the right-hand side of the figure: $\varepsilon^{\text{HB}}_{ab}$ characterises the strength of association, r_{ab} represents the distance between sites a and b, and r^{c}_{ab} the range of the interaction. One should note that significant portions of the hydrogen-bonding association configurations corresponding to site-site overlaps are precluded by the steric interactions between the molecular cores.

appropriate implementation of the TPT1 association contribution within SAFT-VR Mie is developed in the remainder of our paper.

2.2. Wertheim first-order thermodynamic perturbation theory (TPT1) of associating fluids

As we have already mentioned, the Wertheim TPT1 contribution to the thermodynamic properties of molecules that associate is employed within SAFT EOSs. The contribution $A^{\text{assoc.}}$ to the Helmholtz free energy due to association can be expressed in compact form as [41,42]

$$\frac{A^{\text{assoc.}}}{Nk_{\text{B}}T} = \sum_{a=1}^{s} \left(\ln X_a - \frac{X_a}{2} \right) + \frac{s}{2}, \qquad (6)$$

where N represents the number of molecules, k_{B} is the Boltzmann constant, T is the temperature, and s represents the number of association sites per molecule. The fraction of molecules X_a with given sites a not bonded is obtained from the following mass–action relation:

$$X_a = \frac{1}{1 + \rho \sum_{b=1}^{s} X_b \Delta_{ab}}, \qquad (7)$$

where

$$\Delta_{ab} = \int g^{\text{mono.}}(12) f_{ab}(12) \mathrm{d}(12), \qquad (8)$$

and $\rho = N/V$ is the number density. The integrated association strength Δ_{ab} is expressed as an integral over the relative positions and orientations of the two molecules,

denoted here by (12). The RDF $g^{\mathrm{mono.}}(12)$ of the reference non-associated monomers (or, in the case of chain-like molecules, the molecular segments) describes the correlations between particles in the fluid and is specific to the potential chosen to represent the interactions between the molecular segments (e.g., the Mie potential in our current work); the RDF generally depends on both the temperature and the density (as well as the form of the potential). The Mayer function of the association potential, $f_{ab}(12) = \exp[-\Phi_{ab}^{\mathrm{HB}}(12)/(k_{\mathrm{B}}T)] - 1$, which represents the probability that sites a and b on two isolated monomers will bind if the sites are within a certain cutoff distance of each other (for a given relative orientation), depends on the temperature (through the Boltzmann factor), the specific association interaction Φ^{HB}, and the geometry (the type, position, and size) of the sites (see, e.g., Figure 1).

The correlations between particles can be neglected in the zero-density limit (corresponding to $g^{\mathrm{mono.}}(12) = 1$), and the mass–action relation defined in Equation (7) essentially reduces to the form introduced by Hill [9–12] for an associating ideal gas. Guggenheim [138] has discussed the significance of incorporating the Mayer function in the definition for the degree of association (which he refers to as 'sociation') rather than the Boltzmann factor more commonly employed in the description of chemical equilibria. The Mayer function also enters the definition of the integrated association strength Δ_{ab} in Wertheim's treatment of associating fluids, as can be seen from Equation (8).

Owing to the marked structural correlations in a dense fluid, the RDF is not a simple monotonic function and it is therefore apparent that the evaluation of the integral characterising Δ_{ab} is not a trivial task. In order to facilitate the integration, the form of association potential and geometry of the sites are usually chosen to provide an algebraic description, hence the predominance of simple off-centre SW association sites. The integration is carried out over the range of distances for which the site-site association potential is non-zero, and for finite values of the monomer–monomer interaction. The major difficulty in evaluating the integral lies in its functional dependence on the RDF, which must be known over the appropriate range of inter-particle separations and thermodynamic states; unfortunately, the RDF is readily available only for the simplest of models.

2.3. *Radial distribution function of the reference monomer fluid*

An analytical description of the RDF is available in some cases: for example, the Carnahan–Starling EOS [139] for HS fluids yields accurate contact values of the RDF for densities up to the fluid–solid transition, while the expression developed by Boublík [140] for the chemical potential of HS dimers as a function of the intramolecular separation between the two segments can be used to represent the RDF over a moderate range of distances. These algebraic relations are based on well-founded theoretical considerations and their accuracy has been amply demonstrated by comparison with molecular simulations. The empirical expression for the contact value of the LJ fluid developed by Johnson *et al.* [141] also deserves a particular mention; it was obtained by correlating an extensive set of computer-simulation data with a polynomial expression in density and temperature. Perturbation theories [142–144] can also be employed to obtain the RDF of a fluid based on the structure of a simpler reference system; for example, the Barker–Henderson high-temperature perturbation theory [142,143], used in the development of the SAFT-VR EOS [109], can provide a reasonable description of the RDF for a wide range of simple fluids, including the Yukawa, SW, Sutherland, or Mie potentials, based on the RDF of the well-known HS reference system. However, the representation of the RDF obtained with perturbation approaches is not generally of the required accuracy to provide a faithful description of the integrated association strength (cf. Equation (8)) and an alternative route for the RDF is necessary.

Monte Carlo (MC) or molecular dynamics (MD) simulations can be performed for systems with arbitrary intermolecular interactions at the conditions of interest to obtain an essentially exact representation of the full RDF. The use of molecular simulation with an EOS is, however, impractical: for each state point, one would require the RDF and, though computing power is increasing every day, the numerical algorithms are still too computationally intensive to be integrated directly within the EOS.

Another popular route to the RDF of simple fluids is integral-equation theory, which involves the solution of the Ornstein–Zernike (OZ) equation [145]. The OZ equation for a pure (single-component), isotropic, homogeneous fluid of spherical particles can be expressed as

$$g(r) - 1 = c(r) + \rho \int (g(r') - 1)c(|\mathbf{r} - \mathbf{r}'|)\mathrm{d}\mathbf{r}'. \quad (9)$$

In the OZ equation there are two unknowns, the direct correlation function $c(r)$ and the RDF $g(r)$, making it impossible to solve without specifying a closure relation relating the two functions to the potential. There are a number of different closures that can be employed, including the traditional Percus–Yevick (PY), hypernetted chain (HNC), and the mean-spherical approximation (MSA) [146]. For our current work we use the reference hypernetted chain (RHNC) closure [147–150]. Though the MSA integral-equation approach provides an analytical framework for the representation of the pair distribution function and the thermodynamic properties, it is not as accurate as the RHNC closure, particularly in the case soft-core potentials. For example, in the case of the LJ fluid, the description of the vapour-liquid coexistence obtained with the RHNC approach [151] is seen to be highly superior to the corresponding description

obtained with the MSA approach [152]. The RHNC closure can be expressed as

$$c(r) = -\frac{u(r)}{k_B T} + g(r) - 1 - \ln(g(r) - 1) + B(r) , \quad (10)$$

where $B(r)$ is the bridge function, taken to be that of a reference fluid of HSs of diameter σ^{HS}. The parametrisation of Malijevský and Labík [153] can be used to describe the HS bridge function, and σ^{HS} is obtained from a solution of [148,149]

$$\int \left(g(r) - g^{HS}(r)\right)\sigma^{HS}\frac{\partial B^{HS}(r, \sigma^{HS})}{\partial \sigma^{HS}}dr = 0. \quad (11)$$

The OZ relation with the RHNC closure has to be solved numerically as no general analytical form of the solution is available, due in part to the presence of the variable diameter for the HS fluid used to represent the bridge function. The nature of the numerical procedure hampers the direct application of the OZ solution within an EOS, as it requires extensive iterative calculations for each state point. On the other hand, the RHNC integral-equation theory has been shown to provide a very good representation of the RDF and thermodynamic properties of various systems, including the Yukawa [154,155], SW [156], and LJ [151] fluids. The difference between RDF values obtained for simple potential models from the RHNC approach and from molecular simulation is negligible (essentially within the level of accuracy of the simulation). An example of the remarkable agreement is illustrated in Figure 2 for two different Mie fluids characterised by the relatively soft (8-6) and hard (50-6) potential forms.

The RHNC integral-equation theory is not, however, without its shortcomings: there are stable thermodynamic states of the fluid for which RHNC does not have a solution, and, conversely, there are metastable fluid states for which RHNC provides a solution. The region of failure of the RHNC approach does not coincide with the metastable (spinodal) region associated with vapour-liquid equilibrium (VLE); for example, in the case of the LJ model, the region where the RHNC theory fails incorporates super-critical states just above the critical temperature [151]. However, as we shall demonstrate, this will not prove to be overly problematic for our applications: the RHNC solution for the RDF is used first to assess the accuracy of previous approximations within the TPT1 framework; in the case of Mie fluids, we are able to locate the vapour-liquid boundary accurately using the SAFT-VR Mie EOS and the solid-fluid boundary using additional information from molecular simulation and perturbation theory [157], and can thereby identify and ignore erroneous solutions.
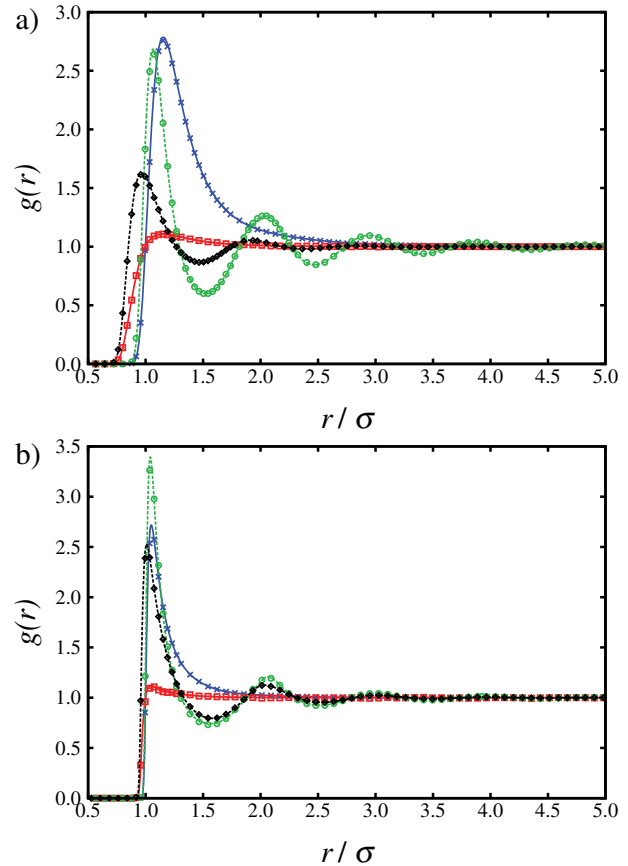

Figure 2. RDFs obtained for fluids comprising Mie particles across the range of liquid densities for relatively (a) soft (8-6) and (b) hard (50-6) forms of the potential. The curves represent the solution of the OZ integral equation with the RHNC closure, and the symbols the corresponding MD data. The temperatures and densities characterising the state of the fluid ($T^* = k_B T/\varepsilon$, $\rho^* = \rho\sigma^3$) are: (a) blue curve and crosses (1.0, 0.01), red curve and squares (10.0, 0.01), green curve and circles (1.0, 0.9), and black curve and diamonds (10.0, 0.9) for the Mie (8-6) fluid; (b) blue curve and crosses (1.0, 0.01), red curve and squares (10, 0.01), green curve and circles (1.0, 0.75), and black curve and diamonds (10.0, 0.75) for the Mie (50-6) fluid (colour online).

3. Application of the Wertheim TPT1 association contribution in SAFT

3.1. Simplification for associating hard-sphere fluids: SAFT-HS

The success of the SAFT EOS can be attributed in large part to its ability to treat associating fluids using the Wertheim TPT1 formalism within an analytical framework. Early on in the development of the SAFT methodology [41], Wertheim's TPT1 was successfully applied to describe the thermodynamic properties and degree of association in systems of associating HSs with one and two bonding sites and comparisons were made with the corresponding molecular-simulation data. Both conical and spherical SW sites were considered as simple models for the association interactions with geometries specifically chosen to provide an

analytical expression for the angle-averaged Mayer function of the potential. The model with two sites extended the description of dimer formation inherent with the one-site model to a treatment of chain aggregates, paving the way towards realistic models for real associating fluids.

In the remainder of our work, we will consider SW bonding sites as this representation of the association interaction is the most prevalent in the context of the SAFT approach. The integrated association strength for off-centre spherical SW sites is obtained as (cf. Equation (8)) [41]

$$\Delta_{ab} = \frac{4\pi}{24(r^{\rm d})^2} F_{ab}$$
$$\times \int_{2r^{\rm d}-r^{\rm c}}^{2r^{\rm d}+r^{\rm c}} g^{\rm mono.}(r)(2r^{\rm d}+r^{\rm c}-r)^2(2r^{\rm c}-2r^{\rm d}+r)r\,{\rm d}r,$$
$$(12)$$

where the (temperature-dependent) magnitude of the Mayer function of the site-site SW association is denoted as

$$F_{ab} = \exp\left[\varepsilon_{ab}^{\rm HB}/(k_{\rm B}T)\right] - 1. \tag{13}$$

In the case of the HS fluid, the lower bound of integration corresponds to the HS diameter σ, since $g^{\rm HS}(r) = 0$ for $r < \sigma$. It was recognised in reference [41] that for short distances outside the HS core, i.e., for short ranges of the site-site interaction, $g^{\rm HS}(r)$ decreases roughly as $1/r^2$, so that the RDF can be represented in terms of its contact value over a range of distances:

$$g^{\rm HS}(r) = \frac{\sigma^2 g^{\rm HS}(\sigma)}{r^2}. \tag{14}$$

This approximation simplifies the equations for the integrated association strength by allowing one to factorise the RDF out of the integral:

$$\Delta_{ab} = \frac{4\pi\sigma^2}{24(r^{\rm d})^2} F_{ab}\, g^{\rm HS}(\sigma)$$
$$\times \int_{\sigma}^{2r^{\rm d}+r^{\rm c}} \frac{(2r^{\rm d}+r^{\rm c}-r)^2(2r^{\rm c}-2r^{\rm d}+r)}{r}\,{\rm d}r.$$
$$(15)$$

The integral is now solely a function of the geometrical parameters of the sites and the quadrature can be carried out to give a compact algebraic expression:

$$\Delta_{ab} = F_{ab}\, g^{\rm HS}(\sigma)\, K_{ab}^{\rm HS}(r^{\rm c}, r^{\rm d}, \sigma), \tag{16}$$

where

$$K_{ab}^{\rm HS} = 4\pi\sigma^2[\ln((r^{\rm c}+2r^{\rm d})/\sigma)(6r^{\rm c3}+18r^{\rm c2}r^{\rm d}-24r^{\rm d3})$$
$$+(r^{\rm c}+2r^{\rm d}-\sigma)(22r^{\rm d2}-5r^{\rm c}r^{\rm d}-7r^{\rm d}\sigma-8r^{\rm c2}$$
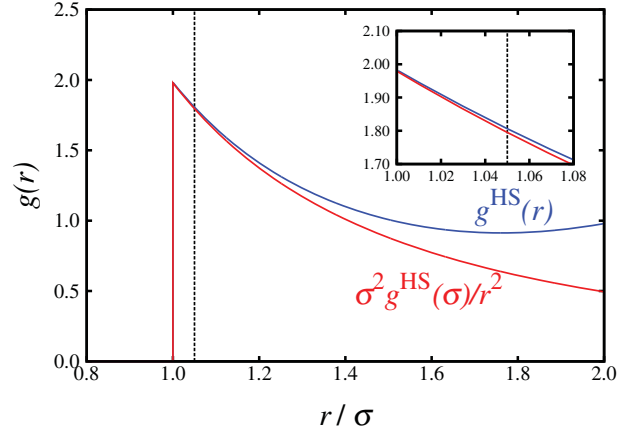$$+r^{\rm c}\sigma+\sigma^2)]/(72r^{\rm d2}) \tag{17}$$

Figure 3. RDF of a HS fluid at a reduced density of $\rho^* = \rho\sigma^3 = 0.45$ obtained with the RHNC integral-equation theory $g^{\rm HS}(r)$ (blue curve) and with the approximate relation $\sigma^2 g^{\rm HS}(\sigma)/r^2$ in terms of the contact value (red curve); the dashed line represents the range of the site-site interaction employed in the study of the associating HSs of reference [41]. A close-up of the region of interest is shown in the inset; the approximation is seen to provide a very good description of the RDF of the fluid for these separations (colour online).

captures the specific geometric nature of the association interaction and is commonly referred to as the bonding volume.

The compressibility factor, internal energy, and fraction of molecules not bonded for HS fluids with one and two bonding sites obtained with this approximate description of the association integral (involving the factorisation of the RDF) have been found to be in very good agreement with the result of the full numerical integration (using the accurate PY solution for $g^{\rm HS}(r)$) and with the simulation data [41]. The accuracy of the factorisation of the RDF from the association integral suggests that the approximation that the RDF decays as $1/r^2$ over short to moderate distances is reasonable for the HS fluid, as can be seen from Figure 3 in the case of the RHNC closure.

The simplification proves to be very accurate and simple, but is limited to HS fluids at low to intermediate densities for systems with short-ranged association interactions. As a consequence of the success and algebraic simplicity of this approximation for the integrated association strength, it has been subsequently used without modification in different versions of the SAFT EOSs, whether or not the reference system is (or can be approximated as) a HS fluid. The principal applications can be found in: the original SAFT EOS [2], where the LJ monomer is treated as a reference HS of diameter $d(T)$, the Barker–Henderson diameter, in order to evaluate the association contribution; the SAFT-HS EOS [158] with a van der Waals treatment of the dispersion attractive contribution; the PC-SAFT EOS [159] where, because the dispersion interactions are added as a perturbation contribution to the HS chain term, the monomer fluid

is effectively the HS fluid; and the cubic-plus-association (CPA) EOS [160], though in this particular case the underlying pair potential is not sufficiently well characterised to obtain a physically representative expression for the integrated association strength.

3.2. Inadequacy of the simplified description for associating square-well fluids: SAFT-VR SW

In the development of the SAFT-VR EOS [109], Δ_{ab} is obtained with the same approximate factorisation as described in the previous section, the main difference being that the monomer system is a SW rather than a HS fluid. Expressions for other intermolecular potentials were also developed in the original paper [109], but the most widely used to date within the SAFT-VR methodology has been the SW potential. In the case of an associating SW fluid, the integrated association strength is approximated as

$$\Delta_{ab} = F_{ab}\, g^{\mathrm{SW}}(\sigma)\, K_{ab}^{\mathrm{HS}}(r^{\mathrm{c}}, r^{\mathrm{d}}, \sigma). \qquad (18)$$

Although an accurate algebraic expression for the contact value of the RDF of the HS fluid is available from the Carnahan–Starling EOS, a corresponding relation is not as forthcoming for the SW system, and hence a first-order Barker–Henderson perturbation expansion (which is consistent with a second-order expansion for the Helmholtz free energy) was used in the SAFT-VR description [109]:

$$g^{\mathrm{SW}}(\sigma) = g^{\mathrm{HS}}(\sigma) + \left(\frac{\varepsilon}{k_{\mathrm{B}}T}\right) g_1^{\mathrm{SW}}(\sigma). \qquad (19)$$

It has been demonstrated that $g(r) \approx g(\sigma)\sigma^2/r^2$ is a good approximation for the HS fluid over short to moderate separations. Unfortunately, such a representation does not turn out to be as reliable for the SW fluid, with the RDF decreasing more rapidly than the assumed inverse quadratic dependence, as is apparent from Figure 4. The use of this approximation for the SW RDF leads to an overestimation of the integrated association strength; as a consequence, the degree of association is enhanced, resulting in an underestimation of the fraction of molecules not bonded, which is apparent from Figure 5.

As the approximate representation of the RDF of the SW fluid is not very good, one could be led to assume that the EOS would not provide an accurate description of the thermodynamic properties of real associating fluids. The approximate treatment of the integrated association strength has, nevertheless, been shown to provide a very good description of the fluid-phase equilibria for different associating fluids and fluid mixtures [47], including challenging systems such as water [137], polyethyleneglycols [161], alkanols, and alkanolamines [162]. Two factors can help to explain this apparent contradiction. In the first instance, the representation of real molecules as chains
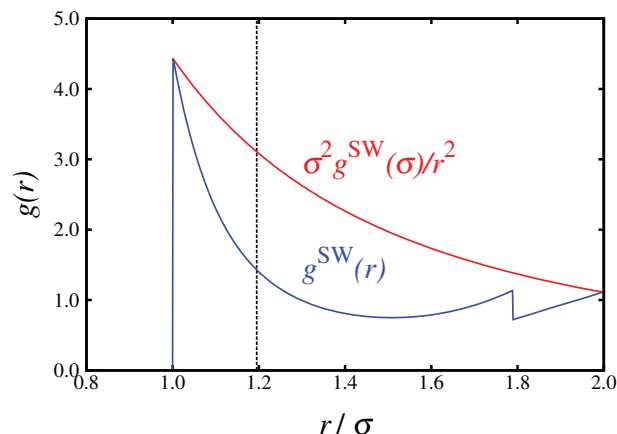
Figure 4. RDF $g^{\mathrm{SW}}(r)$ of a SW fluid of range $\lambda = 1.7889\sigma$ (corresponding to the range of the associating SW model of water described in reference [137]) at a reduced temperature of $T^* = k_{\mathrm{B}}T/\varepsilon = 2.2$ and a reduced density of $\rho^* = \rho\sigma^3 = 0.8$ obtained with the RHNC integral-equation theory (blue curve) and with the approximate relation $\sigma^2 g^{\mathrm{SW}}(\sigma)/r^2$ in terms of the contact value (red curve); the dashed line represents the cutoff range of the site-site interaction employed for the SW model of water [137] (colour online).

of spheres with associating sites is an approximation, and discrepancies in the theory are compensated by refining the intermolecular parameters of the model to the properties of the real fluid. The other reason that can explain why a good description of the fluid-phase behaviour of real systems can be obtained despite the inaccuracy in the evaluation of the
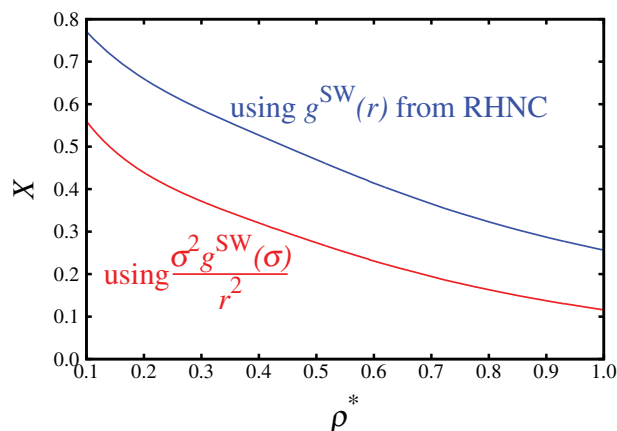
Figure 5. Fraction X of unbonded molecules for an associating SW fluid as a function of the reduced density $\rho^* = \rho\sigma^3$ at a reduced temperature of $T^* = k_{\mathrm{B}}T/\varepsilon = 2.5$. The range of the SW is $\lambda = 1.7889$; the model incorporates one off-centre SW association site placed at $r^{\mathrm{d}}/\sigma = 0.25$ with a cutoff of $r^{\mathrm{c}}/\sigma = 0.69$ (corresponding to parameters of the SW model of water described in reference [137]). A comparison is made between the description obtained using the essentially exact RHNC integral-equation theory to evaluate the integrated association strength (blue curve) and that obtained from the approximation $g^{\mathrm{SW}}(r) \approx \sigma^2 g^{\mathrm{SW}}(\sigma)/r^2$ (red curve) (colour online).

integrated association strength lies in the nature of the properties being examined: phase equilibria involve the equality of pressure and chemical potential of each component in each phase. The pressure and chemical potential correspond to partial derivatives of the Helmholtz free energy with respect to the volume and the number of particles, respectively. A Wertheim TPT1 treatment of these thermodynamic quantities therefore essentially depends on the derivative of the degree of association (through the variable X). As can be seen in Figure 5, the difference between the approximate and exact representation of X is almost constant, resulting in very similar derivatives $\partial X / \partial \rho$ and thus commensurate thermodynamic properties.

3.3. Correlation of simulation data for associating Lennard-Jones fluids: SAFT-LJ and soft-SAFT

In 1995 Müller and Gubbins [163] developed a dipolar SAFT-LJ EOS, using a Stockmayer (a dipolar LJ sphere) model with a focus on describing the properties of water. An association contribution for the monomer reference fluid, which was treated as a LJ system, was developed with the aid of computer-simulation data, and the dipolar contribution was considered with a separate perturbation term [164,165]. For an associating LJ fluid, the integrated association strength can be expressed as (cf. Equation (12))

$$
\Delta_{ab} = \frac{4\pi F_{ab}}{24(r^{\mathrm{d}})^2}
$$
$$
\times \int_{2r^{\mathrm{d}}-r^{\mathrm{c}}}^{2r^{\mathrm{d}}+r^{\mathrm{c}}} g^{\mathrm{LJ}}(r)(2r^{\mathrm{d}} + r^{\mathrm{c}} - r)^2 (2r^{\mathrm{c}} - 2r^{\mathrm{d}} + r) r \, \mathrm{d}r .
$$
(20)

This expression is characterised by five variables: the temperature and density of the thermodynamic state; the strength of the SW site-site interaction $\varepsilon^{\mathrm{HB}}$; and the geometrical parameters of the sites r^{c} and r^{d}. To reduce the complexity, Müller and Gubbins assumed a particular geometry of the sites by setting $r^{\mathrm{d}} = 0.4\sigma$ and $r^{\mathrm{c}} = 0.2\sigma$. As a result, the integrated association strength is given as

$$
\Delta_{ab} = \frac{4\pi F_{ab}}{3.84\sigma^2} \int_{0.6\sigma}^{\sigma} g^{\mathrm{LJ}}(r)(\sigma - r)^2 (r - 0.4\sigma) r \, \mathrm{d}r . \quad (21)
$$

Equation (21) can be written in compact form as

$$
\Delta_{ab} = 4\pi F_{ab} K_{ab}^{\mathrm{LJ}} I, \quad (22)
$$

with $K_{ab}^{\mathrm{LJ}} = \sigma^3$ and

$$
I = \frac{1}{3.84\sigma^5} \int_{0.6\sigma}^{\sigma} g^{\mathrm{LJ}}(r)(\sigma - r)^2 (r - 0.4\sigma) r \, \mathrm{d}r; \quad (23)
$$

we shall refer to the dimensionless integral I as the association kernel. The kernel I can be written in terms of the

dimensionless distance $r^* = r/\sigma$ as

$$
I = \frac{1}{3.84} \int_{0.6}^{1} (1 - r^*)^2 (r^* - 0.4) r^* g^{\mathrm{LJ}}(r^*) \mathrm{d}r^* . \quad (24)
$$

The integral depends only on the temperature and density through the state dependence of the RDF, $g(r; T, \rho)$. Confronted with the need for an accurate representation of the RDF of the LJ fluid, Müller and Gubbins chose to use molecular simulations to obtain structural data over a wide range of conditions; the resulting integral was evaluated numerically and correlated using a two-dimensional polynomial,

$$
I = \sum_{i=0}^{4} \sum_{j=0}^{4} a_{ij} [\rho^*]^i [T^*]^j , \quad (25)
$$

where the 25 a_{ij} coefficients were adjusted to give the best correlation of I. In subsequent work with the SAFT-LJ EOS [166,167], and in the closely related soft-SAFT EOS [168–170], the constraint of a fixed geometry was relaxed in an implicit manner by treating the effective bonding volume K_{ab}^{LJ} as an adjustable parameter; one should point out, however, that when one employs this type of empirical approach the direct correspondence with the geometry of the association site is lost. A very good description of the thermodynamic properties and fluid-phase equilibria of water and other associating fluids can nevertheless be obtained in this way, making this type of approach particularly versatile.

4. Application of the Wertheim TPT1 for associating Mie fluids: SAFT-VR Mie

We now consider associating fluids characterised by the Mie potential treated using the Wertheim TPT1 methodology within the SAFT-VR Mie EOS. In the SAFT-VR Mie approach, molecules are modelled as chains formed from m spherical segments, interacting through the Mie potential (Equation (2)). A principal objective of our work is to develop the best possible description of the thermodynamics and fluid-phase behaviour of associating fluids with a particular focus on water, which is ubiquitous in many mixtures of topical interest, including electrolytes and biological systems.

4.1. Factorisation of the integrated association strength

As a first approximation, we follow the method developed in reference [111], i.e., the approximate factorisation of the contact value of the RDF used in the HS case. Following the treatment presented in Section 3.1, the integrated association strength can be expressed as

$$
\Delta_{ab} = F_{ab} \, g_d^{\mathrm{HS}}(d) \, K_{ab}^{\mathrm{HS}}(r^{\mathrm{c}}, r^{\mathrm{d}}, \sigma, d) , \quad (26)
$$

where $g_d^{HS}(d)$ is the contact value of the RDF of the reference HS fluid of diameter $d(T)$ (the Barker–Henderson diameter), and $K_{ab}^{HS}(r^c, r^d, \sigma, d)$ is the corresponding bonding volume. Models have been proposed for the first four members of the *n*-alkanol homologous series, and a good description of the VLE and single-phase second-derivative properties was demonstrated [111].

In order to develop the best possible model for water, a thorough grid-based parameter-estimation procedure [171] is applied based on a detailed examination of the parameter space by comparison of the computed properties with target experimental data for water from the National Institute of Standards and Technology (NIST) [172]. The multidimensional parameter space is examined in planes defined by discrete pairs of individual parameters, using projections onto contour plots of the percentage absolute average deviation (%AAD $= \frac{1}{n_p} \sum_i^{n_p} |\mathcal{P}_{i,\text{SAFT}} - \mathcal{P}_{i,\text{expt.}}|/|\mathcal{P}_{i,\text{expt.}}|$, where $\mathcal{P}$ represents the set of properties of interest, and n_p the number of data points) of the theoretical description from the experimental values for the vapour pressure and saturated-liquid density from the triple point to 95% of the critical temperature; each point on the grid corresponds to a specific model, while the value of its contour corresponds to the predefined measure of the quality of the model. Closely following the study with the SAFT-VR SW EOS [137], we develop models of water consisting of a single spherical Mie core ($m = 1$) with four association sites (two of type 'e' to represent the electron lone pairs on the oxygen and two of type 'H' to represent the hydrogen atoms, where only 'e – H' bonding is permitted), corresponding to seven adjustable parameters: σ, ε, λ_r, λ_a, r^c, r^d, and ε_{ab}^{HB}. In the case of associating molecules such as water, it is useful to examine models in the $(\varepsilon, \varepsilon_{ab}^{HB})$ plane (cf. references [137] and [173]), as this choice of variables clearly highlights the balance between the dispersive and associative energetic attractive contributions. To reduce the number of parameters that need to be estimated, the exponent characterising the attractive dispersive interaction is fixed to the London value, $\lambda_a = 6$. For the geometry of the site, we fix $r^d = 0.4\sigma$, the same value as used by Müller and Gubbins [163]. This means that for each pair of $(\varepsilon, \varepsilon_{ab}^{HB})$ points on the grid there are now only three adjustable parameters (σ, λ_r, r^c) to optimise, allowing for a more tractable assessment of the optimal multi-dimensional parameter space. The resulting surface is similar to that obtained for the associating SW model of water [137], with the best models located along a single valley, as can be seen in Figure 6.

The best overall representation of the vapour-liquid equilibria is obtained with the model characterised by the parameters given in Table 1. A comparison between the description of the vapour pressures and saturated vapour and liquid densities of water obtained with the SAFT-VR Mie model and that obtained with the SAFT-VR SW model developed in earlier work [137] is shown in Figure 7.
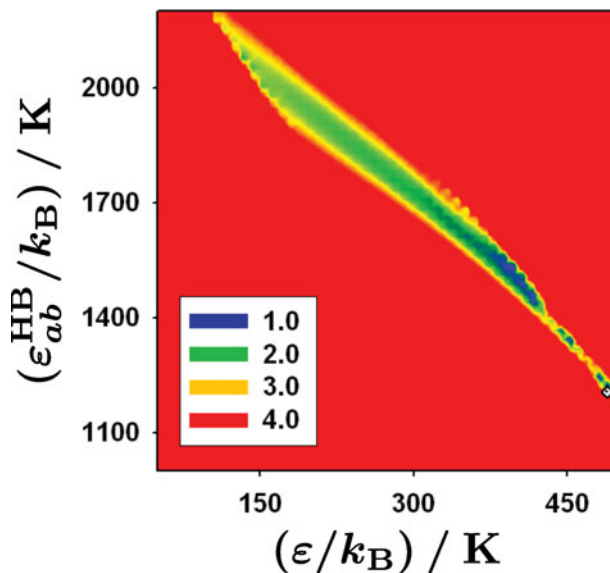

Figure 6. Contour plot in the plane of the dispersion ε and association ε_{ab}^{HB} attractive energies displaying the percentage absolute average deviation %AAD from the experimental values for the vapour pressure and saturated-liquid density [172], obtained with four-site associating Mie models of water from the SAFT-VR Mie EOS [111] with the approximate factorisation of the contact value of the HS RDF in the evaluation of the integrated association strength, Equation (26). The dark blue areas correspond to the lowest values of the %AAD; the diamond corresponds to the 'optimal' model with the parameters given in Table 1 (colour online).

It is rather surprising that though the SAFT-VR Mie EOS is based on a more sophisticated theoretical treatment and has been found to provide a very reliable representation of the properties for a large number of compounds [111,171], the SAFT-VR Mie description for water illustrated here is clearly not as good as that provided by the SAFT-VR SW approach [137]. In the SAFT-VR EOS, the residual Helmholtz free energy is expressed as a sum of three terms, $A^{\text{mono.}}$, A^{chain}, and $A^{\text{assoc.}}$, representing the contribution of the monomer reference fluid, the contribution of forming molecular chains of monomers, and the contribution due to reversible association, respectively. From the previous study of non-associating fluids [111], the monomer and chain terms of SAFT-VR Mie are known to be very accurate; moreover, since water is treated as a spherical molecule ($m = 1$), the chain contribution is not relevant. One is therefore left with the conclusion that the association contribution as currently implemented is not suitable to describe the degree of HB in water and its effect on the thermodynamic properties.

The inaccuracy in the representation of the association contribution stems from the inadequate treatment of the RDF of the Mie fluids in the association contribution. The factorisation of the contact value of the HS RDF from the integrated association strength has been shown to be an

Table 1. Optimal SAFT-VR Mie model parameters for the four-site associating water model obtained using the SAFT-VR Mie EOS [111] with the approximate factorisation of the contact value of the HS RDF in the evaluation of the integrated association strength, Equation (26).

m	$\sigma/\text{Å}$	λ_r	λ_a	$(\varepsilon/k_B)/\text{K}$	$(\varepsilon_{ab}^{HB}/k_B)/\text{K}$	r^c/σ	r^d/σ
1.0	3.1610	52.367	6.0	488.75	1210.0	0.58340	0.40

appropriate approximation for hard-core fluids; for the latter, the RDF is zero inside the core and the integration domain of the association kernel starts at the contact value (which is also the location of the maximum of the RDF) and then decreases outside the repulsive sphere. By contrast, when considering a soft-core interaction like the Mie
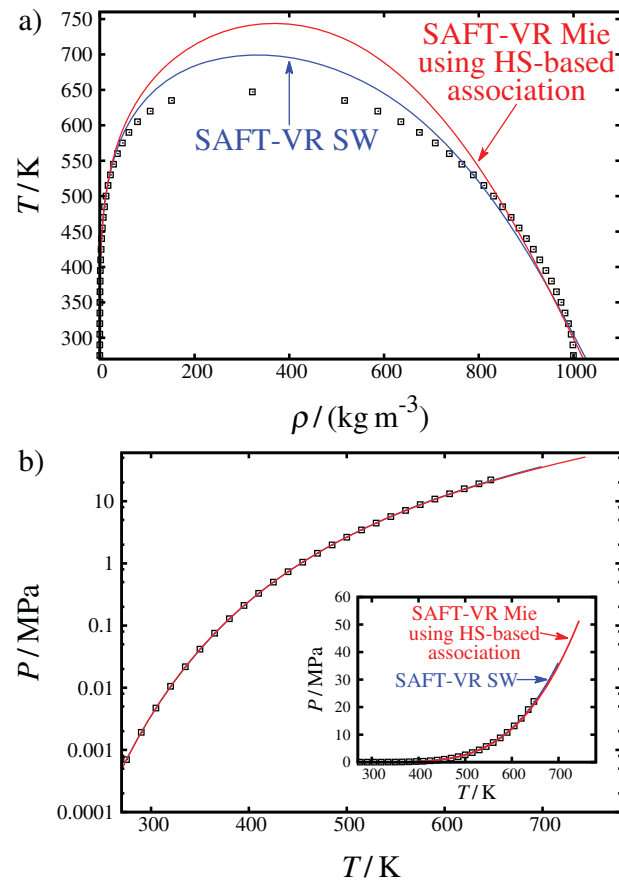
a)

b)

Figure 7. (a) The saturated vapour and liquid densities and (b) the vapour pressure of water: the symbols represent smoothed experimental data from NIST [172]; the blue curves represent the description obtained using the four-site SAFT-VR SW model [137]; and the red curves represent that obtained for the four-site SAFT-VR Mie model presented in Table 1 using the SAFT-VR Mie EOS [111] with the approximate factorisation of the contact value of the HS RDF in the evaluation of the integrated association strength, Equation (26) (colour online).

potential, the integration domain includes intermolecular separations below the contact diameter σ with non-zero values of the RDF in this range, while the maximum can be either below or above σ. As a consequence, the assumption that the RDF decreases as $1/r^2$ from the value at contact fails, as can be seen in Figure 8. This approximation of taking the HS contact value with Equation (14) to represent $g^{\text{Mie}}(r)$ over the range of the association is used for simplicity. A better description would clearly be obtained by using the maximum value, $g_{\max}^{\text{Mie}}(r)$; unfortunately, the distance at which the maximum occurs cannot easily be determined as it depends on temperature, density, and the form of the Mie potential.

The results illustrated in Figure 7 are obtained using the contact value of the RDF of the reference HS fluid of diameter $d(T)$ in the factorisation of the integrated association strength, Equation (26); the use of a similar factorisation with the value of the RDF of the Mie fluid at contact σ provides no improvement. It therefore appears that in order to obtain the integrated association strength more reliably, an accurate representation of the full RDF of the Mie fluid is required.

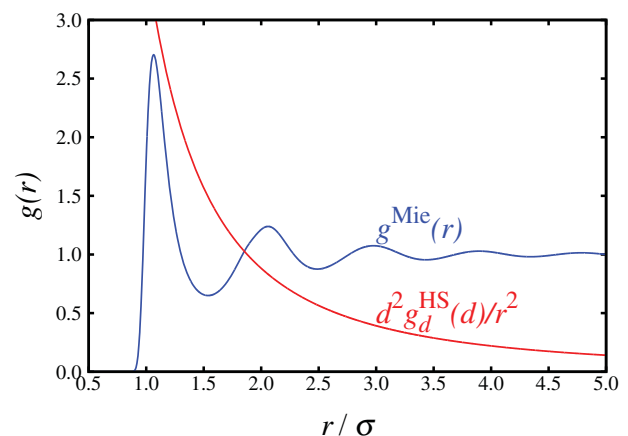Figure 8. RDF of the LJ (Mie 12-6) fluid at $T^* = k_B T/\varepsilon = 1.273$ and $\rho^* = \rho\sigma^3 = 0.85$: the blue curve represents the RDF $g^{\text{Mie}}(r)$ obtained using the RHNC integral-equation theory, while the red curve represents the approximation corresponding to the factorisation of the contact value $g_d^{\text{HS}}(d)$ in the evaluation of the integrated association strength, Equation (26) (colour online).
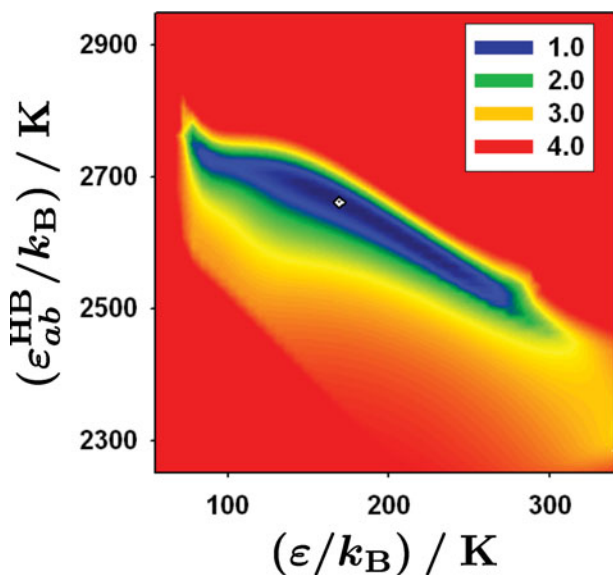
Figure 9. Contour plot in the plane of the dispersion ε and association ε_{ab}^{HB} energies displaying the percentage absolute average deviation %AAD from the experimental values for the vapour pressure and saturated-liquid density [172], obtained with four-site associating SAFT-VR Mie models of water with the SAFT-VR Mie EOS [111] using the SAFT-LJ associating contribution of Müller and Gubbins [163], Equation (25). The dark blue areas correspond to the lowest values of the %AAD; the diamond corresponds to the 'optimal' model with the parameters given in Table 2 (colour online).

4.2. Incorporating the SAFT-LJ integrated association strength into the SAFT-VR Mie EOS for Mie fluids

As we have seen, the approximate expression for the integrated association strength based on the factorisation of the contact value of the RDF is inadequate. We now assess the quality of the description with the Müller and Gubbins [163] association contribution developed for the LJ fluid, cf. Equation (25), as implemented without modification in the SAFT-VR Mie EOS. The incorporation of the SAFT-LJ association term is straightforward and we develop four-site (two 'H' and two 'e') models for water, once again using the 'grid' method to locate the optimal representation of the saturated-liquid density and vapour pressure. The model of water is characterised by seven intermolecular parameters, and the same assumptions are made as in Section 4.1, i.e., the molecule is near spherical so that $m = 1$ and the dispersion energy is assumed to be of the London form with $\lambda_a = 6$. The optimal parameter surface for the %AAD of the theoretical description from the experimental vapour pressures and saturated-liquid densities is shown in Figure 9. The models obtained with the SAFT-LJ association term are found to provide a much improved description compared with that corresponding to the factorisation of the contact value of the RDF; of these, we single out the optimal water model indicated by the white diamond in Figure 9
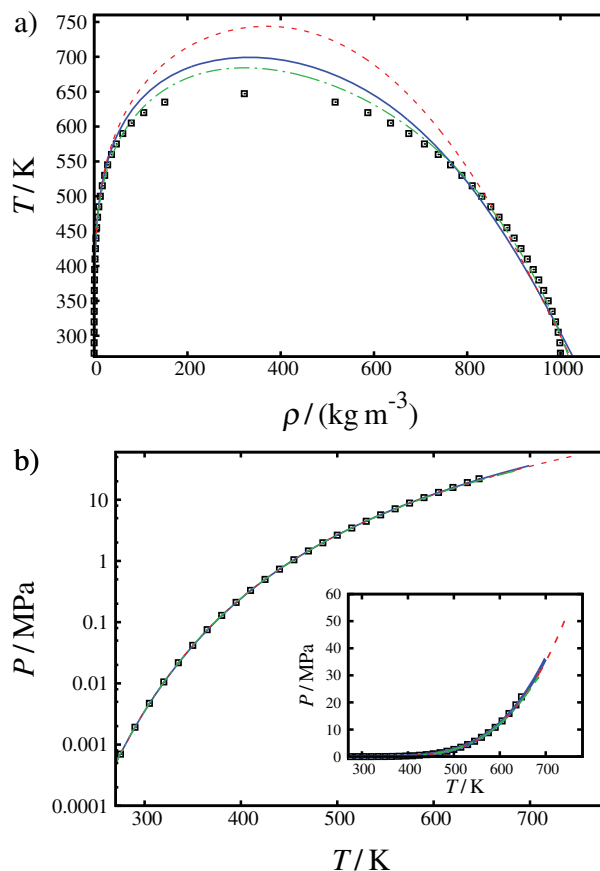
Figure 10. (a) The saturated vapour and liquid densities, and (b) the vapour pressure of water: the symbols represent smoothed experimental data from NIST [172]; the blue continuous curves represent the description obtained using the four-site SAFT-VR SW model [137]; the red dashed curves represent the description obtained for the four-site SAFT-VR Mie model of Table 1 using the SAFT-VR Mie EOS [111] with the approximate factorisation of the contact value of the HS RDF in the evaluation of the integrated association strength, Equation (26); and the green dot-dashed curves represent the description for the four-site SAFT-VR Mie model of Table 2 with the SAFT-LJ association contribution of Müller and Gubbins [163], Equation (25). In (b) the curves are essentially indistinguishable as all models are developed to provide a good description of the vapour pressure, the main difference being in the overshoot of the critical point (colour online).

(see Table 2 for the specific values of the intermolecular parameters of the model).

The use of the SAFT-LJ association contribution within the SAFT-VR Mie EOS provides a good description of the vapour pressure and coexistence densities of water, better overall than both the SAFT-VR Mie model with the factorisation of the HS RDF at contact and the SAFT-VR SW model, as can be seen in Figure 10.

Given that the use of the SAFT-LJ association contribution improves the description of the VLE of water significantly compared with the previous SAFT-VR Mie

Table 2. Optimal SAFT-VR Mie model parameters for the four-site associating water model obtained using the SAFT-VR Mie EOS [111] with the SAFT-LJ associating contribution of Müller and Gubbins [163].

m	$\sigma/\text{Å}$	λ_r	λ_a	$(\varepsilon/k_B)/\text{K}$	$(\varepsilon_{ab}^{HB}/k_B)/\text{K}$	$K_{ab}^{LJ}/\text{Å}^3$
1.0	3.0661	19.697	6.0	170.00	2660.0	3309.2

model, one could be satisfied that the goal of developing an accurate description of the thermodynamics of strongly associating fluids has been achieved. However, a number of important issues need to be emphasised. First of all, the association term of Müller and Gubbins [163] is only strictly applicable for LJ fluids and, as such, incorporating it in the SAFT-VR Mie EOS [111] without constraining the potential to be of the LJ form is inconsistent; though this is not problematic in practical applications, it is unsatisfying from the perspective of a rigorous theoretical treatment. A more important point to recognise is that in the treatment of the association term with the SAFT-LJ approach, the geometry of the association site is varied empirically by using an adjustable bonding volume parameter K_{ab}^{LJ}, which is found to be $\sim 115\sigma^3$ for the model given in Table 2, while the association term is strictly only applicable for the geometry employed by Müller and Gubbins which implies that $K_{ab}^{LJ} = \sigma^3$. The unrealistically large bonding volume brings into question the physical nature of the model and is a consequence of the original choice of geometry (with $r^d = 0.4\sigma$ and $r^c = 0.2\sigma$) which corresponds to an association site which is completely embedded within the spherical molecular core. In order to free ourselves from both the restriction of the LJ association contribution and the use of an implicit geometry, we proceed by developing an association contribution specifically for Mie fluids.

4.3. Novel SAFT-VR Mie association contributions for Mie fluids

It is apparent from the previous section that the incorporation of the SAFT-LJ association contribution into the SAFT-VR Mie EOS provides a much improved description of water. This is because the treatment of Müller and Gubbins [163] is tailored to the LJ soft-core (12-6) fluid, which is a particular case of the Mie potential. In order to improve on the good representation that such a treatment provides, we follow a similar approach with the aim of developing a generic Mie association contribution that is appropriate for potentials of varying form.

We continue to consider off-centre SW association sites to retain a tractable Mayer function, so that the integrated association strength can still be expressed in a factorised form as

$$\Delta_{ab} = F_{ab} K_{ab} I , \qquad (27)$$

where $K_{ab} = \sigma^3$, and the dimensionless association kernel is

$$I = \frac{4\pi}{24(r^d)^2\sigma^3} \int_{2r^d-r^c}^{2r^d+r^c} g^{Mie}(r)(2r^d + r^c - r)^2 \\ \times (2r^c - 2r^d + r)r\,dr . \qquad (28)$$

The RDF of the Mie fluid is obtained with the RHNC integral-equation approach for a wide range of conditions; this allows one to determine the kernel I numerically and then correlate the resulting data with a convenient empirical function. We opt not to correlate the RDF itself as the complex oscillatory functional form required to obtain a good description of the RDF, such as that proposed by Matteoli and Mansoori [174], prevents a straightforward analytical integration.

Two association contributions are developed in our current work: in the first, more generic, form, we determine the association kernel using the RDF of the Mie fluid with a suitable fixed geometry of the association site; alternatively, we take a leaf out of the Müller and Gubbins book and employ the RDF of the LJ fluid to provide a simpler representation of the association kernel, but using a different fixed geometry of the association site from that used by these authors (now chosen to allow more realistic values of the bonding volume K_{ab}).

In the case where we consider the RDF of the Mie fluid, the variables that need to be taken into account are the thermodynamic state defined by the dimensionless temperature $T^* = k_B T/\varepsilon$ and density $\rho^* = \rho\sigma^3$, and four model parameters: the two exponents λ_r and λ_a that characterise the Mie potential, and the geometrical parameters of the sites r^c and r^d. The other SAFT-VR Mie molecular parameters do not need to be considered explicitly as the association term is developed as a perturbation from the monomer fluid, whereby it is independent of the molecular chain length m; the hydrogen-bonding energy can be factored out of the integral with the Mayer function, and the size of the monomer segment and dispersion energy are taken into account implicitly, through T^* and ρ^*. To simplify the correlation, the dimensionality of the problem is reduced by fixing the attractive exponent to its London-dispersion value of $\lambda_a = 6$ and the position of the site is taken as $r^d = 0.4\sigma$ (cf. Section 4.1). Broad intervals are considered in the determination of the association kernel I for the remaining four
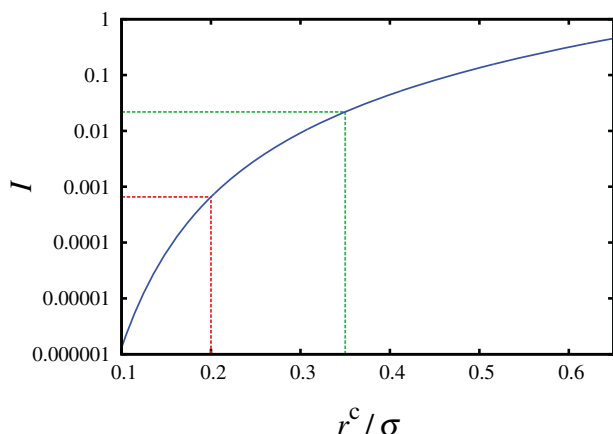
Figure 11. Values of the association kernel I as a function of the range r^c of the site-site association interaction for a Mie (20-6) potential at $T^* = k_B T/\varepsilon = 8.2$ and $\rho^* = \rho\sigma^3 = 0.75$ calculated using the Mie RDF from RHNC integral-equation theory; the lines indicate the values of I corresponding to the particular cases $r^c = 0.2\sigma$ (the value adopted by Müller and Gubbins [163]; red) and $r^c = 0.35\sigma$ (the value adopted in our current work; green) (colour online).

variables:

$$
\begin{aligned}
T^* &\in [0.1; 10] &\quad &\text{(100 values)}; \\
\rho^* &\in [10^{-10}; 1.25] &\quad &\text{(30 values)}; \\
\lambda_r &\in [8; 50] &\quad &\text{(22 values)}; \\
r^c/\sigma &\in [0.2; 0.6] &\quad &\text{(41 values).}
\end{aligned} \tag{29}
$$

After removing all the thermodynamic states that fall within the VLE envelopes of the corresponding Mie fluid from the data-set, a total of 2050,000 data points are retained for I.

To make the problem more manageable, one of the variables can be constrained. Since the temperature and density need to be taken into account explicitly, one can fix either the repulsive exponent of the Mie potential λ_r or the range of the association interaction r^c and use a bonding-volume parameter following the SAFT-LJ/soft-SAFT approaches. Fixing the repulsive exponent would sever the important link between the generic reference-fluid contribution and the association contribution, as we would no longer consider the association of the general Mie fluids but that of a particular form of potential. It is therefore preferable to fix the geometry of the association sites, thus maintaining consistency with the other contributions of the SAFT-VR Mie EOS, to the detriment of the link between the association parameters and the explicit site geometry. For the value of the range of the association interaction, we select a value of $r^c = 0.35\sigma$, which increases the magnitude of the association kernel, as shown in Figure 11. This range of the site-site interaction is larger than that used by Müller and Gubbins [163] ($r^c = 0.2\sigma$), allowing us to obtain more realistic values of the bonding volume parameter by considering

a geometry for which the association site is more accessible. Note the logarithmic scale in Figure 11; although the increase in r^c is less than a factor of 2, the resulting increase in I is between one and two orders of magnitude, whereby a much smaller effective bonding volume is required to represent the association kernel.

Following these simplifications, we now correlate the remaining 50,000 data points with three variables. The association kernel I is correlated with a general expression based on a combination of polynomials:

$$
I(T^*, \rho^*, \lambda_r) = \sum_{i=0}^{i+j\leqslant 10} \sum_{j=0} a_{ij}(\lambda_r)[\rho^*]^i[T^*]^j . \tag{30}
$$

where $a_{ij}(\lambda_r)$ are 66 adjustable coefficients. The dependence of these coefficients on the repulsive exponent of the Mie potential λ_r is

$$
a_{ij}(\lambda_r) = \sum_{k=0}^{6} b_{i,j,k}[\lambda_r]^k , \tag{31}
$$

where $b_{i,j,k}$ are $66 \times 7 = 462$ adjustable coefficients given in Tables A2–A8 of Appendix 1. With these coefficients, one reproduces very accurately the 50,000 values of the association kernel obtained using the RHNC integral-equation theory for the RDF of the Mie fluid, with a corresponding %AAD of 0.155%.

In order to simplify further the representation of the association contribution and reduce the number of coefficients required for an accurate representation, one can employ the RDF of the LJ (12-6) fluid (as obtained with the RHNC approach) to evaluate the integral. The association kernel I can then be represented as

$$
I(T^*, \rho^*) = \sum_{i=0}^{i+j\leqslant 10} \sum_{j=0} c_{ij}[\rho^*]^i[T^*]^j . \tag{32}
$$

The values of the corresponding 66 c_{ij} coefficients are given in Table A1 of Appendix 1.

Once the association kernel has been determined using either the generic Mie (Equation (30)) or the LJ (Equation (32)) forms, the integrated association strength for the associating Mie fluid can be expressed in the usual factorised form as

$$
\Delta_{ab} = F_{ab} K_{ab} I, \tag{33}
$$

where, in line with the treatment described in Section 4.2, K_{ab} can now be taken to represent an adjustable bonding-volume parameter to allow one to consider different site geometries in an empirical manner. The association strength Δ_{ab} is then used to determine the association contribution to the Helmholtz free energy of the associating Mie fluid
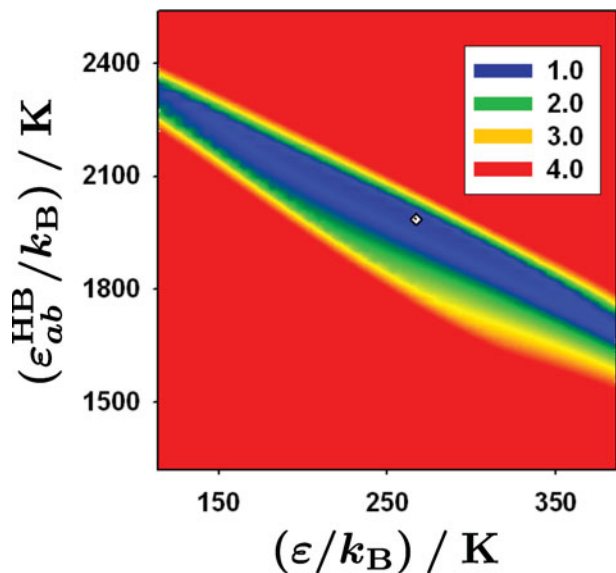
Figure 12. Contour plot in the plane of the dispersion ε and association ε_{ab}^{HB} energies displaying the percentage absolute average deviation %AAD from the experimental values for the vapour pressure and saturated-liquid density [172], obtained with four-site associating SAFT-VR Mie models of water with the SAFT-VR Mie EOS [111] using our novel LJ-based association kernel, Equation (32). The dark blue areas correspond to the lowest values of the %AAD; the diamond corresponds to the 'optimal' model with the parameters given in Table 3 (colour online).

Figure 13. Contour plot in the plane of the dispersion ε and association ε_{ab}^{HB} energies displaying the percentage absolute average deviation %AAD from the experimental values for the vapour pressure and saturated-liquid density [172], obtained with four-site associating SAFT-VR Mie models of water with the SAFT-VR Mie EOS [111] using our novel generic Mie association kernel, Equation (30). The dark blue areas correspond to the lowest values of the %AAD; the diamond corresponds to the 'optimal' model with the parameters given in Table 3 (colour online).
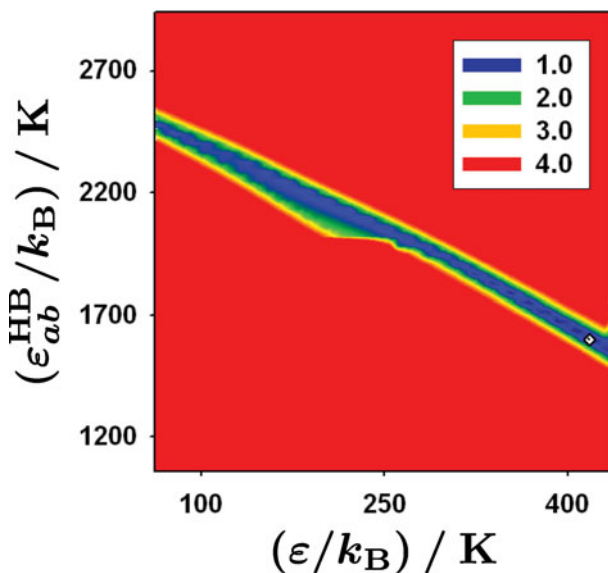
in the usual manner with the Wertheim TPT1 formalism, cf. Equations (6)–(8). Our improved and versatile representation of the association thermodynamics can then be combined with the monomer and chain contributions to the Helmholtz free energy of the SAFT-VR Mie EOS [111] for a reliable description of associating fluids and fluid mixtures.

5. Representing the thermodynamic properties of real associating fluids

5.1. Water

With this novel, generic, and accurate association contribution to the Helmholtz free energy for Mie fluids at hand, we are now in a position to develop an optimal SAFT-VR Mie description for water based on a four-site (two 'H' and two 'e') association model [137]. As in the previous sections, we examine a grid of models in the plane of the dispersive and associative attractive energies (ε, ε_{ab}^{HB}). The contours of Figures 12 and 13 are displayed representing the %AAD of the theoretical description from the experimental data [172] for the vapour pressure and saturated-liquid density of water (from the triple point to 95% of the critical temperature) using our novel LJ (Equation (32)) or generic Mie (Equation (30)) association kernels, respectively; at each point on the (ε, ε_{ab}^{HB}) surface, the size σ, repulsive exponent

λ_r, and bonding-volume K_{ab} parameters are estimated to optimise the representation of the vapour-liquid equilibria, treating the molecular core as spherical (corresponding to $m = 1$ in the SAFT description) and keeping the attractive exponent fixed at its London-dispersion value (*i.e.*, $\lambda_a = 6$). The intermolecular potential parameters for the best overall generic Mie model obtained on the surface are reported in Table 3, while the performance of the model for the VLE of water can be assessed in Figure 14.

It is apparent from Figure 14 that the SAFT-VR Mie model with the new generic Mie association contribution provides an improved representation of the vapour-liquid equilibria of water compared to that with the model obtained using the Müller and Gubbins [163] association contribution or our novel LJ kernel. The improvement is rather modest, however, leading to the conclusion that the quality of the description obtained using an association integral based on the LJ RDF is at least in part due to a decoupling of the reference fluids used to describe the dispersive and associative contributions of the EOS. This introduces an extra degree of freedom: when the repulsive exponent λ_r is changed, only the dispersive free-energy contribution is affected with the Müller and Gubbins association term remaining of the LJ form, while with our new treatment of the association kernel both the reference monomer and association contributions to the free energy of the associating Mie fluid are impacted simultaneously. On the other hand, the generic Mie model

Table 3. Optimal SAFT-VR Mie model parameters for the four-site associating water model obtained using the SAFT-VR Mie EOS [111] with our novel LJ (Equation (32)) or generic Mie (Equation (30)) association kernels.

Kernel	m	$\sigma/\text{Å}$	λ_r	λ_a	$(\varepsilon/k_B)/\text{K}$	$(\varepsilon_{ab}^{HB}/k_B)/\text{K}$	$K_{ab}/\text{Å}^3$
LJ	1.0	3.0063	17.020	6.0	266.68	1985.4	101.69
Mie	1.0	3.0555	35.823	6.0	418.00	1600.0	496.66

of water is more rigorous as it retains a variable repulsive exponent, a key feature of the SAFT-VR Mie EOS; moreover, by selecting a large range $r^c = 0.35$ for the association interaction as the basis for our correlation, the optimal value of the bonding volume parameter is significantly reduced, corresponding to $K_{ab} \sim 17\sigma^3$.

An overshoot of the predicted critical temperature can still be observed with the Mie formulation of the theory; the overshoot is less significant than that obtained with the SAFT-VR SW model of water [137]. In the development of the SAFT-VR Mie EOS, the perturbation expansion of the monomer reference contribution is taken to third order to capture some of the higher-body near-critical fluctuations in a semi-empirical manner [111]. Although the resulting algebraic expression does not, of course, yield universal values of the critical exponent (but rather leads to the usual quadratic mean-field form close to the critical point), a marked improvement of the shape of the phase envelope is obtained for non-associating compounds. On the other hand, the association contribution is developed using the Wertheim TPT1 two-body description, and as a consequence, does not incorporate these additional fluctuation contributions. It is therefore not surprising to find a small overshoot in the critical temperature for strong associating fluids such as water. A proper renormalisation-group treatment would have to be employed in this regard (e.g., as implemented in a number of studies within the SAFT formalism [175–178]), but this is beyond the scope of our current work.

The use of the generic Mie model leads to a clear improvement in the quality of the description of other thermodynamic properties, such as the single-phase density, the Joule–Thomson coefficient, and the isobaric heat capacity (see the five isobars depicted in Figure 15). Our SAFT-VR Mie model provides a good description of the heat capacity and Joule–Thomson coefficient. A deterioration of the description of some other thermodynamic properties such as the isothermal compressibility and speed of sound is, however, found at lower temperatures, partly due to omission of single-phase densities in the parameter-estimation procedure and partly due to the well-known and challenging anomalous behaviour of water. We did not include single-phase properties when developing the models for water to enable a direct comparison of the parameter-estimation procedure using a similar objective function for all models, including models based on the SW potential [137]. A

detailed assessment of the description of the isothermal compressibility, speed of sound, isothermal heat capacity, and other derivative properties of water and associating fluids with the SAFT-VR Mie EOS is the subject of on-going work.

Due to the additional number of adjustable intermolecular parameters necessary to describe associating components, an increased degeneracy of the model parameter space is found. A number of studies of water using EOSs of the SAFT family based on the Wertheim TPT1 have been undertaken to assess the description of additional properties in order to discriminate between models or to confirm the physical validity of the underlying interactions. A property that is widely considered in this regard is the degree of HB association of the fluid: the fraction of non-bonded OH groups in water obtained experimentally by Luck [179] using overtone infrared (IR) spectroscopy has been assessed with different versions of SAFT and related EOSs [137,163,170,180–191]. This property is particularly appealing when dealing with theories of associating fluids because the monomer fraction is obtained directly with a Wertheim TPT1 description from Equation (7) and its magnitude is sensitive to the specific model used.

The degree of association in water can be determined directly from molecular simulations of the popular atomistic models of water, including the SPC/E [115] and TIP4P/2005 [119] intermolecular potentials. A comparison of the main thermodynamic properties provided by these force fields has been presented in reference [120], and their performance in describing the VLE of water has already been assessed [192–195]. Here, we undertake additional canonical (*NVT*) MC [196] simulations of $N = 360$ water molecules represented with the SPC/E and TIP4P/2005 models for states along the vapour-liquid coexistence envelope [192–195] to determine the OH distribution function $g^{OH}(r)$ and assess the extent of HB. In the case of the liquid phase, 50,000 equilibration cycles (each corresponding to N separate MC trial displacements and reorientational moves) are carried out, followed by 50,000 cycles to accumulate the averages; of the order of 100,000 cycles are required to obtain reasonable statistics for the distribution functions of the vapour phase. The Ewald summation technique [196] is employed to account for the long-range electrostatic interactions: the range of the cutoff of the Ewald sum is taken as $R^{EW} = 0.4L$, where L is the density-dependent dimension of the simulation cell, and the width of the compensating
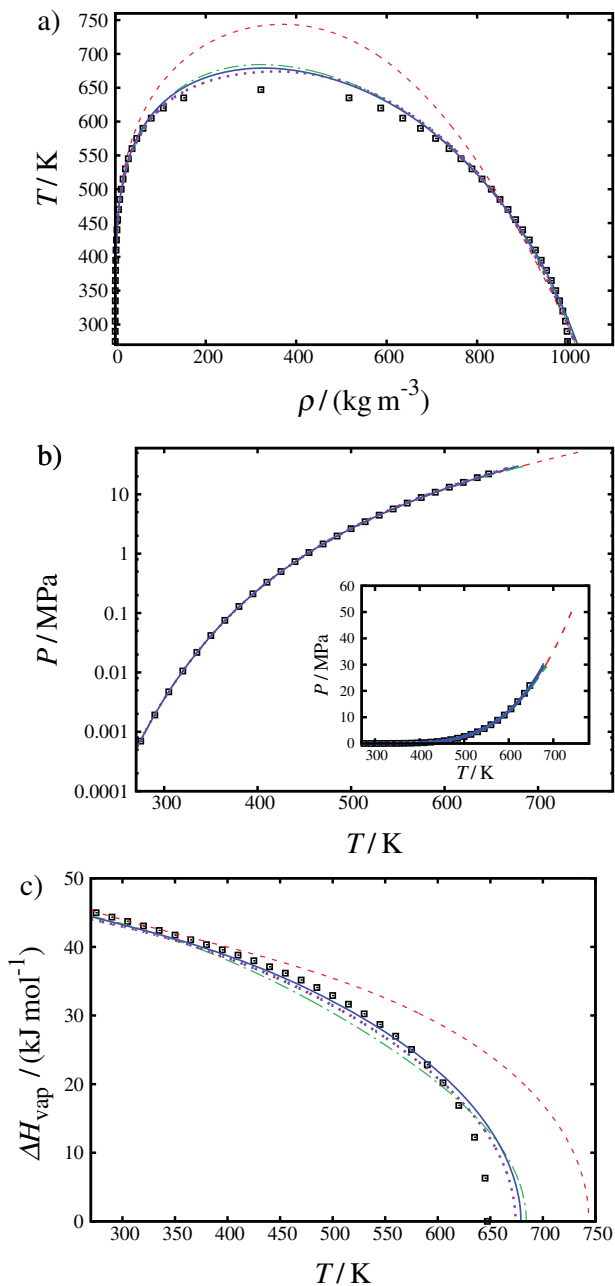
Figure 14. (a) The saturated vapour and liquid densities, (b) the vapour pressure, and (c) the enthalpy of vaporisation of water: the symbols represent smoothed experimental data from NIST [172]; the red dashed curves represent the description obtained for the four-site SAFT-VR Mie model of Table 1 using the SAFT-VR Mie EOS [111] with the approximate factorisation of the contact value of the HS RDF in the evaluation of the integrated association strength, Equation (26); the green dot-dashed curves represent the four-site SAFT-VR Mie model of Table 2 with the SAFT-LJ association contribution of Müller and Gubbins [163], Equation (25); the purple dotted curves represent the four-site SAFT-VR Mie model of Table 3 with the newly developed association kernel based on the LJ RDF, Equation (32); and the blue continuous curves represent the four-site SAFT-VR Mie model of Table 3 with the newly developed association kernel based on the generic Mie RDF, Equation (30) (colour online).
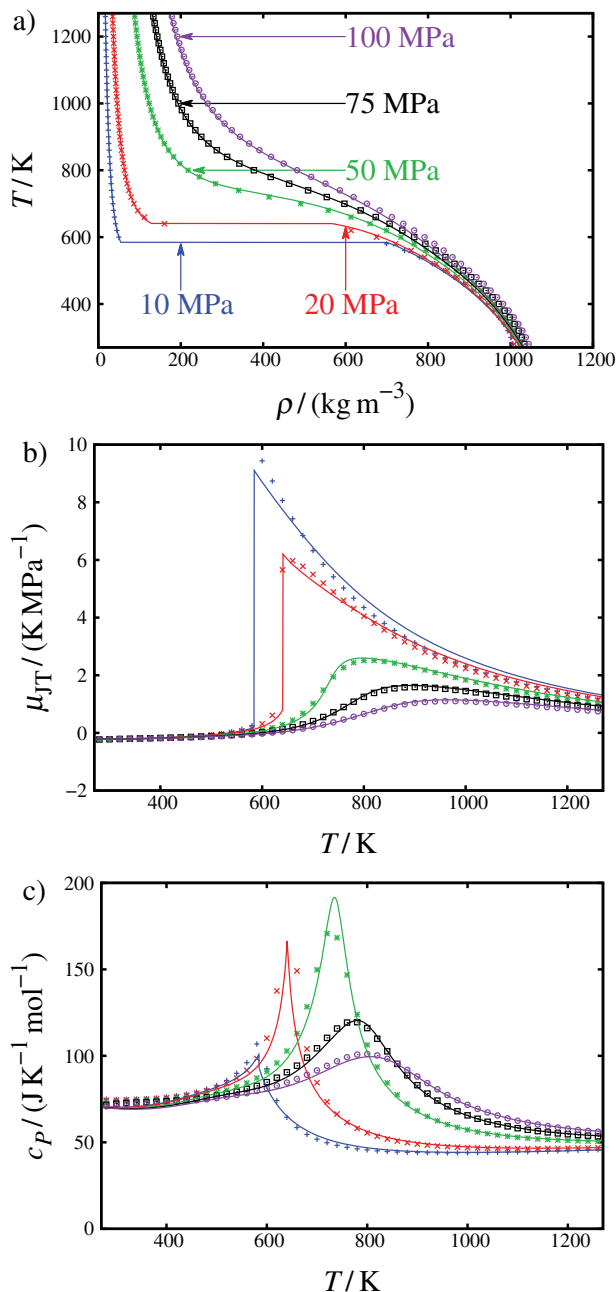
Figure 15. Single-phase isobaric properties of water, including (a) the density, (b) the Joule–Thomson coefficient, and (c) the isobaric heat capacity, at pressures of $P = 10$ (blue curves and pluses), 20 (red curves and crosses), 50 (green curves and asterisks), 75 (black curves and squares), and 100 (purple curves and circles) MPa: the symbols represent smoothed experimental data from NIST [172]; the curves represent the description obtained with the SAFT-VR Mie EOS [111] for the SAFT-VR Mie model of Table 3 using the newly developed association kernel based on the generic Mie RDF, Equation (30) (colour online).

screening charge is $\alpha^{EW} = 3/R^{EW}$. This choice provides a compromise between the accuracy of the Ewald sum and speed of the computation.

The number of hydrogen bonds n^{OH} associated with each H_2O molecule can be extracted directly from the coordination number which is determined by integrating the OH distribution function $g^{OH}(r)$ up to a specified cutoff distance r_c:

$$n^{OH} = 4\pi\rho \int_0^{r_c} r^2 g^{OH}(r)\mathrm{d}r \,. \tag{34}$$

If one assumes that a single water molecule can mediate a maximum of four (two acceptor and two donator) hydrogen bonds, then, because each hydrogen bond is shared between two water molecules, there can be a maximum of two hydrogen bonds per molecule. In the limit of complete association, the maximum number of hydrogen bonds in water is thus $N_{max}^{HB} = 2N$. The total number of OH hydrogen bonds per water molecule n^{HB} can be obtained as

$$n^{HB} = \frac{N^{HB}}{N} = 2n^{OH} \,, \tag{35}$$

where the factor of 2 is a consequence of the need to consider both the O and H atoms as the origin in the transcription of the coordination numbers obtained from $g^{OH}(r)$. The fraction of the total possible number of OH hydrogen bonds that are free is then simply given by

$$\begin{aligned} f_{free}^{OH} &= \frac{2N - N^{HB}}{2N} \\ &= 1 - n^{OH} \,. \end{aligned} \tag{36}$$

In a Wertheim TPT1 description, the fraction of free OH groups for the four-site SAFT models of water is obtained directly as an output of the theory from the fractions of molecules not bonded at the H or e site, cf. Equation (7):

$$f_{free}^{OH} = X_H = X_e \,; \tag{37}$$

the reader is directed to the thorough analysis of reference [137] for further details.

Mountain [197] has suggested a unique geometrical definition of the extent of HB for use in the simulation of atomistic models by setting the integration limit of Equation (34) to $r_c = 2.4$ Å. In the case of the TIP4P model [197], $n^{HB} \sim 1.8$ at 273 K and 0.999 g cm^{-3}. This geometric measure is broadly consistent with the degree of HB determined using an alternative energetic definition: $n^{HB} \sim 1.7$ at 298 K, 0.958 g cm^{-3}, and 0.101 MPa (see reference [198]) and $n^{HB} \sim 1.8$ at 298 K, 1.006 g cm^{-3}, and 0.1 MPa (see reference [199]). Both Kalinichev and Bass [200] and Chialvo and Cummings [201] have concluded that the geometric definition proposed by Mountain successfully represents the degree of HB in the system under normal conditions (away from the critical region). Kalinichev and
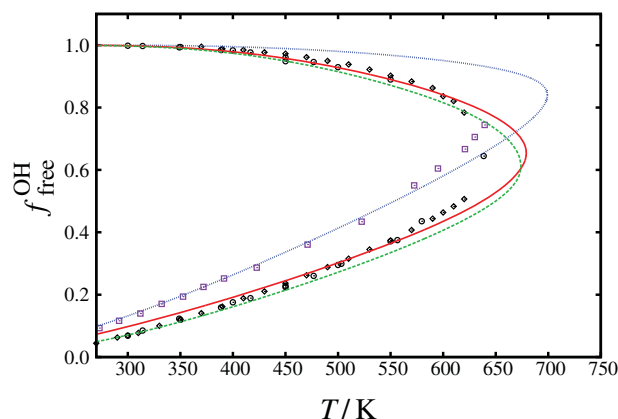
Figure 16. Fraction of free OH hydrogen bonds for the vapour and liquid states of water along the coexistence curve: the purple squares represent the values obtained from the IR spectroscopic data of Luck [179]; the black symbols are our new molecular simulation data for the SPC/E (circles) and TIP4P/2005 (diamonds) force fields; and the curves represent the corresponding theoretical description obtained with the SAFT-VR SW model [137] (blue dotted curve), and the predictions with the SAFT-VR Mie models of Table 3 using the association kernels based on the LJ (green dashed curve) and Mie (red continuous curve) RDFs (colour online).

Bass [200] have also shown that the typical energetic criterion for a hydrogen bond corresponding to a cutoff of -10 kJ mol^{-1} coincides with the simple geometric criterion of Mountain for water under ambient conditions.

The fractions of non-bonded OH groups obtained from our simulations of the SPC/E and TIP4P/2005 force fields are compared in Figure 16 and Table 4 with the values obtained from the analysis of the IR spectroscopic data by Luck [179] and from the representation of the degree of association obtained with the SAFT-VR SW model [137] and the SAFT-VR Mie models of Table 3 using the association kernels based on the LJ (Equation (32)) and generic Mie RDFs (Equation (30)). At ambient conditions the number of hydrogen bonds per water molecule in the saturated-liquid phase predicted with the generic SAFT-VR Mie description of the association is $n^{HB} \sim 1.85$, which is in very good correspondence with the simulation data for the SPC/E and TIP4P/2005 models and with the experimental value of $n^{HB} \sim 1.9$ obtained by Soper and Phillips [202] from an analysis of the structure determined by neutron scattering. On the other hand, the corresponding value of $n^{HB} \sim 1.7$ obtained by Luck [179] from IR spectroscopic data appears to suggest a slightly lower degree of association.

The agreement between the previously developed SAFT-VR SW model and the experimental data of Luck [179] is not surprising as these data were used to discriminate between models that provided a very similar description of the vapour pressure and saturated-liquid density [137]. It is evident that the degrees of HB obtained from the MC simulations of the SPC/E and TIP4P-2005 force

Table 4. Fraction of free OH hydrogen bonds for the saturated vapour (vap.) and liquid (liq.) states of water along the coexistence curve obtained by molecular simulation compared with the predictions from the SAFT-VR Mie models using the association kernels based on the LJ (Equation (32)) and generic Mie (equation (30)) RDFs. The vapour–liquid coexistence densities for the TIP4P/2005 and SPC/E models are taken directly from the literature [192–195].

Liquid (liq.) states

T/K	TIP4P/2005		SPC/E		LJ kernel (32)		Mie kernel (30)	
liq.	$\rho/(\text{g cm}^{-3})$	f^{OH}_{free}	$\rho/(\text{g cm}^{-3})$	f^{OH}_{free}	$\rho/(\text{g cm}^{-3})$	f^{OH}_{free}	$\rho/(\text{g cm}^{-3})$	f^{OH}_{free}
252.10	0.992	0.025			1.028	0.038	1.032	0.060
270.00	1.000	0.044			1.018	0.049	1.022	0.073
290.00	0.999	0.063			1.006	0.063	1.011	0.089
300.00	0.997	0.069	1.005	0.069	1.000	0.071	1.005	0.098
310.00	0.993	0.077			0.994	0.079	0.999	0.106
314.14					0.991	0.082	0.997	0.110
330.00	0.984	0.100	0.987	0.085	0.981	0.095	0.987	0.124
348.85			0.949	0.123	0.968	0.112	0.974	0.142
350.00	0.971	0.120	0.961	0.120	0.967	0.113	0.973	0.143
370.00	0.959	0.141	0.932	0.159	0.953	0.132	0.959	0.162
388.70					0.938	0.150	0.944	0.180
390.00	0.943	0.162	0.911	0.175	0.937	0.151	0.943	0.182
400.00					0.929	0.161	0.935	0.192
410.00	0.923	0.189			0.921	0.172	0.926	0.202
416.67			0.903	0.189	0.915	0.179	0.920	0.209
430.00	0.905	0.210	0.864	0.229	0.903	0.193	0.907	0.223
450.00	0.883	0.237	0.874	0.224	0.884	0.214	0.887	0.245
450.00					0.884	0.214	0.887	0.245
470.00	0.861	0.262	0.834	0.261	0.864	0.237	0.865	0.267
476.76					0.857	0.245	0.857	0.275
490.00	0.835	0.288	0.792	0.296	0.842	0.260	0.841	0.290
500.00			0.790	0.299	0.830	0.272	0.829	0.302
503.19					0.826	0.276	0.825	0.306
510.00	0.807	0.315	0.703	0.371	0.818	0.284	0.816	0.314
530.00	0.775	0.345	0.703	0.375	0.792	0.309	0.789	0.339
550.00	0.741	0.374			0.763	0.335	0.759	0.364
556.52					0.753	0.344	0.749	0.373
570.00	0.703	0.407	0.612	0.435	0.731	0.362	0.727	0.391
579.71					0.714	0.376	0.710	0.405
590.00	0.650	0.444			0.695	0.391	0.690	0.420
600.00	0.629	0.464			0.675	0.406	0.670	0.435
610.00	0.598	0.483			0.654	0.423	0.649	0.451
620.00	0.561	0.506			0.631	0.440	0.625	0.468
638.60			0.273	0.644	0.137	0.755	0.125	0.789

Vapour (vap.) states

T/K	TIP4P/2005		SPC/E		LJ kernel (32)		Mie kernel (30)	
vap.	$\rho/(\text{g cm}^{-3})$	f^{OH}_{free}	$\rho/(\text{g cm}^{-3})$	f^{OH}_{free}	$\rho/(\text{g cm}^{-3})$	f^{OH}_{free}	$\rho/(\text{g cm}^{-3})$	f^{OH}_{free}
300.00			7.400×10^{-6}	0.998	2.600×10^{-5}	0.997	2.599×10^{-5}	0.998
314.14			1.480×10^{-5}	0.997	5.417×10^{-5}	0.996	5.423×10^{-5}	0.997
348.85			8.990×10^{-5}	0.993	2.483×10^{-4}	0.990	2.485×10^{-4}	0.992
350.00			8.800×10^{-5}	0.994	2.597×10^{-4}	0.989	2.598×10^{-4}	0.992
370.00	1.891×10^{-4}	0.995	4.660×10^{-4}	0.984	5.382×10^{-4}	0.984	5.373×10^{-4}	0.988
388.70			5.620×10^{-4}	0.983	9.882×10^{-4}	0.978	9.841×10^{-4}	0.982
390.00	3.966×10^{-4}	0.988			1.028×10^{-3}	0.978	1.024×10^{-3}	0.982
400.00					1.385×10^{-3}	0.974	1.377×10^{-3}	0.979
410.00	7.590×10^{-4}	0.985	1.000×10^{-3}	0.976	1.837×10^{-3}	0.970	1.823×10^{-3}	0.975
416.67					2.200×10^{-3}	0.967	2.181×10^{-3}	0.973
430.00	1.379×10^{-3}	0.977	2.710×10^{-3}	0.961	3.102×10^{-3}	0.960	3.066×10^{-3}	0.967
450.00	2.342×10^{-3}	0.972	3.390×10^{-3}	0.948	4.997×10^{-3}	0.949	4.917×10^{-3}	0.958
450.00					4.997×10^{-3}	0.949	4.917×10^{-3}	0.958
470.00	3.850×10^{-3}	0.961	5.060×10^{-3}	0.946	7.738×10^{-3}	0.936	7.576×10^{-3}	0.947
476.76					8.901×10^{-3}	0.932	8.699×10^{-3}	0.943
490.00	6.090×10^{-3}	0.949	8.160×10^{-3}	0.929	1.159×10^{-2}	0.922	1.129×10^{-2}	0.935
500.00					1.404×10^{-2}	0.915	1.363×10^{-2}	0.928
510.00	9.350×10^{-3}	0.938			1.689×10^{-2}	0.907	1.635×10^{-2}	0.921
530.00	1.415×10^{-2}	0.922	2.240×10^{-2}	0.890	2.406×10^{-2}	0.890	2.314×10^{-2}	0.906
550.00	2.130×10^{-2}	0.902			3.364×10^{-2}	0.871	3.213×10^{-2}	0.890
570.00	3.160×10^{-2}	0.884			4.639×10^{-2}	0.851	4.399×10^{-2}	0.872
590.00	4.630×10^{-2}	0.863			6.339×10^{-2}	0.828	5.964×10^{-2}	0.852
600.00	5.930×10^{-2}	0.836			7.400×10^{-2}	0.816	6.932×10^{-2}	0.841
610.00	7.440×10^{-2}	0.821			8.642×10^{-2}	0.802	8.055×10^{-2}	0.829
620.00	1.030×10^{-1}	0.784			1.011×10^{-1}	0.787	9.368×10^{-2}	0.816

Table 5. Optimal SAFT-VR Mie model parameters for methanol, ammonia, and hydrogen sulphide obtained using the SAFT-VR Mie EOS [111] with our novel generic Mie (Equation (30)) association kernel.

Compound	m	$\sigma/\text{Å}$	λ_r	λ_a	$(\varepsilon/k_B)/\text{K}$	$(\varepsilon_{ab}^{HB}/k_B)/\text{K}$	$K_{ab}/\text{Å}^3$
CH_3OH	1.7989	3.1425	16.968	6.0	276.92	2156.0	222.18
NH_3	1.0	3.3309	36.832	6.0	323.70	1105.0	560.73
H_2S	1.0	3.7820	31.311	6.0	243.28	585.72	1880.4

fields and the predictions with our novel SAFT-VR Mie models are in remarkable agreement, and that the values from neither approach are consistent with those reported by Luck. The issue about possible inconsistencies in the values for the degree of association in water, methanol, and ethanol estimated by Luck from IR spectroscopic data has been raised before [186,189,191]. We reiterate that the neutron scattering data of Soper and Phillips [202], though only available for limited thermodynamic conditions, is consistent with the corresponding values predicted theoretically with the SAFT-VR Mie models of water and by simulation with the SPC/E and TIP4P/2005 models, but is not in line with the IR data of Luck.

The basic features of the degree of association are qualitatively similar, with a very high fraction of free OH hydrogen bonds in the vapour phase and a much lower one in the liquid phase increasing rapidly up to the critical point. The fraction of monomers at the critical point is, however, quite different where the spectroscopic data of Luck suggest $f_{\text{free}}^{OH} > 0.8$, while the simulation data and SAFT-VR Mie models are consistent with a lower value of ~ 0.6. The discrepancy between the extent of association obtained here with the SAFT-VR Mie models and simulation data, on one hand, and the spectroscopic data of Luck, on the other, echoes the conclusions of Liang *et al.* [191], who used water + alkane liquid-liquid equilibrium (LLE) data to discriminate between parameter sets for the PC-SAFT EOS and found that models developed to provide a good description of the LLE phase envelope lead to an overestimate of the degree of association. The optimal models obtained by Liang *et al.* [191] result in a very similar degree of association to that predicted with our SAFT-VR Mie models. Though it is generally inadvisable to contradict the evidence of experimental findings, the striking similarity of the description obtained using two different techniques (a rigorous perturbation theory for associating fluids and molecular simulation for well-established atomistic force fields) with very different approaches for the characterisation of the degree of association (the treatment of association in the SAFT-VR Mie EOS is based on the Wertheim TPT1 statistical mechanical formalism, while structural/geometric information is employed in the molecular simulation), coupled with the non-trivial nature of the experimental analysis of the spectroscopic data, leads one to question whether the estimates of Luck are an accurate quantification of the degree HB in water.

5.2. Other associating compounds: methanol, ammonia, and hydrogen sulphide

Having assessed our novel methodology for the treatment of association with the SAFT-VR Mie EOS using the association kernel based on the generic Mie RDF, Equation (30), in the specific case of water as a prototypical associating fluid, we now turn our attention to other associating fluids: methanol (CH_3OH), ammonia (NH_3), and hydrogen sulphide (H_2S). Methanol is modelled as a dimer of chain length $m = 1.7989$ with three association sites (two sites of type 'e' representing the lone pairs of electrons on the oxygen atom and a site of type 'H' to represent the hydrogen atom); ammonia is modelled as a spherical core corresponding to $m = 1$ with four association sites, three of type 'H' and one of type 'e'; and hydrogen sulphide is described with the same scheme as water, a spherical core with $m = 1$ and four association sites, two of type 'H' and two of type 'e'; in each case, only 'e–H' bonding is allowed.

The SAFT-VR Mie intermolecular parameters developed for these three associating molecules are reported in Table 5, with the corresponding vapour-liquid equilibria and thermodynamic properties represented in Figures 17–22. The SAFT-VR Mie EOS [111] is employed with the newly developed association kernel based on the generic Mie RDF, Equation (30) to describe the associating compounds in this instance. The SAFT-VR Mie model of methanol provides an excellent description of the VLE, although, as expected for any treatment with a classical

Table 6. Intermolecular potential parameters for the model LJ (12-6) binary mixture of components 1 and 2, with thermodynamic states corresponding to the van der Waals one-fluid (vdW1) and two-fluid (vdW2) mixing rules under consideration at $T = 400$ K and $\rho = 1.0$ Å^3. The corresponding reduced temperature and density are defined as $T_{\text{vdW1},x}^* = k_B T/\varepsilon_{\text{vdW1},x}$ and $\rho_{\text{vdW1},x}^* = \rho\sigma_{\text{vdW1},x}^3$ for the vdW1 recipe; and $T_{\text{vdW2},ij}^* = k_B T/\varepsilon_{ij}$ and $\rho_{\text{vdW2},ij}^* = \rho\sigma_{ij}^3$ for the vdW2 recipe.

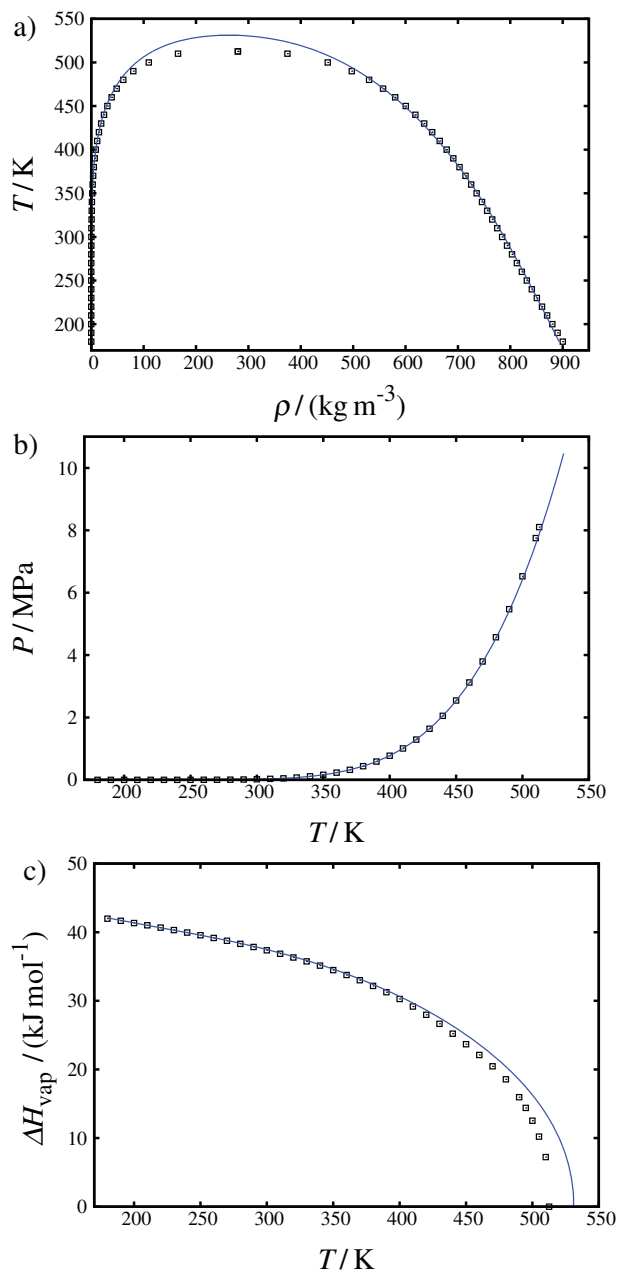| i-j	$\sigma_{ij}/\text{Å}$	$(\varepsilon_{ij}/k_B)/\text{K}$	$T_{\text{vdW2},ij}^*$	$\rho_{\text{vdW2},ij}^*$
1–1	0.928	160	2.50	0.800
2–2	0.843	250	1.60	0.600
1–2	0.886	200	2.00	0.695
	$\sigma_{\text{vdW1},x}/\text{Å}$	$(\varepsilon_{\text{vdW1},x}/k_B)/\text{K}$	$T_{\text{vdW1},x}^*$	$\rho_{\text{vdW1},x}^*$
	0.897	189	2.12	0.723

Figure 17.   (a) The saturated vapour and liquid densities, (b) the vapour pressure, and (c) the enthalpy of vaporisation of methanol: the symbols represent smoothed experimental data from NIST [172]; the curves represent the description obtained with the SAFT-VR Mie EOS [111] for the SAFT-VR Mie model of Table 5 using the newly developed association kernel based on the generic Mie RDF, Equation (30).

Figure 18.   Single-phase isobaric properties of methanol, including (a) the density, (b) the Joule–Thomson coefficient, and (c) the isobaric heat capacity, at pressures of $P = 1$ (blue curves and pluses), 2 (red curves and crosses), 5 (green curves and asterisks), 10 (black curves and squares), and 20 (purple curves and circles) MPa: the symbols represent smoothed experimental data from NIST [172]; the curves represent the description obtained with the SAFT-VR Mie EOS [111] for the SAFT-VR Mie model of Table 5 using the newly developed association kernel based on the generic Mie RDF, Equation (30) (colour online).

EOS, there is again a slight overshoot of the critical point (corresponding to ~4% in temperature). The description of the VLE of ammonia is also of high quality, as shown in Figure 19; the overshoot of the critical temperature is very small (2 K, or 0.5%), and there is a small consistent underestimate in the enthalpy of vaporisation of ~1 kJ mol^{-1}

from the experimental values. The single-phase density and isobaric heat capacity of ammonia are well described with the SAFT-VR Mie EOS, while the representation of the Joule–Thomson coefficient is less accurate (see Figure 20).
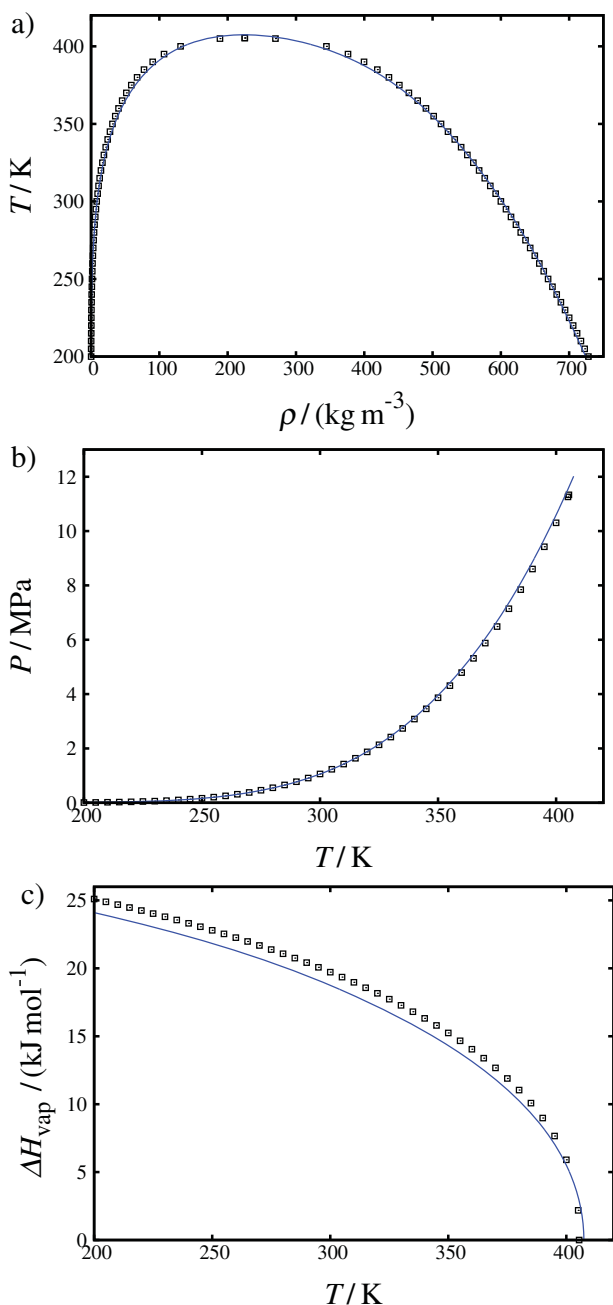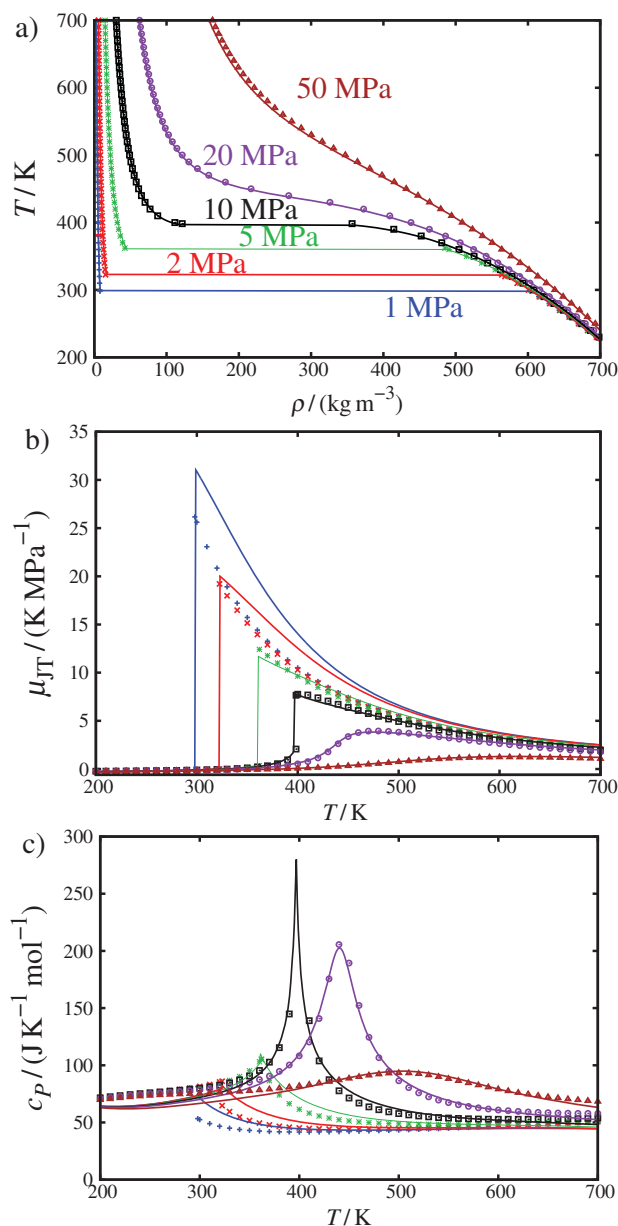
Figure 19. (a) The saturated vapour and liquid densities, (b) the vapour pressure, and (c) the enthalpy of vaporisation of ammonia: the symbols represent smoothed experimental data from NIST [172]; and the curves represent the description obtained with the SAFT-VR Mie EOS [111] for the SAFT-VR Mie model of Table 5 using the newly developed association kernel based on the generic Mie RDF, Equation (30).

Figure 20. Single-phase isobaric properties of ammonia, including (a) the density, (b) the Joule–Thomson coefficient, and (c) the isobaric heat capacity, at pressures of $P = 1$ (blue curves and pluses), 2 (red curves and crosses), 5 (green curves and asterisks), 10 (black curves and squares), 20 (purple curves and circles), and 50 (brown curves and triangles) MPa: the symbols represent smoothed experimental data from NIST [172]; the curves represent the description obtained with the SAFT-VR Mie EOS [111] for the SAFT-VR Mie model of Table 5 using the newly developed association kernel based on the generic Mie RDF, Equation (30) (colour online).

The SAFT-VR Mie model of hydrogen sulphide provides a description of the VLE which is quite similar to that obtained for ammonia, with a good representation of the experimental data, a very small overshoot of the critical point, and a slight underestimate of the enthalpy of vapor-

isation. In Figure 21 we also include, for comparison, the description obtained with a non-associating model of hydrogen sulphide. (A non-associating model is physically reasonable for H_2S as this is a weakly HB substance, while a non-associating model of water or ammonia would be
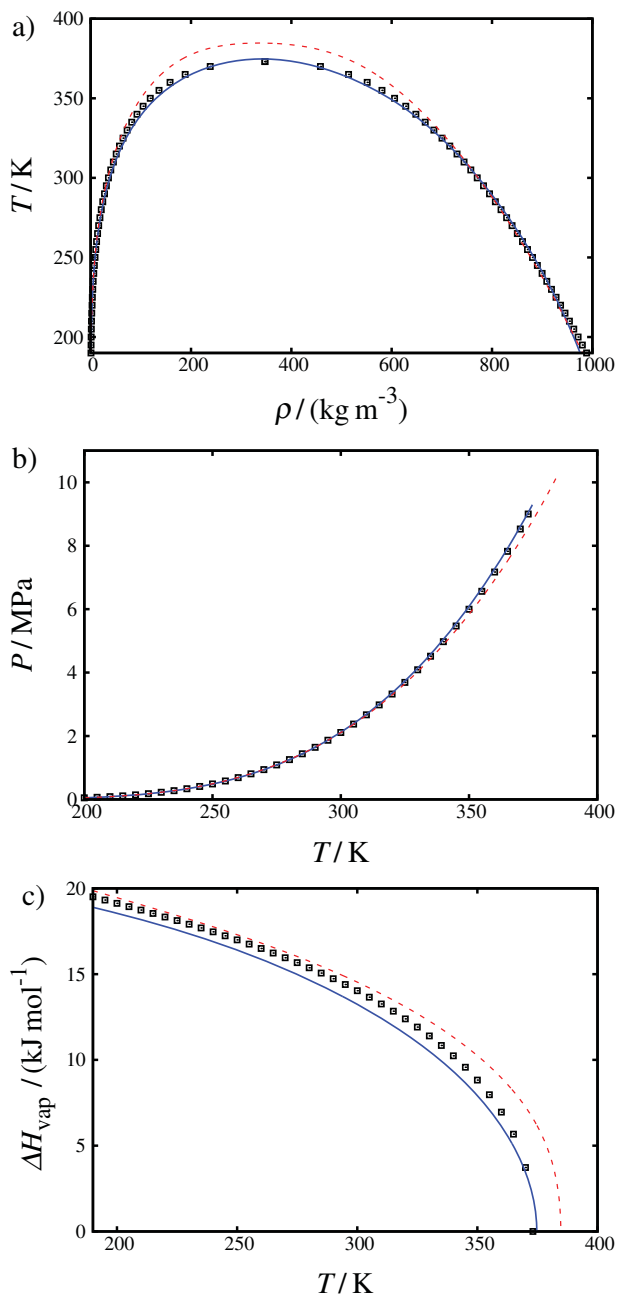
Figure 21. (a) The saturated vapour and liquid densities, (b) the vapour pressure, and (c) the enthalpy of vaporisation of hydrogen sulphide: the symbols represent smoothed experimental data from NIST [172]; the blue continuous curves represent the description obtained with the SAFT-VR Mie EOS [111] for the SAFT-VR Mie model of Table 5 using the newly developed association kernel based on the generic Mie RDF, Equation (30), and the red dashed curve the corresponding description with an non-associating model (colour online).
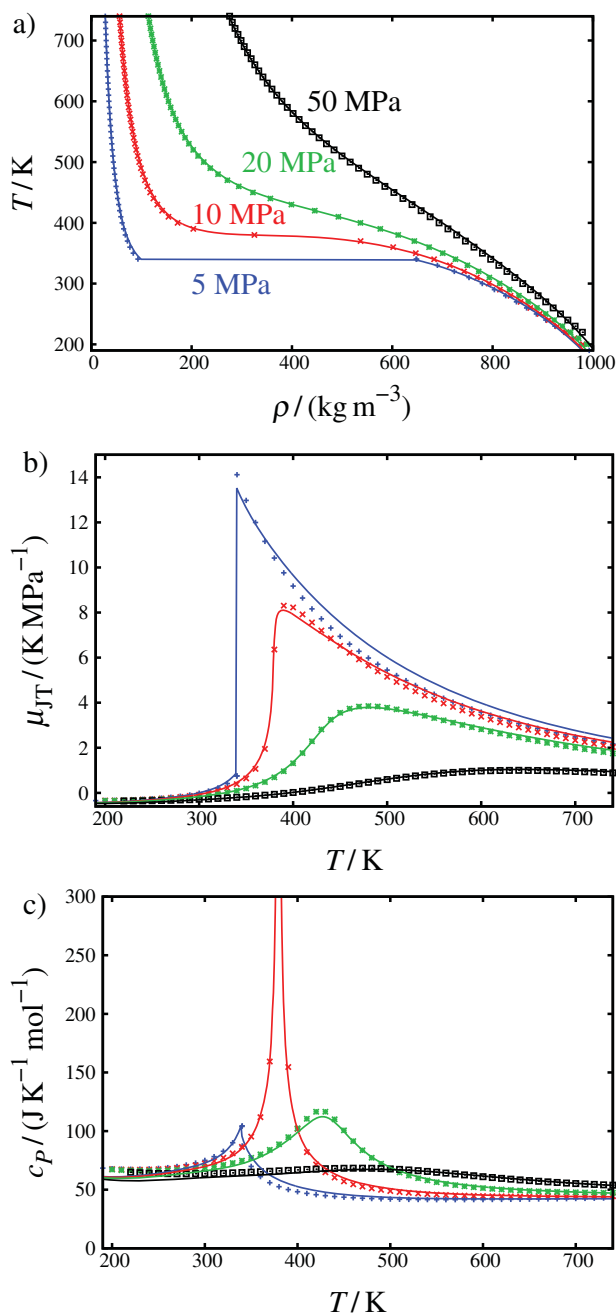

Figure 22. Single-phase isobaric properties of hydrogen sulphide, including (a) the density, (b) the Joule–Thomson coefficient, and (c) the isobaric heat capacity, at pressures of $P = 5$ (blue curves and pluses), 10 (red curves and crosses), 20 (green curves and asterisks), and 50 (black curves and squares) MPa: the symbols represent smoothed experimental data from NIST [172]; and the curves represent the description obtained with the SAFT-VR Mie EOS [111] for the SAFT-VR Mie model of Table 5 using the newly developed association kernel based on the generic Mie RDF, Equation (30) (colour online).

inappropriate.) The associating SAFT-VR Mie model of hydrogen sulphide performs better for the VLE, providing a better description of the vapour pressure and a smaller overshoot of the critical point; as can be seen in Figure 22, the associating model of H_2S also offers a very good repre-

sentation of the single-phase densities and derivative properties, with an accuracy similar to that obtained with the SAFT-VR Mie EOS for non-associating fluids.

6. Application to mixtures of associating Mie fluids: SAFT-VR Mie

A key goal of our research is the representation of the fluid-phase equilibria of mixtures. A reliable description of the thermodynamic properties of mixtures of associating molecules is therefore a prerequisite. The first task at hand is to extend the treatment of the association contribution to the Helmholtz free energy, which we formulated for pure fluids in Section 4.3, to mixtures. This involves the development of an appropriate mixing rule for the association term of the mixture (characterised by the association strength) and combining rules for the parameters that define the corresponding association interactions between the different molecular species. In the case of a mixture of associating fluids, the association strength Δ_{abij} between SW sites a and b on components i and j can be expressed as a simple generalisation of Equation (33) for the pure component:

$$\Delta_{abij} = F_{abij} \, K_{abij} \, I_{ij}, \tag{38}$$

where the corresponding Mayer function of the site-site SW association is

$$F_{abij} = \exp\left[\varepsilon_{abij}^{\mathrm{HB}}/(k_{\mathrm{B}}T)\right] - 1, \tag{39}$$

K_{abij} is the empirical bonding volume parameter, and I_{ij} is the generalisation of the association kernel which can be determined using expressions based on either the generic Mie form (Equation (30)) or the LJ (Equation (32)) form. As the association kernel is based on an integral over the RDF of the reference fluid (cf. Equation (8)), a mixing rule that best describes the RDF $g_{ij}^{\mathrm{Mie}}(r_{ij})$ between the i and j components of mixtures of Mie particles is also expected to provide the most appropriate representation of the association strength Δ_{abij} described with the association kernels I_{ij}.

6.1. Mixing rules for the association contribution

We first compare the van der Waals one-fluid (vdW1) and two-fluid (vdW2) mixing rules by describing the RDF between the various species of the mixture with that of an equivalent pure-component system; for more information on the use of van der Waals mixing rules to describe mixtures, we direct the reader to the books of Lee [146], and of Rowlinson and Swinton [203].

In order to assess the adequacy of the mixing rules for the structure of a mixture of LJ (12-6) particles, we perform MD simulations [196], comparing the resulting RDFs to those obtained using the RHNC integral-equation theory with the different mixing rules. The MD simulation consists of a binary mixture of $N_1 = 5000$ particles of type 1 and $N_2 = 3000$ of type 2, in a $V = 8000$ Å^3 cubic box at $T = 400$ K; the specific values of the intermolecular param-

eters defining the LJ particles are given in Table 6, together with a characterisation of the thermodynamic states, chosen such that the mixture is supercritical and thereby will not phase separate at these conditions.

The composition-dependent van der Waals one-fluid parameters $\sigma_{\mathrm{vdW1},x}$ and $\varepsilon_{\mathrm{vdW1},x}$ for the effective single-component system are defined as

$$\sigma_{\mathrm{vdW1},x}^3 = \sum_i \sum_j x_i x_j \sigma_{ij}^3 \tag{40}$$

and

$$\varepsilon_{\mathrm{vdW1},x} = \frac{\sum_i \sum_j x_i x_j \sigma_{ij}^3 \varepsilon_{ij}}{\sigma_{\mathrm{vdW1}}^3}, \tag{41}$$

where $x_i = N_i/N$ is the mole fraction of component i. A detailed discussion of the treatment of the unlike size σ_{ij} and energy ε_{ij} parameters is made in Section 6.2.

For the particular binary mixture being considered (with a mole fraction of $x_1 = 5000/8000 = 0.625$ and $x_2 = 3000/8000 = 0.375$), the effective one-fluid particle diameter is obtained as $\sigma_{\mathrm{vdW1},x} = 0.897$ Å, and the well depth as $\varepsilon_{\mathrm{vdW1},x}/k_{\mathrm{B}} = 189$ K, corresponding to an effective dimensionless number density of $\rho_{\mathrm{vdW1},x}^* = \rho\sigma_{\mathrm{vdW1},x}^3 = 0.723$ and temperature of $T_{\mathrm{vdW1},x}^* = k_{\mathrm{B}}T/\varepsilon_{\mathrm{vdW1},x} = 2.12$. In the case of the van der Waals two-fluid mixing rule, the dimensionless number density and temperature are defined directly in terms of the individual pair parameters as $\rho_{\mathrm{vdW2},ij}^* = \rho\sigma_{ij}^3$ and $T_{\mathrm{vdW2},ij}^* = k_{\mathrm{B}}T/\varepsilon_{ij}$, respectively.

An analysis of the structure of the binary mixture is made by comparing the like 1–1 and 2–2 RDFs, $g_{11}(r_{11})$ and $g_{22}(r_{22})$, obtained by molecular simulation with the corresponding functions obtained with the RHNC integral-equation theory using the reduced variables defined with the different van der Waals mixing rules. It is apparent from Figure 23 that the description obtained for both $g_{11}(r_{11})$ and $g_{22}(r_{22})$ using a combination of the one-fluid mixing rule for the size parameter $\sigma_{\mathrm{vdW1},x}$ and the two-fluid rule for the energetic parameter $\varepsilon_{\mathrm{vdW2},ij}$ is superior to that provided by using one-fluid mixing rules for both $\sigma_{\mathrm{vdW1},x}$ and $\varepsilon_{\mathrm{vdW1},x}$, or by using two-fluid mixing rules for both $\sigma_{\mathrm{vdW2},ij}$ and $\varepsilon_{\mathrm{vdW2},ij}$, or by using the two-fluid mixing rule for $\sigma_{\mathrm{vdW2},ij}$ and the one-fluid rule for $\varepsilon_{\mathrm{vdW1},x}$. We therefore opt for the combined one-fluid/two-fluid mixing rules for the size/energy parameters to represent the thermodynamic properties of the associating mixtures. It is important to note at this stage that the combined use of a one-fluid description of size parameters and a two-fluid description of the energy parameters is consistent with the treatment employed for the first- and second-order perturbation contributions at the core of the SAFT-VR Mie [111] and SAFT-γ [77] EOSs.

In summary, the appropriate dimensionless temperature and density which enter the association kernels $I_{ij}(T^*, \rho^*, \lambda_{r,ij})$ (Equation (30)) and $I_{ij}(T^*, \rho^*)$ (Equation
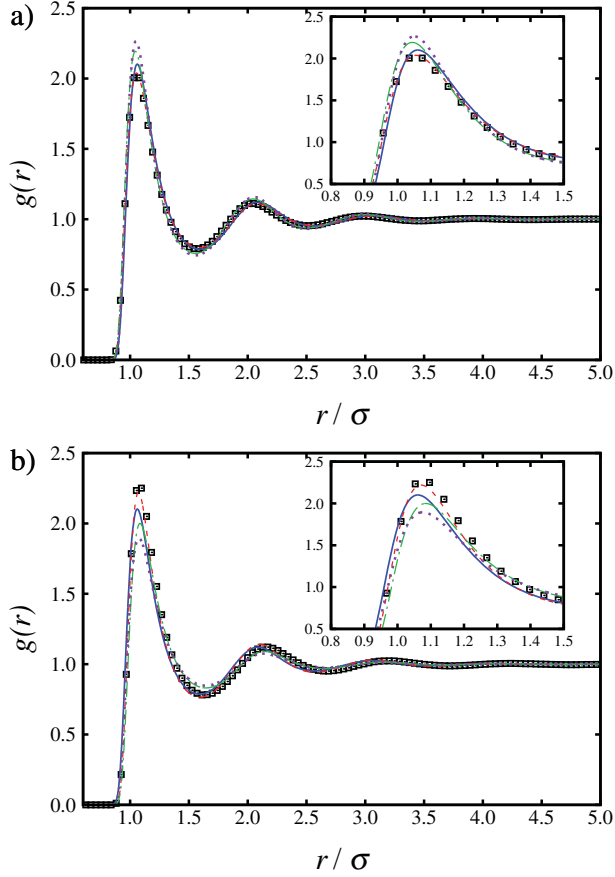
Figure 23. Comparison of the pair RDFs of a binary mixture of LJ species 1 and 2 (characterised by the parameters given in Table 6) for a composition of $x_1 = 0.625$ obtained from MD simulations at a temperature of $T = 400$ K (symbols) with the corresponding RDFs from the RHNC integral-equation theory (curves). (a) $g_{11}(r_{11})$ and (b) $g_{22}(r_{22})$ determined from the RHNC theory with the various mixing rules: the blue continuous curves corresponds to $g(r; T^*_{\text{vdW1},x}, \rho^*_{\text{vdW1},x})$; the red dashed curves to $g(r; T^*_{\text{vdW2},ij}, \rho^*_{\text{vdW1},x})$; the purple dotted curves to $g(r; T^*_{\text{vdW1},x}, \rho^*_{\text{vdW2},ij})$; and the green dot-dashed curves to $g(r; T^*_{\text{vdW2},ij}, \rho^*_{\text{vdW2},ij})$ (colour online).

(32)) are

$$T^* = T^*_{\text{vdW2},ij} = k_B T / \varepsilon_{ij} , \qquad (42)$$

and

$$\rho^* = \rho^*_{\text{vdW1},x} = \rho \sigma^3_{\text{vdW1},x} . \qquad (43)$$

If one employs the association kernel developed for the generic Mie associating fluid, the exponent characterising the unlike repulsive interactions between the Mie cores also has to be specified explicitly to evaluate $I_{ij}(T^*, \rho^*, \lambda_{r, ij})$.

6.2. Combining rules for the unlike parameters

It is common practice to employ combining rules for the unlike intermolecular potential parameters for use within EOSs to simplify the representation of multicomponent mixtures. A general discussion can be found in reference [203]; for a particular application to mixtures of components with interactions of the SW or Mie forms, see references [110,111].

The unlike size parameters are invariably obtained from a simple arithmetic mean (Lorentz combining rule) as

$$\sigma_{ij} = \frac{\sigma_{ii} + \sigma_{jj}}{2} . \qquad (44)$$

This formulation corresponds to the conventional additive treatment of the particle diameters.

In the case of molecules represented with the Mie potential, the values of the repulsive $\lambda_{r, ij}$ and attractive $\lambda_{a, ij}$ exponents for the i–j unlike interaction have to be specified; a geometric criterion (Berthelot-like combining rule) for the van der Waals attractive constants of the Mie potential can be used to express the exponents as [111]

$$\lambda_{k,ij} = 3 + \sqrt{(\lambda_{k,ii} - 3)(\lambda_{k,jj} - 3)}, \quad k = a, r, \qquad (45)$$

though a London-dispersion form is commonly chosen for the attractive exponents, whereby $\lambda_{a, ij} = \lambda_{a, ii} = \lambda_{a, jj} = 6$. It should also be noted that occasionally it may be fruitful to refine the value of the unlike repulsive $\lambda_{r, ij}$ exponents between the different species to improve the treatment of challenging mixtures where the fluid-phase behaviour is very sensitive to the precise form of the potential. In this case, the repulsive exponent can be estimated directly from experimental data of the mixture.

The unlike attractive dispersive energy parameters ε_{ij} can be characterised with an expression of the Berthelot geometric-mean form:

$$\varepsilon_{ij} = \frac{\sqrt{\sigma^3_{ii} \sigma^3_{jj}}}{\sigma^3_{ij}} \sqrt{\varepsilon_{ii} \varepsilon_{jj}} . \qquad (46)$$

For non-ideal mixtures, however, one often finds that the energetic interactions between unlike species exhibit large deviations from the Berthelot-like combining rule. In order to improve the description of the fluid-phase behaviour of the mixture, a binary correction parameter k_{ij} can be introduced as

$$\varepsilon_{ij} = (1 - k_{ij}) \frac{\sqrt{\sigma^3_{ii} \sigma^3_{jj}}}{\sigma^3_{ij}} \sqrt{\varepsilon_{ii} \varepsilon_{jj}}, \qquad (47)$$

where k_{ij} for each binary interaction is estimated from the data of the appropriate mixture. In essence, one is determining the unlike energetic interaction of the mixture independently from the like interactions which are estimated from pure-component data.

In the case of mixtures of associating molecules treated within the Wertheim TPT1 approach, one has to specify

the unlike energetic and bonding-volume parameters for the various site-site interactions. The association-energy parameters for the SW interactions of sites a on component i and sites b on component j can be expressed in terms of the corresponding Berthelot combining rule as

$$\varepsilon_{abij}^{\mathrm{HB}} = \sqrt{\varepsilon_{aaii}^{\mathrm{HB}} \varepsilon_{bbjj}^{\mathrm{HB}}} . \tag{48}$$

As for the unlike dispersive energies, deviations from the geometric mean can be found for the association interactions, and in this case these can be estimated from experimental data for the corresponding mixture of associating molecules.

The unlike site-site bonding-volume parameters have to be determined in order to complete the specification of the unlike interactions for associating mixtures. A simple arithmetic-mean rule can be employed for size parameters of this type. In the case of the bonding volumes between sites a on component i and sites b on component j, one can average the cube root of the corresponding values for the like interactions:

$$K_{abij} = \left(\frac{3\sqrt{K_{abii}} + 3\sqrt{K_{abjj}}}{2} \right)^3 . \tag{49}$$

In certain cases, however, it is also necessary to refine the K_{abij} bonding-volume parameters between different associating species to improve the description of the thermodynamic properties and phase behaviour of the associating mixture.

In the final part of our paper, the combining rules developed here are used to describe the fluid-phase equilibria of mixtures of real associating fluids with the SAFT-VR Mie EOS [111] using our novel association kernel, Equation (38). The choice of combining rule and any required unlike deviation parameter will be specified where appropriate.

7. Representing the thermodynamic properties of mixtures of real associating fluids

7.1. *Binary aqueous mixtures of methanol, methane, carbon dioxide, or hydrogen sulphide*

Once the mixing and combining rules have been specified, the SAFT-VR Mie EOS can be used to represent the fluid-phase equilibria of mixtures of real associating molecules. Binary mixtures of the compounds represented with the association models developed in Sections 5.1 and 5.2 are assessed using the association contribution with the newly developed kernel $I_{ij}(T^*, \rho^*, \lambda_{r,ij})$ based on the generic Mie RDF, Equation (30), with the mixing rules for the dimensionless temperature and density defined in Equations (42) and (43), respectively. Aqueous mixtures comprising non-associating components such as methane and carbon diox-
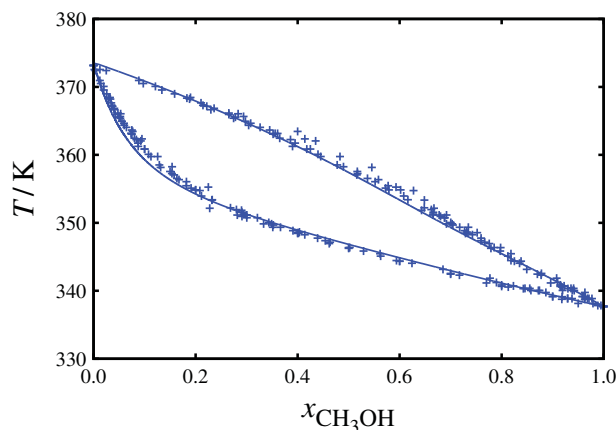

Figure 24. Isobaric temperature-mole fraction representation of the vapour-liquid equilibria of the water + methanol binary mixture at $P = 1$ atm: the symbols represent the experimental data [205–210], and the curves the description obtained using the SAFT-VR Mie EOS with our novel treatment of the association contribution based on the generic Mie kernel, Equation (30).

ide are also considered in view of their key relevance to natural gas reservoirs and significant topical interest.

We start with an examination of the water + methanol binary mixture, as it is one of the few examples of aqueous mixtures that exhibit a near-ideal type I vapour-liquid phase behaviour with a continuous critical locus, according to the classification of van Konynenburg and Scott [203,204]. An isobaric slice of the temperature-composition VLE of this mixture at $P = 1$ atm calculated with the SAFT-VR Mie EOS is shown in Figure 24. The model adopted for water is that from Table 3 (with the generic Mie association contribution), and that for methanol is specified in Table 5. In this case, only a small deviation from the geometric-mean combining rule for the unlike dispersive energy is required, corresponding to a binary parameter of $k_{ij} = 0.04$ in Equation (47), to provide good agreement with the experimental data [205–210] for the vapour-liquid envelope; the 'standard' combining rules defined in Section 6.2 are employed for all other unlike interaction parameters.

More challenging non-ideal binary mixtures comprising water as a component exhibit type III fluid-phase behaviour, according to the van Konynenburg and Scott [204] classification; these systems are characterised by large regions of vapour-liquid and liquid-liquid fluid-phase equilibria with a discontinuous vapour-liquid critical locus. Typical examples of type III behaviour include binary mixtures of: water + methane; water + hydrogen sulphide; and water + carbon dioxide. The pure-component model parameters for methane and carbon dioxide are developed in reference [171], and are reproduced in Table 7 for completeness.

It has been demonstrated [211] that for the extreme phase separation exhibited by such systems, a single binary

Table 7. Optimal SAFT-VR Mie model parameters for methane and carbon dioxide obtained using the SAFT-VR Mie EOS.

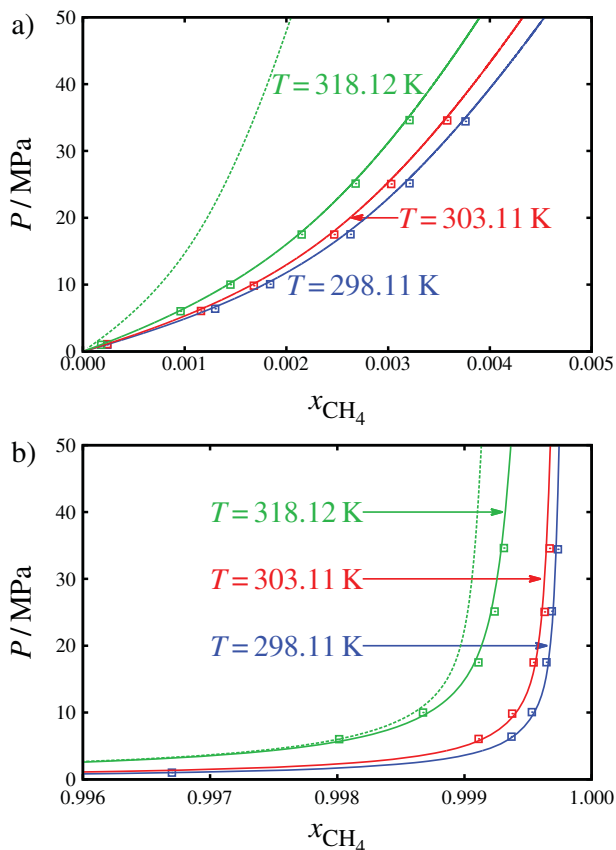| Compound	m	$\sigma/\text{Å}$	λ_r	λ_a	$(\varepsilon/k_B)/\text{ K}$
CH_4	1.0	3.7366	12.319	6.000	151.45
CO_2	1.6936	3.0465	18.067	6.000	235.73

a)

b)

Figure 25. Isothermal pressure-mole fraction representation of the vapour-liquid equilibria of the water + methane binary mixture at $T = 298.11$, 303.11, and 318.12 K: (a) water-rich phase; (b) methane-rich phase. The symbols represent the experimental data [212], and the curves represent the description obtained using the SAFT-VR Mie EOS with our novel treatment of the association contribution based on the generic Mie kernel, Equation (30), and the binary interaction parameters k_{ij} given in Table 8; the dashed green curves represent the results obtained for the $T = 318.12$ K isotherm with $k_{ij} = 0$ (colour online).

interaction parameter k_{ij} cannot be used to describe both phases adequately. Accordingly, we estimate separate k_{ij} values to describe the unlike interactions for each phase.

For the water + methane system, the SAFT-VR Mie models characterised by the parameters in Tables 3 (the generic Mie association model), 7, and 8 provide a good description of the experimental data [212] for the fluid-phase equilibria, as can be seen in Figure 25. While judging the physical relevance of a binary parameter is not easy, requiring a detailed analysis to obtain a theoretically sound esti-

Table 8. Binary interaction parameters k_{ij} for the unlike dispersive energy, Equation (47), of the water + methane binary mixture.

	k_{ij}		
Phase	298.11 K	303.11 K	318.12 K
H_2O rich	−0.083	−0.069	−0.053
CH_4 rich	0.080	0.080	0.080

Table 9. Binary interaction parameters k_{ij} for the unlike dispersive energy, Equation (47), of the water + carbon dioxide binary mixture; the unlike repulsive exponent is set to $\lambda_{r,ij} = 13$ in all cases.

	k_{ij}		
Phase	323.2 K	348 K	373.2 K
H_2O rich	−0.594	−0.554	−0.530
CO_2 rich	−0.454	−0.443	−0.445

Table 10. Binary interaction parameters k_{ij} for the unlike dispersive energy, Equation (47), and the unlike associative energy ε_{abij}^{HB} and the unlike bonding volume K_{abij} of the water + hydrogen sulphide binary mixture.

Phase	k_{ij}	$(\varepsilon_{abij}^{HB}/k_B)/\text{ K}$	$K_{abij}/\text{Å}^3$
H_2O rich	−0.004	1080.0	870.00
H_2S rich	0.219		

mate [211], it is clear from the values reported in Table 8 that the optimal k_{ij} for the methane-rich phase is small and positive, with no discernible temperature dependence, while that for the water-rich phase is small, negative, and is evidently sensitive to temperature. (We note in passing that a temperature dependence is also to be expected for the methane-rich phase [211]; that one is not seen is probably due to the relatively narrow range of temperatures considered here.) Although the magnitudes of k_{ij} are found be relatively small, the impact on the fluid-phase behaviour is significant, especially in the aqueous phase, as can be seen from the dashed curves in Figure 25, which represent the results obtained for $T = 318.12$ K for the Berthelot-like geometric combining rule, corresponding to $k_{ij} = 0$.

In the case of the water + carbon dioxide binary mixture, we refine the unlike repulsive exponent $\lambda_{r,ij}$ to improve the quality of the representation of the fluid-phase behaviour, as this is a crucial mixture of interest. The optimal description is obtained by using a value of $\lambda_{r,ij} = 13$, which is used for both phases at all temperatures to keep the number of adjustable parameters at a tractable level. The estimated values of the binary energetic parameters k_{ij} given in Table 9 are found to be negative, quite large, and temperature-dependent for both phases. A good description of the experimental fluid-phase equilibrium data
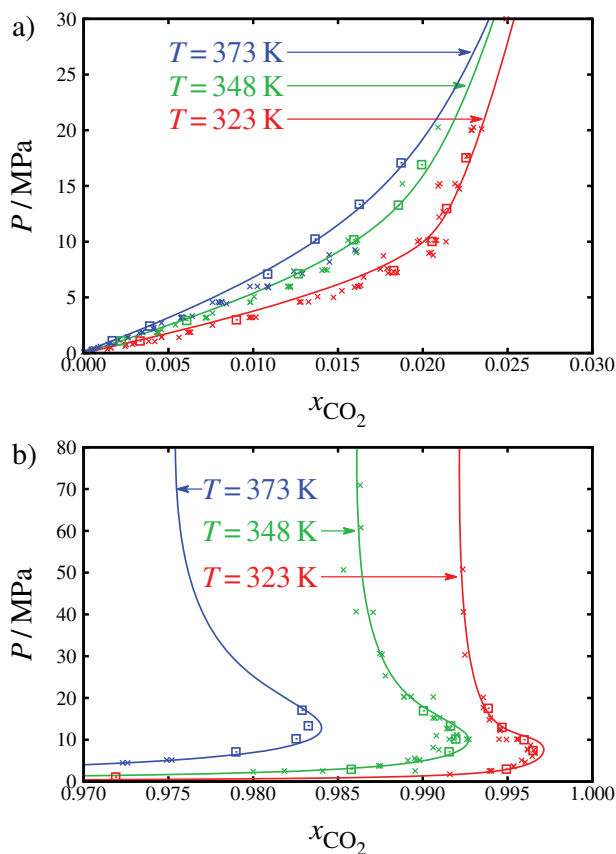
Figure 26. Isothermal pressure-mole fraction representation of the vapour-liquid equilibria of the water + carbon dioxide binary mixture at $T = 323$, 348, and 373 K: (a) water-rich phase, (b) carbon dioxide rich phase. The symbols represent the experimental data [213–221], and the curves represent the description obtained using the SAFT-VR Mie EOS with our novel treatment of the association contribution based on the generic Mie kernel, Equation (30), and the binary interaction parameters k_{ij} given in Table 9.
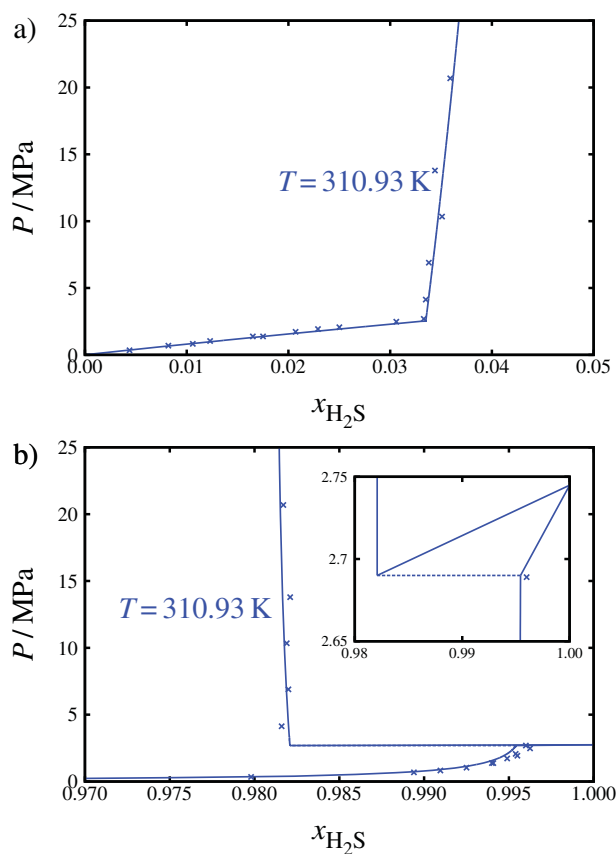
Figure 27. Isothermal pressure-mole fraction representation of the fluid-phase equilibria of the water + hydrogen sulphide system: (a) water-rich phase, (b) hydrogen sulphide-rich phase. The symbols represent experimental data [220,222], and curves represent the SAFT-VR Mie description with our novel treatment of the association contribution based on the generic Mie kernel, Equation (30), and the binary interaction parameters k_{ij} given in Table 10; the region around the three-phase line is enlarged in the inset.

[213–221] is obtained with the SAFT-VR Mie EOS using these intermolecular potential models: as can be seen from Figure 26, the maximum in the solubility of water in the carbon dioxide rich phase can be accurately reproduced.

Hydrogen sulphide is an associating fluid which exhibits a strong non-ideality when mixed with water. This leads to deviations for the standard combining rules, and as a consequence, there are more mixture parameters to estimate. We choose to estimate the value of k_{ij} for the deviation of the unlike dispersive energy along with the unlike associative energy ε_{abij}^{HB} and bonding-volume K_{abij} parameters. The optimal values of the parameters estimated from a comparison of the description obtained using the SAFT-VR Mie EOS with the experimental fluid-phase equilibrium data [220,222] are reported in Table 10. This SAFT-VR Mie model provides a good description of both the vapour-liquid and liquid-liquid equilibria exhibited by this mixture, as can be seen in Figure 27.

The overall description of mixtures of associating fluids with the SAFT-VR Mie EOS is found to be very satisfying, and our novel generic association contribution and the corresponding mixing rules are seen to be appropriate for the accurate representation of the fluid-phase equilibria of these systems.

8. Conclusions

In this paper, we have provided a detailed assessment of the implementation of the Wertheim first-order perturbation theory of associating fluids for reference interactions based on the Mie (generalised LJ) potential. A central goal of our work has been the implementation of an accurate, yet algebraic, Wertheim TPT1 treatment of the association contribution to the Helmholtz free energy within the latest version of the statistical associating fluid theory for Mie potentials of variable repulsive/attractive range (SAFT-VR Mie) [111]. We have shown that a proper description of the

RDF of the reference fluid is a prerequisite for the faithful treatment of the effect of the association interactions on the thermodynamic properties of the associating fluid. A high-fidelity representation of the structure of the generic Mie fluid (obtained with the RHNC integral-equation theory) was incorporated in the integral for the association strength which is at the heart of the Wertheim TPT1 approach. By choosing a physically reasonable geometry for the sites which mediate the association interactions, we obtained a semi-empirical algebraic representation of the association contribution appropriate for generic Mie fluids with a varying form of interaction over a wide range of thermodynamic conditions. A more compact expression has also been formulated by using the structure of a reference LJ fluid to evaluate the association integral, without a significant loss of accuracy in the description of the fluid-phase equilibria of real associating fluids. A key advantage of the algebraic formulation developed here is that the expressions can be incorporated in a straightforward manner within other commonly used versions of the SAFT EOS, such as soft-SAFT, PC-SAFT, and SAFT-γ, as well as the CPA implementation of the Wertheim TPT1 approach in a cubic EOS.

Our generic treatment of the Wertheim TPT1 association contribution in the SAFT-VR Mie EOS was used to determine the fluid-phase behaviour and other derived thermodynamic properties of real associating fluids to a high level of reliability. In the particularly challenging case of water, one can represent the vapour-liquid equilibria very accurately; though some of the anomalies exhibited by water (such as the density and compressibility maximum) are not reproduced by the SAFT-VR Mie EOS, the overall description of the thermodynamic properties was found to be very good considering that the theory is fully algebraic. We have also reported a detailed comparison of the degree of HB obtained by using the SAFT-VR Mie EOS for a four-site association model of water and that obtained by direct molecular simulation for the popular SPC/E and TIP4P/2005 distributed-charge models: the extent of association obtained from the theory with our new association contribution was found to be in remarkable agreement with that obtained by molecular simulations from an analysis of the coordination number using the accepted geometric definition of the hydrogen bond. The degree of association obtained with the SAFT-VR Mie EOS and molecular simulations is consistent with that obtained from neutron scattering data at ambient conditions, but not with the analysis of IR overtone spectroscopy of water along vapour-liquid co-existence. The description of vapour-liquid equilibria and single-phase thermodynamic properties of other real associating fluids such as methanol, ammonia, and hydrogen sulphide was also found to be very good.

In the final part of our paper, the novel treatment of the association contribution in the SAFT-VR Mie EOS was generalised to mixtures. A combined one-fluid and two-fluid description of the thermodynamic and structural properties of the mixtures was found to be the most appropriate. The fluid-phase (vapour-liquid and liquid-liquid) equilibria of some representative mixtures of associating molecules were determined with the theory and compared with the corresponding experimental data. The reliable description of the phase behaviour obtained for aqueous mixtures of methanol, methane, carbon dioxide, and hydrogen sulphide clearly demonstrates that our novel association contribution is also appropriate for the thermodynamic properties of mixtures.

We are currently using the SAFT-VR Mie and SAFT-γ Mie EOSs with the enhanced treatment of the association contribution to study a wide variety of complex multicomponent mixtures comprising associating molecules. The SAFT-γ algebraic platform is also being employed to develop course-grained force fields based on the Mie potential for a variety of systems [223–226], including water [227], which can be used reliably in large-scale molecular simulations.

Disclosure statement

No potential conflict of interest was reported by the authors.

References

[1] W.G. Chapman, K.E. Gubbins, G. Jackson, and M. Radosz, Fluid Phase Equilib. **52**, 31 (1989).
[2] W.G. Chapman, K.E. Gubbins, G. Jackson, and M. Radosz, Ind. Eng. Chem. Res. **29**, 1709 (1990).

[3] G.A. Jeffrey, *An Introduction to Hydrogen Bonding* (Oxford University Press, New York, 1997).

[4] Y. Maréchal, *The Hydrogen Bond and the Water Molecule* (Elsevier, Amsterdam, The Netherlands, 2007).

[5] E. Arunan, G.R. Desiraju, R.A. Klein, J. Sadlej, S. Scheiner, I. Alkorta, D.C. Clary, R.H. Crabtree, J.J. Dannenberg, P. Hobza, H.G. Kjaergaard, A.C. Legon, B. Mennucci, and D.J. Nesbitt, Pure Appl. Chem. **83**, 1619 (2011).

[6] E. Arunan, G.R. Desiraju, R.A. Klein, J. Sadlej, S. Scheiner, I. Alkorta, D.C. Clary, R.H. Crabtree, J.J. Dannenberg, P. Hobza, H.G. Kjaergaard, A.C. Legon, B. Mennucci, and D.J. Nesbitt, Pure Appl. Chem. **83**, 1637 (2011).

[7] J. Lennard-Jones and J.A. Pople, Proc. R. Soc. A **205**, 155 (1951).

[8] J.A. Pople, Proc. R. Soc. A **205**, 163 (1951).

[9] T.L. Hill, J. Chem. Phys. **23**, 617 (1955).

[10] T.L. Hill, J. Chem. Phys. **23**, 623 (1955).

[11] T.L. Hill, *Statistical Mechanics* (McGraw-Hill, New York, NY, 1956).

[12] T.L. Hill, *Introduction to Statistical Thermodynamics* (Addison-Wesley, Reading, 1960).

[13] E.A. Guggenheim, *Mixtures* (Oxford University Press, Oxford, 1952).

[14] J.A. Barker and W. Fock, Discuss. Faraday Soc. **15**, 188 (1953).

[15] H.C. Andersen, J. Chem. Phys. **59**, 4714 (1973).

[16] H.C. Andersen, J. Chem. Phys. **61**, 4985 (1974).

[17] L.W. Dahl and H.C. Andersen, J. Chem. Phys. **78**, 1962 (1983).

[18] L.W. Dahl and H.C. Andersen, J. Chem. Phys. **78**, 1980 (1983).

[19] D. Chandler and L.R. Pratt, J. Chem. Phys. **65**, 2925 (1976).

[20] F. Hirata, Bull. Chem. Soc. Japan **50**, 1032 (1977).

[21] J.S. Høye and K. Olaussen, Phys. A **104**, 435 (1980).

[22] A. Ben-Naim, J. Chem. Phys. **52**, 5531 (1970).

[23] A. Ben-Naim, J. Chem. Phys. **54**, 3682 (1971).

[24] A. Ben-Naim and F.H. Stillinger, 'Aspects of the Statistical-Mechanical Theory of Water' in *Water and Aqueous Solutions: Structure, Thermodynamic and Transport Processes*, edited by R.A. Horne (Wiley, New York, 1972).

[25] A. Ben-Naim, Mol. Phys. **24**, 705 (1972).

[26] S.L. Carnie, D.Y.C. Chan, and G.R. Walker, Mol. Phys. **43**, 1115 (1981).

[27] G.N. Patey and S.L. Carnie, J. Chem. Phys. **78**, 5183 (1983).

[28] P.T. Cummings and G. Stell, Mol. Phys. **51**, 253 (1984).

[29] P.T. Cummings and G. Stell, Mol. Phys. **55**, 33 (1985).

[30] G. Stell and Y. Zhou, J. Chem. Phys. **91**, 3618 (1989).

[31] Y. Zhou and G. Stell, J. Chem. Phys. **96**, 1504 (1992).

[32] Y.V. Kalyuzhnyi and G. Stell, Mol. Phys. **78**, 1247 (1993).

[33] W.R. Smith and I. Nezbeda, J. Chem. Phys. **81**, 3694 (1984).

[34] J. Kolafa and I. Nezbeda, Mol. Phys. **61**, 161 (1987).

[35] I. Nezbeda, J. Kolafa, and Y.V. Kalyuzhnyi, Mol. Phys. **68**, 143 (1989).

[36] Y.V. Kalyuzhnyi and I. Nezbeda, Mol. Phys. **73**, 703 (1991).

[37] M.S. Wertheim, J. Stat. Phys. **35**, 19 (1984).

[38] M.S. Wertheim, J. Stat. Phys. **35**, 35 (1984).

[39] M.S. Wertheim, J. Stat. Phys. **42**, 459 (1986).

[40] M.S. Wertheim, J. Stat. Phys. **42**, 477 (1986).

[41] G. Jackson, W.G. Chapman, and K.E. Gubbins, Mol. Phys. **65**, 1 (1988).

[42] W.G. Chapman, G. Jackson, and K.E. Gubbins, Mol. Phys. **65**, 1057 (1988).

[43] E.A. Müller and K.E. Gubbins, Ind. Eng. Chem. Res. **40**, 2193 (2001).

[44] I.G. Economou, Ind. Eng. Chem. Res. **41**, 953 (2002).

[45] P. Paricaud, A. Galindo, and G. Jackson, Fluid Phase Equilib. **194**, 87 (2002).

[46] S.P. Tan, H. Adidharma, and M. Radosz, Ind. Eng. Chem. Res. **47**, 8063 (2008).

[47] C. McCabe and A. Galindo, 'SAFT associating fluids and fluid mixtures' in *Applied Thermodynamics of Fluids*, edited by A.R.H. Goodwin, J.V. Sengers, and C.J. Peters (Royal Society of Chemistry, London, 2010).

[48] G.M. Kontogeorgis and G.K. Folas, *Thermodynamic Models for Industrial Applications* (Wiley, New York, 2010).

[49] H. Docherty and A. Galindo, Mol. Phys. **104**, 3551 (2006).

[50] M.S. Wertheim, J. Chem. Phys. **87**, 7323 (1987).

[51] E.A. Müller and K.E. Gubbins, Mol. Phys. **80**, 957 (1993).

[52] S. Phan, E. Kierlik, M. Rosinberg, H. Yu, and G. Stell, J. Chem. Phys. **99**, 5326 (1993).

[53] R.P. Sear and G. Jackson, Phys. Rev. E **50**, 386 (1994).

[54] R.P. Sear and G. Jackson, Mol. Phys. **81**, 801 (1994).

[55] K. Shukla and W.G. Chapman, Mol. Phys. **98**, 2045 (2000).

[56] B.D. Marshall and W.G. Chapman, J. Chem. Phys. **138**, 174109 (2013).

[57] M.S. Wertheim, J. Chem. Phys. **85**, 2929 (1986).

[58] W.G. Chapman, J. Chem. Phys. **93**, 4299 (1990).

[59] A.L. Archer and G. Jackson, Mol. Phys. **73**, 881 (1991).

[60] W.R. Smith, I. Nezbeda, M. Strnad, B. Triska, S. Labík, and A. Malijevský, J. Chem. Phys. **109**, 1052 (1998).

[61] M.D. Amos and G. Jackson, Mol. Phys. **74**, 191 (1991).

[62] M.D. Amos and G. Jackson, J. Chem. Phys. **96**, 4604 (1992).

[63] R.P. Sear, M.D. Amos, and G. Jackson, Mol. Phys. **80**, 777 (1993).

[64] A.L. Archer, M.D. Amos, G. Jackson, and I.A. McLure, Int. J. Thermophys. **17**, 201 (1996).

[65] F.J. Blas and L.F. Vega, Mol. Phys. **92**, 135 (1997).

[66] H. Adidharma and M. Radosz, Fluid Phase Equilib. **158**, 165 (1999).

[67] C. McCabe, A. Gil-Villegas, G. Jackson, and F. del Río, Mol. Phys. **97**, 551 (1999).

[68] M. Banaszak and M. Radosz, Fluid Phase Equilib. **193**, 179 (2002).

[69] J. Gross, O. Spuhl, F. Tumakaka, and G. Sadowski, Ind. Eng. Chem. Res. **42**, 1266 (2003).

[70] Y. Peng, H. Zhao, and C. McCabe, Mol. Phys. **104**, 571 (2006).

[71] P. Morgado, H. Zhao, F.J. Blas, C. McCabe, L.P.N. Rebelo, and E.J.M. Filipe, J. Phys. Chem. B **111**, 2856 (2007).

[72] A. Lymperiadis, C.S. Adjiman, A. Galindo, and G. Jackson, J. Chem. Phys. **127**, 234903 (2007).

[73] A. Lymperiadis, C.S. Adjiman, G. Jackson, and A. Galindo, Fluid Phase Equilib. **274**, 85 (2008).

[74] Y. Peng, K.D. Goff, M.C. dos Ramos, and C. McCabe, Fluid Phase Equilib. **277**, 131 (2009).

[75] V. Papaioannou, C.S. Adjiman, G. Jackson, and A. Galindo, Fluid Phase Equilib. **306**, 82 (2011).

[76] K. Paduszyński and U. Domańska, Ind. Eng. Chem. Res. **51**, 12967 (2012).

[77] V. Papaioannou, T. Lafitte, C. Avendaño, C.S. Adjiman, G. Jackson, E.A. Müller, and A. Galindo, J. Chem. Phys. **140**, 054107 (2014).

[78] E. Sauer, M. Stavrou, and J. Gross, Ind. Eng. Chem. Res. **53**, 14854 (2014).

[79] D. Ghonasgi, V. Perez, and W.G. Chapman, J. Chem. Phys. **101**, 6880 (1994).

[80] D. Ghonasgi and W.G. Chapman, J. Chem. Phys. **102**, 2585 (1995).

[81] R.P. Sear and G. Jackson, Mol. Phys. **87**, 517 (1996).

[82] A. Galindo, S.J. Burton, G. Jackson, D.P. Visco Jr, and D.A. Kofke, Mol. Phys. **100**, 2241 (2002).

[83] A.S. Avlund, G.M. Kontogeorgis, and W.G. Chapman, Mol. Phys. **109**, 1759 (2011).

[84] B.D. Marshall and W.G. Chapman, Phys. Rev. E **87**, 052307 (2013).

[85] B.D. Marshall and W.G. Chapman, J. Chem. Phys. **139**, 054902 (2013).

[86] R.P. Sear and G. Jackson, Mol. Phys. **82**, 1033 (1994).

[87] R.P. Sear and G. Jackson, J. Chem. Phys. **105**, 1113 (1996).

[88] B.D. Marshall, A. Haghmoradi, and W.G. Chapman, J. Chem. Phys. **140**, 164101 (2014).

[89] Y.V. Kalyuzhnyi, H. Docherty, and P.T. Cummings, J. Chem. Phys. **133**, 044502 (2010).

[90] Y.V. Kalyuzhnyi, H. Docherty, and P.T. Cummings, J. Chem. Phys. **135**, 014501 (2011).

[91] Y.V. Kalyuzhnyi, B.D. Marshall, W.G. Chapman, and P.T. Cummings, J. Chem. Phys. **139**, 044909 (2013).

[92] B.D. Marshall and W.G. Chapman, J. Chem. Phys. **139**, 104904 (2013).

[93] B.D. Marshall and W.G. Chapman, Soft Matter **9**, 11346 (2013).

[94] B.D. Marshall, W.G. Chapman, and M.M. Telo da Gama, Phys. Rev. E **88**, 060301 (2013).

[95] T. Mohorič, T. Urbic, and B. Hribar-Lee, J. Chem. Phys. **140**, 024502 (2014).

[96] J. Chang, Korean J. Chem. Eng. **31**, 374 (2014).

[97] R.P. Sear, J. Chem. Phys. **111**, 4800 (1999).

[98] N. Kern and D. Frenkel, J. Chem. Phys. **118**, 9882 (2003).

[99] F. Sciortino, E. Bianchi, J.F. Douglas, and P. Tartaglia, J. Chem. Phys. **126**, 194903 (2007).

[100] E. Bianchi, P. Tartaglia, E. Zaccarelli, and F. Sciortino, J. Chem. Phys. **128**, 144504 (2008).

[101] J.M. Tavares, P.I.C. Teixeira, and M.M. Telo da Gama, Phys. Rev. E **80**, 021506 (2009).

[102] J.M. Tavares, P.I.C. Teixeira, M.M. Telo da Gama, and F. Sciortino, J. Chem. Phys. **132**, 234502 (2010).

[103] J. Russo, J.M. Tavares, P.I.C. Teixeira, M.M. Telo da Gama, and F. Sciortino, Phys. Rev. Lett. **106**, 085703 (2011).

[104] F. Romano and F. Sciortino, Nature Mat. **10**, 171 (2011).

[105] J.M. Tavares, L. Rovigatti, and F. Sciortino, J. Chem. Phys. **137**, 044901 (2012).

[106] L. Rovigatti, J.M. Tavares, and F. Sciortino, Phys. Rev. Lett. **111**, 168302 (2013).

[107] R. Fantoni and G. Pastore, J. Chem. Phys. **141**, 074108 (2014).

[108] W.M. Jacobs, D.W. Oxtoby, and D. Frenkel, J. Chem. Phys. **140**, 204109 (2014).

[109] A. Gil-Villegas, A. Galindo, P.J. Whitehead, S.J. Mills, G. Jackson, and A.N. Burgess, J. Chem. Phys. **106**, 4168 (1997).

[110] A. Galindo, L.A. Davies, A. Gil-Villegas, and G. Jackson, Mol. Phys. **93**, 241 (1998).

[111] T. Lafitte, A. Apostolakou, C. Avendaño, A. Galindo, C.S. Adjiman, E.A. Müller, and G. Jackson, J. Chem. Phys. **139**, 154504 (2013).

[112] F.H. Stillinger and A. Rahman, J. Chem. Phys. **60**, 1545 (1974).

[113] F.H. Stillinger, Adv. Chem. Phys. **31**, 1 (1975).

[114] H.J.C. Berendsen, J.P.M. Postma, W.F. van Gunsteren, and J. Hermans, 'Interaction Models for Water in Relation to Protein Hydration' in *Intermolecular Forces*, edited by B. Pullman (Reidel, Dordrecht, 1981).

[115] H.J.C. Berendsen, J.R. Grigera, and T.P. Straatsma, J. Phys. Chem. **91**, 6269 (1987).

[116] W.L. Jorgensen, J. Am. Chem. Soc. **103**, 335 (1981).

[117] W.L. Jorgensen, J. Chandrasekhar, J.D. Madura, R.W. Impey, and M.L. Klein, J. Chem. Phys. **79**, 926 (1983).

[118] M.W. Mahoney and W.L. Jorgensen, J. Chem. Phys. **112**, 8910 (2000).

[119] J.L.F. Abascal and C. Vega, J. Chem. Phys. **123**, 234505 (2005).

[120] C. Vega and J.L.F. Abascal, Phys. Chem. Chem. Phys. **13**, 19663 (2011).

[121] J.D. Bernal and R.H. Fowler, J. Chem. Phys. **1**, 515 (1933).

[122] J.S. Rowlinson, Trans. Faraday Soc. **45**, 974 (1949).

[123] J.S. Rowlinson, Trans. Faraday Soc. **47**, 120 (1951).

[124] N. Bjerrum, Kgl. Danske Videnskab, Selskab, Mat. fys. Medd. **27**, 1 (1951).

[125] I. Nezbeda, J. Molec. Liq. **73–74**, 317 (1997).

[126] K.A.T. Silverstein, A.D.J. Haymet, and K.A. Dill, J. Am. Chem. Soc. **120**, 3166 (1998).

[127] T.M. Truskett and K.A. Dill, J. Chem. Phys. **117**, 5101 (2002).

[128] K.A. Dill, T.M. Truskett, V. Vlachy, and B. Hribar-Lee, Ann. Rev. Biophys. Biomol. Struct. **34**, 173 (2005).

[129] W. Bol, Mol. Phys. **45**, 605 (1982).

[130] M.S. Wertheim, J. Chem. Phys. **88**, 1145 (1988).

[131] G. Mie, Ann. Phys. (Berlin) **316**, 657 (1903).

[132] E. Grüneisen, Z. Elektrochem. Angew. Phys. Chem. **17**, 737 (1911).

[133] E. Grüneisen, Ann. Phys. (Berlin) **344**, 257 (1912).

[134] J.E. Jones, Proc. R. Soc. London A **106**, 441 (1924).

[135] J.E. Jones, Proc. R. Soc. London A **106**, 463 (1924).

[136] J.E. Lennard-Jones, Proc. Phys. Soc. **43**, 461 (1931).

[137] G.N.I. Clark, A.J. Haslam, A. Galindo, and G. Jackson, Mol. Phys. **104**, 3561 (2006).

[138] E.A. Guggenheim, Trans. Faraday Soc. **56**, 1159 (1960).

[139] N.F. Carnahan and K.E. Starling, J. Chem. Phys. **51**, 635 (1969).

[140] T. Boublík, Mol. Phys. **59**, 775 (1986).

[141] J.K. Johnson, E.A. Müller, and K.E. Gubbins, J. Phys. Chem. **98**, 6413 (1994).

[142] J.A. Barker and D. Henderson, J. Chem. Phys. **47**, 4714 (1967).

[143] J.A. Barker and D. Henderson, J. Chem. Phys. **47**, 2856 (1967).

[144] J.D. Weeks, D. Chandler, and H.C. Andersen, J. Chem. Phys. **54**, 5237 (1971).

[145] L.S. Ornstein and F.Z. Zernike, Proc. Acad. Sci. Amsterdam **17**, 793 (1914).

[146] L.L. Lee, *Molecular Thermodynamics of Nonideal Fluids* (Butterworths, Stoneham, MA, 1988).

[147] F. Lado, Phys. Rev. A **8**, 2548 (1973).

[148] F. Lado, Phys. Lett. A **89**, 196 (1982).

[149] F. Lado, S.M. Foiles, and N.W. Ashcroft, Phys. Rev. A **28**, 2374 (1983).

[150] Y. Rosenfeld and N.W. Ashcroft, Phys. Rev. A **20**, 1208 (1979).

[151] E. Lomba, Mol. Phys. **68**, 87 (1989).

[152] D.-M. Duh and A.D.J. Haymet, J. Chem. Phys. **103**, 2625 (1995).

[153] A. Malijevský and S. Labík, Mol. Phys. **60**, 663 (1987).

[154] E. Lomba and N.G. Almarza, J. Chem. Phys. **100**, 8367 (1994).

[155] Y.V. Kalyuzhnyi and P.T. Cummings, Mol. Phys. **87**, 1459 (1996).

[156] A. Gil-Villegas, C. Vega, F. del Río, and A. Malijevský, Mol. Phys. **86**, 857 (1995).

[157] N. Ramrattan, C. Avendaño, E.A. Müller, and A. Galindo, Mol. Phys. **113**, 932 (2015).

[158] A. Galindo, P.J. Whitehead, G. Jackson, and A.N. Burgess, J. Phys. Chem. **100**, 6781 (1996).

[159] J. Gross and G. Sadowski, Ind. Eng. Chem. Res. **41**, 5510 (2002).

[160] G.M. Kontogeorgis, E.C. Voutsas, I.V. Yakoumis, and D.P. Tassios, Ind. Eng. Chem. Res. **35**, 4310 (1996).

[161] G.N.I. Clark, A. Galindo, G. Jackson, S. Rogers, and A.N. Burgess, Macromolecules **41**, 6582 (2008).

[162] J. Rodriguez, N. MacDowell, F. Llovell, C.S. Adjiman, G. Jackson, and A. Galindo, Mol. Phys. **110**, 1325 (2012).

[163] E.A. Müller and K.E. Gubbins, Ind. Eng. Chem. Res. **34**, 3662 (1995).

[164] C.G. Gray and K.E. Gubbins, *Theory of Molecular Fluids,* Vol. 1 (Clarendon Press, Oxford, 1984).

[165] G. Stell, J.C. Rasaiah, and H. Narang, Mol. Phys. **27**, 1393 (1974).

[166] T. Kraska and K.E. Gubbins, Ind. Eng. Chem. Res. **35**, 4727 (1996).

[167] T. Kraska and K.E. Gubbins, Ind. Eng. Chem. Res. **35**, 4738 (1996).

[168] F.J. Blas and L.F. Vega, Ind. Eng. Chem. Res. **37**, 660 (1998).

[169] F.J. Blas and L.F. Vega, J. Chem. Phys. **109**, 7405 (1998).

[170] L.F. Vega, F. Llovell, and F.J. Blas, J. Phys. Chem. B **113**, 7621 (2009).

[171] S. Dufal, A.J. Haslam, T. Lafitte, A. Galindo, and G. Jackson, AIChE J., in press, doi: 10.1002/aic.14808 (2015).

[172] P. Linstrom and W. Mallard, editors, *NIST Chemistry Web-Book, NIST Standard Reference Database Number 69* (National Institute of Standards and Technology, Gaithersburg, MD, 2013).

[173] M.C. dos Ramos, H. Docherty, F.J. Blas, and A. Galindo, Fluid Phase Equilib. **276**, 116 (2009).

[174] E. Matteoli and G.A. Mansoori, J. Chem. Phys. **103**, 4672 (1995).

[175] C. McCabe and S.B. Kiselev, Ind. Eng. Chem. Res. **43**, 2839 (2004).

[176] F. Llovell and L.F. Vega, J. Supercrit. Fluids **41**, 204 (2007).

[177] O. Vilaseca, F. Llovell, J. Yustos, R.M. Marcos, and L.F. Vega, J. Supercrit. Fluids **55**, 755 (2010).

[178] E. Forte, F. Llovell, L.F. Vega, J.P.M. Trusler, and A. Galindo, J. Chem. Phys. **134**, 154102 (2011).

[179] W.A.P. Luck, Angew. Chem. Int. Edn. **19**, 28 (1980).

[180] H. Kahl and S. Enders, Fluid Phase Equilib. **172**, 27 (2000).

[181] E.K. Karakatsani, T. Spyriouni, and I.G. Economou, AIChE J. **51**, 2328 (2005).

[182] N. von Solms, M.L. Michelsen, C.P. Passos, S.O. Derawi, and G.M. Kontogeorgis, Ind. Eng. Chem. Res. **45**, 5368 (2006).

[183] S. Aparicio-Martínez and K.R. Hall, Fluid Phase Equilib. **254**, 112 (2007).

[184] A. Grenner, G.M. Kontogeorgis, M.L. Michelsen, and G.K. Folas, Mol. Phys. **105**, 1797 (2007).

[185] I. Tsivintzelis, A. Grenner, I.G. Economou, and G.M. Kontogeorgis, Ind. Eng. Chem. Res. **47**, 5651 (2008).

[186] G.M. Kontogeorgis, I. Tsivintzelis, N. von Solms, A. Grenner, D. Bøgh, M. Frost, A. Knage-Rasmussen, and I.G. Economou, Fluid Phase Equilib. **296**, 219 (2010).

[187] T. Soria, F. Sánchez, S. Pereda, and S. Bottini, Fluid Phase Equilib. **296**, 116 (2010).

[188] G. Niño-Amézquita, D. van Putten, and S. Enders, Fluid Phase Equilib. **332**, 40 (2012).

[189] G.M. Kontogeorgis, Chem. Eng. Res. Design **91**, 1840 (2013).

[190] I. Tsivintzelis, D. Bøgh, E. Karakatsani, and G.M. Kontogeorgis, Fluid Phase Equilib. **365**, 112 (2014).

[191] X. Liang, I. Tsivintzelis, and G.M. Kontogeorgis, Ind. Eng. Chem. Res. **53**, 14493 (2014).

[192] G.C. Boulougouris, I.G. Economou, and D.N. Theodorou, J. Phys. Chem. B **102**, 1029 (1998).

[193] J.R. Errington and A.Z. Panagiotopoulos, J. Phys. Chem. B **102**, 7470 (1998).

[194] M. Lísal, W.R. Smith, and I. Nezbeda, Fluid Phase Equilib. **181**, 127 (2001).

[195] C. Vega, J.L.F. Abascal, and I. Nezbeda, J. Chem. Phys. **125**, 034503 (2006).

[196] D. Frenkel and B. Smit, *Understanding Molecular Simulation from Algorithms to Applications* (Academic Press, San Diego, CA, 1996).

[197] R.D. Mountain, J. Chem. Phys. **90**, 1866 (1989).

[198] W.L. Jorgensen and J.D. Madura, Mol. Phys. **56**, 1381 (1985).

[199] J.D. Madura, B.M. Pettitt, and D.F. Calef, Mol. Phys. **64**, 325 (1988).

[200] A.G. Kalinichev and J.D. Bass, Chem. Phys. Lett. **231**, 301 (1994).

[201] A.A. Chialvo and P.T. Cummings, 'Molecular-Based Modeling of Water and Aqueous Solutions at Supercritical Conditions' in *Advances in Chemical Physics*, Vol. 109, edited by I. Prigogine and S.A. Rice (John Wiley & Sons, Hoboken, NJ, 1999), p. 115.

[202] A.K. Soper and M.G. Phillips, Chem. Phys. **107**, 47 (1986).

[203] J.S. Rowlinson and F.L. Swinton, *Liquids and Mixtures, 3rd Edition* (Butterworths, London, 1982).

[204] P.H. van Konynenburg and R.L. Scott, Phil. Trans. R. Soc. **298**, 495 (1980).

[205] G. Bredig and R. Bayer, Z. Phys. Chem. **130**, 1 (1927).

[206] J.G. Dunlop, M.Sc. thesis, Brooklyn Polytechnic Inst., New York, 1948.

[207] H.E. Hughes and J.O. Maloney, Chem. Eng. Progr. **48**, 192 (1952).

[208] S.I. Green and R.E. Vener, Ind. Eng. Chem. **47**, 103 (1955).

[209] J. Ocon and F. Rebolleda, An. R. Soc. Esp. Fis. Quim. Ser. B **54**, 525 (1958).

[210] R.S. Ramalho, F.M. Tiller, W.J. James, and D.W. Bunch, Ind. Eng. Chem. **53**, 895 (1961).

[211] A.J. Haslam, A. Galindo, and G. Jackson, Fluid Phase Equilib. **266**, 105 (2008).

[212] A. Chapoy, C. Coquelet, and D. Richon, Fluid Phase Equilib. **214**, 101 (2003).

[213] S.-X. Hou, G.C. Maitland, and J.P.M. Trusler, J. Supercrit. Fluids **73**, 87 (2013).

[214] Y.D. Zel'venskii, Zh. Fiz. Khim. **14**, 1250 (1937).

[215] C.R. Coan and A.D. King Jr., J. Am. Chem. Soc. **93**, 1857 (1971).

[216] A. Zawisza and B. Malesinska, J. Chem. Eng. Data **26**, 388 (1981).

[217] J. Kiepe, S. Horstmann, K. Fischer, and J. Gmehling, Ind. Eng. Chem. Res. **41**, 4393 (2002).

[218] R. Wiebe and V.L. Gaddy, J. Am. Chem. Soc. **63**, 475 (1941).

[219] R. D'Souza, J.R. Patrick, and A.S. Teja, Can. J. Chem. Eng. **66**, 319 (1988).

[220] P.C. Gillespie and G.M. Wilson, Tech. Rep. (GPA Research Report RR-48), 1982.

[221] A. Bamberger, G. Sieder, and G. Maurer, J. Supercrit. Fluids **17**, 97 (2000).

[222] F.T. Selleck, L.T. Carmichael, and B.H. Sage, Ind. Eng. Chem. **44**, 2219 (1952).

[223] C. Avendaño, T. Lafitte, A. Galindo, C.S. Adjiman, G. Jackson, and E.A. Müller, J. Phys. Chem. B **115**, 11154 (2011).

[224] C. Avendaño, T. Lafitte, C.S. Adjiman, A. Galindo, E.A. Müller, and G. Jackson, J. Phys. Chem. B **117**, 2717 (2013).

[225] T. Lafitte, C. Avendaño, V. Papaioannou, A. Galindo, C.S. Adjiman, G. Jackson, and E.A. Müller, Mol. Phys. **110**, 1189 (2012).

[226] E.A. Müller and G. Jackson, Ann. Rev. Chem. Biomol. Eng. **5**, 405 (2014).

[227] O. Lobanova, C. Avendaño, E.A. Müller, and G. Jackson, Mol. Phys. **113**, 1228 (2015).

Appendix 1. Correlation coefficients for LJ-based and Mie-based association kernels

The values of the correlation coefficients that appear in the association kernels equations (30) and (32) are presented in the subsequent tables.

A downloadable file with the coefficients conveniently formatted for computer code is available as Supplemental Material (follow the Supplemental Material link from the article home page).

Table A1. $c_{i,j}$ coefficients for the association kernel correlation in the LJ-based association term, Equation (32).

i	j	$c_{i,j}$	i	j	$c_{i,j}$	i	j	$c_{i,j}$	i	j	$c_{i,j}$
0	0	$7.56425183020431 \times 10^{-2}$	1	6	$-4.84863997651451 \times 10^{-4}$	3	4	$3.17171522104923 \times 10^{-2}$	6	0	$-6.21028065719194 \times 10^{-1}$
0	1	$-1.28667137050961 \times 10^{-1}$	1	7	$4.35262491516424 \times 10^{-5}$	3	5	$-2.91368915845693 \times 10^{-3}$	6	1	$-1.92883360342573 \times 10^{-1}$
0	2	$1.28350663231605 \times 10^{-1}$	1	8	$-2.07789181640066 \times 10^{-6}$	3	6	$1.30193710011706 \times 10^{-4}$	6	2	$2.84109761066570 \times 10^{-1}$
0	3	$-7.25321780970292 \times 10^{-2}$	1	9	$4.13749349344802 \times 10^{-8}$	3	7	$-2.14505500786531 \times 10^{-6}$	6	3	$-1.57606767372364 \times 10^{-2}$
0	4	$2.57782547511452 \times 10^{-2}$	2	0	$-5.65116428942893 \times 10^{-1}$	4	0	2.13713180911797	6	4	$3.68599073256615 \times 10^{-4}$
0	5	$-6.01170055221687 \times 10^{-3}$	2	1	1.00930692226792	4	1	-2.02798460133021	7	0	11.608353281802900
0	6	$9.33363147191978 \times 10^{-4}$	2	2	$-6.60166945915607 \times 10^{-1}$	4	2	$3.36709255682693 \times 10^{-1}$	7	1	$7.42215544511197 \times 10^{-1}$
0	7	$-9.55607377143667 \times 10^{-5}$	2	3	$2.14492212294301 \times 10^{-1}$	4	3	$1.18106507393722 \times 10^{-3}$	7	2	$-8.23976531246117 \times 10^{-2}$
0	8	$6.19576039900837 \times 10^{-6}$	2	4	$-3.88462990166792 \times 10^{-2}$	4	4	$-6.00058423301506 \times 10^{-3}$	7	3	$1.86167650098254 \times 10^{-3}$
0	9	$-2.30466608213628 \times 10^{-7}$	2	5	$4.06016982985030 \times 10^{-3}$	4	5	$6.26343952584415 \times 10^{-4}$	8	0	-10.2632535542427
0	10	$3.74605718435540 \times 10^{-9}$	2	6	$-2.39515566373142 \times 10^{-4}$	4	6	$-2.03636395699819 \times 10^{-5}$	8	1	$-1.25035689035085 \times 10^{-1}$
1	0	$1.34228218276565 \times 10^{-1}$	2	7	$7.25488368831468 \times 10^{-6}$	5	0	$-3.00527494795524 \times 10^{-1}$	8	2	$1.14299144831867 \times 10^{-2}$
1	1	$-1.82682168504886 \times 10^{-1}$	2	8	$-8.58904640281928 \times 10^{-8}$	5	1	2.89920714512243	9	0	$4.65297446837297 \times 10^{-1}$
1	2	$7.71662412959262 \times 10^{-2}$	3	0	$-3.87336382687019 \times 10^{-1}$	5	2	$-5.67134839686498 \times 10^{-1}$	9	1	$-1.92518067137033 \times 10^{-3}$
1	3	$-7.17458641164565 \times 10^{-4}$	3	1	$-2.11614570109503 \times 10^{-1}$	5	3	$5.18085125423494 \times 10^{-2}$	10	0	$-8.67296219639940 \times 10^{-1}$
1	4	$-8.72427344283170 \times 10^{-3}$	3	2	$4.50442894490509 \times 10^{-1}$	5	4	$-2.39326776760414 \times 10^{-3}$			
1	5	$2.97971883605287 \times 10^{-3}$	3	3	$-1.76931752538907 \times 10^{-1}$	5	5	$4.15107362643844 \times 10^{-5}$			

Table A2. $b_{i,j,k=0}$ coefficients for the association kernel correlation in the Mie-based association term, Equation (30).

i	j	$b_{i,j,k=0}$
0	0	$1.329707021820683 \times 10^{-2}$
0	1	$-1.77199122935443 \times 10^{-2}$
0	2	$2.93736747694974 \times 10^{-2}$
0	3	$-2.05527304404423 \times 10^{-2}$
0	4	$8.61683420907605 \times 10^{-3}$
0	5	$-2.28505275303600 \times 10^{-3}$
0	6	$3.90171133200072 \times 10^{-4}$
0	7	$-4.26035888869942 \times 10^{-5}$
0	8	$2.86246920519487 \times 10^{-6}$
0	9	$-1.07315320963937 \times 10^{-7}$
0	10	$1.70912976772329 \times 10^{-9}$
1	0	$-4.65504528847432 \times 10^{-2}$
1	1	$3.32597325549352 \times 10^{-1}$
1	2	$-3.26575316241193 \times 10^{-1}$
1	3	$1.44653671541451 \times 10^{-1}$
1	4	$-3.63193315289496 \times 10^{-2}$
1	5	$5.69934220115537 \times 10^{-3}$
1	6	$-5.81966173216051 \times 10^{-4}$
1	7	$3.83608167089024 \times 10^{-5}$
1	8	$-1.50305409953983 \times 10^{-6}$
1	9	$2.66749257811143 \times 10^{-8}$
2	0	$1.64972499633366 \times 10^{-1}$
2	1	$-9.74898725377830 \times 10^{-1}$
2	2	$9.19082550772666 \times 10^{-1}$
2	3	$-3.67978443660284 \times 10^{-1}$
2	4	$7.88054156983951 \times 10^{-2}$
2	5	$-9.81102799831725 \times 10^{-3}$
2	6	$7.17901835772044 \times 10^{-4}$
2	7	$-2.91191052989125 \times 10^{-5}$
2	8	$5.17207032026779 \times 10^{-7}$
3	0	$-5.53080054304108 \times 10^{-1}$
3	1	1.07124021914524
3	2	$-9.14915281734471 \times 10^{-1}$
3	3	$3.28132391309741 \times 10^{-1}$
3	4	$-5.77909160509185 \times 10^{-2}$
3	5	$5.39941935098940 \times 10^{-3}$
3	6	$-2.49522541631115 \times 10^{-4}$
3	7	$4.36324500072586 \times 10^{-6}$
4	0	$6.97481173735912 \times 10^{-1}$
4	1	$-1.27802319197572 \times 10^{-1}$
4	2	$2.38559496985344 \times 10^{-1}$
4	3	$-1.24364954974360 \times 10^{-1}$
4	4	$1.83583032370354 \times 10^{-2}$
4	5	$-1.33946361388127 \times 10^{-3}$
4	6	$3.68888649118614 \times 10^{-5}$
5	0	$-6.82258598593205 \times 10^{-3}$
5	1	$-2.96768597044265 \times 10^{-1}$
5	2	$3.46077751701231 \times 10^{-1}$
5	3	$1.22496582163678 \times 10^{-2}$
5	4	$-8.05951611068984 \times 10^{-4}$
5	5	$5.01775524378700 \times 10^{-5}$
6	0	-2.46482416179796
6	1	-1.45370322973416
6	2	$-4.48827080921154 \times 10^{-1}$
6	3	$-5.66229179136722 \times 10^{-3}$
6	4	$-1.80870029200998 \times 10^{-4}$
7	0	8.78388694047369
7	1	3.23807384513205
7	2	$2.81816142695178 \times 10^{-1}$
7	3	$3.40169105539079 \times 10^{-3}$
8	0	$-1.35178089781880 \times 10^{1}$
8	1	-2.48217551606281
8	2	$-7.83334040233511 \times 10^{-2}$
9	0	9.42415649943917
9	1	$6.87363680163044 \times 10^{-1}$
10	0	-2.46151453173016

Table A3. $b_{i,j,k=1}$ coefficients for the association integral correlation in the Mie-based association term, Equation (30).

i	j	$b_{i,j,k=1}$
0	0	$5.56479463564548 \times 10^{-4}$
0	1	$-2.82932524693843 \times 10^{-4}$
0	2	$-2.12156862728691 \times 10^{-3}$
0	3	$2.24197388058698 \times 10^{-3}$
0	4	$-1.15385075260200 \times 10^{-3}$
0	5	$3.45261305021541 \times 10^{-4}$
0	6	$-6.36772702454557 \times 10^{-5}$
0	7	$7.32538316171651 \times 10^{-6}$
0	8	$-5.10881831259873 \times 10^{-7}$
0	9	$1.97049247692837 \times 10^{-8}$
0	10	$-3.21285622252695 \times 10^{-10}$
1	0	$4.92332122696642 \times 10^{-2}$
1	1	$-1.34456183191719 \times 10^{-1}$
1	2	$1.08517185632299 \times 10^{-1}$
1	3	$-4.25401431513956 \times 10^{-2}$
1	4	$9.54409805564329 \times 10^{-3}$
1	5	$-1.31479859839035 \times 10^{-3}$
1	6	$1.13485041044446 \times 10^{-4}$
1	7	$-5.97590027689909 \times 10^{-6}$
1	8	$1.73112888670222 \times 10^{-7}$
1	9	$-2.01831274082934 \times 10^{-9}$
2	0	$-1.58447251265296 \times 10^{-1}$
2	1	$4.30576656790814 \times 10^{-1}$
2	2	$-3.42386658999542 \times 10^{-1}$
2	3	$1.26318819450003 \times 10^{-1}$
2	4	$-2.57089028169037 \times 10^{-2}$
2	5	$3.10740070593876 \times 10^{-3}$
2	6	$-2.26247702797060 \times 10^{-4}$
2	7	$9.40337471999922 \times 10^{-6}$
2	8	$-1.75927011626452 \times 10^{-7}$
3	0	$1.30961541597078 \times 10^{-1}$
3	1	$-3.58137806097004 \times 10^{-1}$
3	2	$3.23521260711548 \times 10^{-1}$
3	3	$-1.13820803061658 \times 10^{-1}$
3	4	$1.92702466504444 \times 10^{-2}$
3	5	$-1.69264438876774 \times 10^{-3}$
3	6	$7.20470394807155 \times 10^{-5}$
3	7	$-1.12895786020720 \times 10^{-6}$
4	0	$-6.78784049001058 \times 10^{-2}$
4	1	$-1.59716521155965 \times 10^{-1}$
4	2	$-4.08260244006866 \times 10^{-2}$
4	3	$3.97261699377944 \times 10^{-2}$
4	4	$-6.68853458452261 \times 10^{-3}$
4	5	$4.90515978818942 \times 10^{-4}$
4	6	$-1.26640904345952 \times 10^{-5}$
5	0	$6.11672146147809 \times 10^{-1}$
5	1	$2.57963755040360 \times 10^{-1}$
5	2	$-1.50206376568020 \times 10^{-1}$
5	3	$3.87683716563604 \times 10^{-3}$
5	4	$1.13887448052591 \times 10^{-4}$
5	5	$-2.67212361539355 \times 10^{-5}$
6	0	-1.27512696874714
6	1	$4.21048118713917 \times 10^{-1}$
6	2	$1.22792263121120 \times 10^{-1}$
6	3	$-1.58386412295998 \times 10^{-3}$
6	4	$1.98370689434891 \times 10^{-4}$
7	0	$2.69957785723510 \times 10^{-1}$
7	1	$-8.99401835359301 \times 10^{-1}$
7	2	$-5.93934567946635 \times 10^{-2}$
7	3	$-1.10977335239395 \times 10^{-3}$
8	0	1.49379616940916
8	1	$6.28459498670159 \times 10^{-1}$
8	2	$1.77032259427776 \times 10^{-2}$
9	0	-1.50913781396606
9	1	$-1.66624388301135 \times 10^{-1}$
10	0	$4.44942467424175 \times 10^{-1}$

Table A4. $b_{i,j,k=2}$ coefficients for the association integral correlation in the Mie-based association term, Equation (30).

i	j	$b_{i,j,k=2}$	i	j	$b_{i,j,k=2}$	i	j	$b_{i,j,k=2}$	i	j	$b_{i,j,k=2}$
0	0	$4.68753836985661 \times 10^{-5}$	1	6	$-9.31205117458790 \times 10^{-6}$	3	4	$-2.04736822270412 \times 10^{-3}$	6	0	$2.60822991454304 \times 10^{-1}$
0	1	$-2.01534029276569 \times 10^{-4}$	1	7	$4.07198179416416 \times 10^{-7}$	3	5	$1.71672501041056 \times 10^{-4}$	6	1	$-6.26432527852684 \times 10^{-2}$
0	2	$4.08971640196116 \times 10^{-4}$	1	8	$-7.24002263850399 \times 10^{-9}$	3	6	$-6.91918528995779 \times 10^{-6}$	6	2	$-9.59839254636274 \times 10^{-2}$
0	3	$-3.34428221392103 \times 10^{-4}$	1	9	$-2.85054817786792 \times 10^{-11}$	3	7	$1.02234151256019 \times 10^{-7}$	6	3	$2.23341727285368 \times 10^{-3}$
0	4	$1.54951071291061 \times 10^{-4}$	2	0	$2.11014984424621 \times 10^{-2}$	4	0	$2.67157884350682 \times 10^{-2}$	6	4	$-2.78886526475732 \times 10^{-5}$
0	5	$-4.39272547633533 \times 10^{-5}$	2	1	$-4.95382445219106 \times 10^{-2}$	4	1	$6.04022182900132 \times 10^{-3}$	7	0	$-1.79706752593973 \times 10^{-1}$
0	6	$7.86877804626315 \times 10^{-6}$	2	2	$3.71909493534914 \times 10^{-2}$	4	2	$8.22450412680841 \times 10^{-3}$	7	1	$9.89212484451187 \times 10^{-2}$
0	7	$-8.92538365355001 \times 10^{-7}$	2	3	$-1.32662359974178 \times 10^{-2}$	4	3	$-5.02124889994980 \times 10^{-3}$	7	2	$3.88197187439871 \times 10^{-3}$
0	8	$6.20541126317064 \times 10^{-8}$	2	4	$2.64252348906371 \times 10^{-3}$	4	4	$8.03630265796884 \times 10^{-4}$	7	3	$1.51511550199890 \times 10^{-4}$
0	9	$-2.40904019797940 \times 10^{-9}$	2	5	$-3.16720398760111 \times 10^{-4}$	4	5	$-5.55280746686634 \times 10^{-5}$	8	0	$-3.15900588187112 \times 10^{-2}$
0	10	$3.99225753392296 \times 10^{-11}$	2	6	$2.32682269109226 \times 10^{-5}$	4	6	$1.30402695735287 \times 10^{-6}$	8	1	$-6.07681438566115 \times 10^{-2}$
1	0	$-6.36142804034125 \times 10^{-3}$	2	7	$-9.93969228161767 \times 10^{-7}$	5	0	$-1.31004401410042 \times 10^{-1}$	8	2	$-1.41908354521815 \times 10^{-3}$
1	1	$1.48870088793584 \times 10^{-2}$	2	8	$1.93247731973246 \times 10^{-8}$	5	1	$-9.85163509226622 \times 10^{-3}$	9	0	$9.26908832419059 \times 10^{-2}$
1	2	$-1.12930088940554 \times 10^{-2}$	3	0	$-2.04522546881708 \times 10^{-2}$	5	2	$1.28544254818812 \times 10^{-2}$	9	1	$1.51506077043458 \times 10^{-2}$
1	3	$4.23537018032177 \times 10^{-3}$	3	1	$4.56627841733661 \times 10^{-2}$	5	3	$-2.16912930642026 \times 10^{-4}$	10	0	$-3.12717011022248 \times 10^{-2}$
1	4	$-9.09633136025822 \times 10^{-4}$	3	2	$-3.75241588712114 \times 10^{-2}$	5	4	$-4.55721397631024 \times 10^{-5}$			
1	5	$1.18406467168496 \times 10^{-4}$	3	3	$1.25888572116524 \times 10^{-2}$	5	5	$4.78472396442476 \times 10^{-6}$			

Table A5. $b_{i,j,k=3}$ coefficients for the association integral correlation in the Mie-based association term, Equation (30).

i	j	$b_{i,j,k=3}$	i	j	$b_{i,j,k=3}$	i	j	$b_{i,j,k=3}$	i	j	$b_{i,j,k=3}$
0	0	$-1.52750755540612 \times 10^{-6}$	1	6	$2.92850782905453 \times 10^{-7}$	3	4	$1.07391347801278 \times 10^{-4}$	6	0	$-3.40226871507608 \times 10^{-7}$
0	1	$6.65734616244750 \times 10^{-6}$	1	7	$-5.67255537711216 \times 10^{-9}$	3	5	$-8.69254977310800 \times 10^{-6}$	6	1	$-1.95358884282327 \times 10^{-2}$
0	2	$-1.49163457856162 \times 10^{-5}$	1	8	$-3.50155347187566 \times 10^{-10}$	3	6	$3.38632787324714 \times 10^{-7}$	6	2	$4.20143444237083 \times 10^{-3}$
0	3	$1.28251715836463 \times 10^{-5}$	1	9	$1.64319946681537 \times 10^{-11}$	3	7	$-4.90436065438310 \times 10^{-9}$	6	3	$2.97766652427410 \times 10^{-4}$
0	4	$-6.13363502620892 \times 10^{-6}$	2	0	$-1.27835416513710 \times 10^{-3}$	4	0	$-2.96574649489361 \times 10^{-3}$	6	4	$-8.36498131244475 \times 10^{-6}$
0	5	$1.77374828289499 \times 10^{-6}$	2	1	$2.72631887421459 \times 10^{-3}$	4	1	$7.37340818584580 \times 10^{-4}$	7	0	$1.51044087021239 \times 10^{-6}$
0	6	$-3.21719278338969 \times 10^{-7}$	2	2	$-1.95876152374924 \times 10^{-3}$	4	2	$-7.62065788926240 \times 10^{-4}$	7	1	$1.64362361737192 \times 10^{-2}$
0	7	$3.67816571475073 \times 10^{-8}$	2	3	$6.80170219619246 \times 10^{-4}$	4	3	$-9.27089410962249 \times 10^{-5}$	7	2	$-5.27606737824625 \times 10^{-3}$
0	8	$-2.57070860278200 \times 10^{-9}$	2	4	$-1.33171449466011 \times 10^{-4}$	4	4	$3.15097078455367 \times 10^{-4}$	7	3	$-9.32930119768768 \times 10^{-6}$
0	9	$1.00187848111417 \times 10^{-10}$	2	5	$1.58508191731109 \times 10^{-5}$	4	5	$-4.64683975120556 \times 10^{-5}$	8	0	$-4.39666318131193 \times 10^{-3}$
0	10	$-1.66615681224878 \times 10^{-12}$	2	6	$-1.17119945008334 \times 10^{-6}$	4	6	$3.00942802764189 \times 10^{-6}$	8	1	$2.87829011566385 \times 10^{-3}$
1	0	$3.52707112753263 \times 10^{-4}$	2	7	$5.09014996522337 \times 10^{-8}$	5	0	$-6.47808066443911 \times 10^{-8}$	8	2	$5.24103094975034 \times 10^{-5}$
1	1	$-7.61494022700993 \times 10^{-4}$	2	8	$-1.01109171728229 \times 10^{-9}$	5	1	$1.04319873447675 \times 10^{-2}$	9	0	$-1.59566365617165 \times 10^{-3}$
1	2	$5.51126114938543 \times 10^{-4}$	3	0	$1.64258140843764 \times 10^{-3}$	5	2	$-7.75429459116355 \times 10^{-4}$	9	1	$-6.67764807450442 \times 10^{-4}$
1	3	$-1.97194099229223 \times 10^{-4}$	3	1	$-2.94360803306568 \times 10^{-3}$	5	3	$-3.79064014723981 \times 10^{-4}$	10	0	$8.61407443430205 \times 10^{-4}$
1	4	$3.97623327839760 \times 10^{-5}$	3	2	$2.15659810736663 \times 10^{-3}$	5	4	$-1.60783833898331 \times 10^{-5}$			
1	5	$-4.65836276873807 \times 10^{-6}$	3	3	$-6.85370482291315 \times 10^{-4}$	5	5	$4.71880061366660 \times 10^{-6}$			

Table A6. $b_{i,j,k=4}$ coefficients for the association integral correlation in the Mie-based association term, Equation (30).

i	j	$b_{i,j,k=4}$
0	0	$-3.6720123092920 \times 10^{-8}$
0	1	$6.6543123492297 \times 10^{-8}$
0	2	$8.0975325026481 \times 10^{-8}$
0	3	$-1.2934963796981 \times 10^{-7}$
0	4	$7.7503494236271 \times 10^{-8}$
0	5	$-2.5044244953800 \times 10^{-8}$
0	6	$4.8196976488644 \times 10^{-9}$
0	7	$-5.6833586091982 \times 10^{-10}$
0	8	$4.0254465205731 \times 10^{-11}$
0	9	$-1.5705713578918 \times 10^{-12}$
0	10	$2.5901806515018 \times 10^{-14}$
1	0	$-1.0053309818631 \times 10^{-5}$
1	1	$2.0497378545526 \times 10^{-5}$
1	2	$-1.4236452555262 \times 10^{-5}$
1	3	$4.8485962653371 \times 10^{-6}$
1	4	$-9.0328739452153 \times 10^{-7}$
1	5	$8.9540398525651 \times 10^{-8}$
1	6	$-3.0517547707806 \times 10^{-9}$
1	7	$-2.5120622755009 \times 10^{-10}$
1	8	$2.8588833754456 \times 10^{-11}$
1	9	$-8.3571369169993 \times 10^{-13}$
2	0	$3.9828982666092 \times 10^{-5}$
2	1	$-7.9206614738454 \times 10^{-5}$
2	2	$5.4906684115785 \times 10^{-5}$
2	3	$-1.8640273539785 \times 10^{-5}$
2	4	$3.5960461123929 \times 10^{-6}$
2	5	$-4.2513658323379 \times 10^{-7}$
2	6	$3.1470188558904 \times 10^{-8}$
2	7	$-1.3794201076325 \times 10^{-9}$
2	8	$2.7662589483315 \times 10^{-11}$
3	0	$-6.2260615260380 \times 10^{-5}$
3	1	$9.7866185935570 \times 10^{-5}$
3	2	$-6.5471112754411 \times 10^{-5}$
3	3	$1.9839479230395 \times 10^{-5}$
3	4	$-3.014589729 \times 10^{-6}$
3	5	$2.38076582 \times 10^{-7}$
3	6	$-9.121372355 \times 10^{-9}$
3	7	$1.332987814 \times 10^{-10}$
4	0	$1.248106387 \times 10^{-4}$
4	1	$-5.136120521 \times 10^{-5}$
4	2	$3.094328537 \times 10^{-5}$
4	3	$-1.020097512 \times 10^{-5}$
4	4	$1.397144136 \times 10^{-6}$
4	5	$-8.5503442 79 \times 10^{-8}$
4	6	$1.711500449 \times 10^{-9}$
5	0	$-3.740440991 \times 10^{-4}$
5	1	$5.607960504 \times 10^{-5}$
5	2	$1.846261271 \times 10^{-6}$
5	3	$1.342885286 \times 10^{-6}$
5	4	$-1.946146552 \times 10^{-7}$
5	5	$1.141578637 \times 10^{-8}$
6	0	$6.72078359176232 \times 10^{-4}$
6	1	$-1.38031320636187 \times 10^{-4}$
6	2	$-3.14894396008512 \times 10^{-6}$
6	3	$5.76785692862702 \times 10^{-8}$
6	4	$-3.88710150387342 \times 10^{-8}$
7	0	$-6.09145837554261 \times 10^{-4}$
7	1	$1.48275594790438 \times 10^{-4}$
7	2	$2.61353677755675 \times 10^{-7}$
7	3	$2.91087061127825 \times 10^{-7}$
8	0	$2.52724106819134 \times 10^{-4}$
8	1	$-7.36076398 6864788 \times 10^{-5}$
8	2	$-1.00642768627400 \times 10^{-6}$
9	0	$-2.49258677 87548 \times 10^{-5}$
9	1	$1.59720037817341 \times 10^{-5}$
10	0	$-7.70341617155424 \times 10^{-6}$

Table A7. $b_{i,j,k=5}$ coefficients for the association integral correlation in the Mie-based association term, Equation (30).

i	j	$b_{i,j,k=5}$
0	0	$1.88048156944327 \times 10^{-9}$
0	1	$-5.20041750295709 \times 10^{-9}$
0	2	$4.35881692094647 \times 10^{-9}$
0	3	$-1.90967917025464 \times 10^{-9}$
0	4	$4.36098784939288 \times 10^{-10}$
0	5	$-4.66145781784596 \times 10^{-11}$
0	6	$2.56821311477203 \times 10^{-13}$
0	7	$4.53836639240824 \times 10^{-13}$
0	8	$-4.35569028016719 \times 10^{-14}$
0	9	$1.51660179879606 \times 10^{-15}$
0	10	$-1.34231785680549 \times 10^{-17}$
1	0	$1.44492319539037 \times 10^{-7}$
1	1	$-2.81833237588783 \times 10^{-7}$
1	2	$1.88795822312826 \times 10^{-7}$
1	3	$-6.12284776821388 \times 10^{-8}$
1	4	$1.04054640162243 \times 10^{-8}$
1	5	$-7.91894115995732 \times 10^{-10}$
1	6	$-1.78097006314277 \times 10^{-11}$
1	7	$8.46173387258907 \times 10^{-12}$
1	8	$-6.29468789021339 \times 10^{-13}$
1	9	$1.62914975397206 \times 10^{-14}$
2	0	$-6.16808609401052 \times 10^{-7}$
2	1	$1.16624214027143 \times 10^{-6}$
2	2	$-7.85736422030061 \times 10^{-7}$
2	3	$2.61841021616088 \times 10^{-7}$
2	4	$-4.99004695268396 \times 10^{-8}$
2	5	$5.85970807128971 \times 10^{-9}$
2	6	$-4.33266245043971 \times 10^{-10}$
2	7	$1.90360900947593 \times 10^{-11}$
2	8	$-3.82506468133384 \times 10^{-13}$
3	0	$1.08977129458469 \times 10^{-6}$
3	1	$-1.59381377689636 \times 10^{-6}$
3	2	$9.99496177147637 \times 10^{-7}$
3	3	$-2.91595858554532 \times 10^{-7}$
3	4	$4.326523797 \times 10^{-8}$
3	5	$-3.362778684 \times 10^{-9}$
3	6	$1.282166014 \times 10^{-10}$
3	7	$-1.917029734 \times 10^{-12}$
4	0	$-2.259714868 \times 10^{-6}$
4	1	$1.119175754 \times 10^{-6}$
4	2	$-5.651590331 \times 10^{-7}$
4	3	$1.626275899 \times 10^{-7}$
4	4	$-2.099187596 \times 10^{-8}$
4	5	$1.227562914 \times 10^{-9}$
4	6	$-2.324142752 \times 10^{-11}$
5	0	$6.178830434 \times 10^{-6}$
5	1	$-1.202803829 \times 10^{-6}$
5	2	$8.664999355 \times 10^{-8}$
5	3	$-3.132630663 \times 10^{-8}$
5	4	$3.532659092 \times 10^{-9}$
5	5	$-1.815059958 \times 10^{-10}$
6	0	$-1.08048264112286 \times 10^{-5}$
6	1	$2.17366900821365 \times 10^{-6}$
6	2	$-1.53022515538303 \times 10^{-8}$
6	3	$2.11500280833261 \times 10^{-9}$
6	4	$4.74260725560735 \times 10^{-10}$
7	0	$1.01466386059898 \times 10^{-5}$
7	1	$-2.10287523493265 \times 10^{-6}$
7	2	$1.91184417519603 \times 10^{-8}$
7	3	$-4.48828024315313 \times 10^{-9}$
8	0	$-4.89026741776877 \times 10^{-6}$
8	1	$9.75457041464072 \times 10^{-7}$
8	2	$1.00074660431270 \times 10^{-8}$
9	0	$1.04333009405285 \times 10^{-6}$
9	1	$-2.00783047336916 \times 10^{-7}$
10	0	$-5.01517451094617 \times 10^{-8}$

Table A8. $b_{i,j,k=6}$ coefficients for the association integral correlation in the Mie-based association term, Equation (30).

i	j	$b_{i,j,k=6}$	i	j	$b_{i,j,k=6}$	i	j	$b_{i,j,k=6}$	i	j	$b_{i,j,k=6}$
0	0	$-1.84421844661105 \times 10^{-11}$	1	6	$3.82442150265529 \times 10^{-13}$	3	4	$-2.48716300671280 \times 10^{-10}$	6	0	$6.55633333711198 \times 10^{-8}$
0	1	$5.39073389355030 \times 10^{-11}$	1	7	$-7.05793035532524 \times 10^{-14}$	3	5	$1.91426474551801 \times 10^{-11}$	6	1	$-1.31376750286488 \times 10^{-8}$
0	2	$-5.61963272868663 \times 10^{-11}$	1	8	$4.59807633591802 \times 10^{-15}$	3	6	$-7.31095625646731 \times 10^{-13}$	6	2	$3.55287199097211 \times 10^{-10}$
0	3	$3.23187813505929 \times 10^{-11}$	1	9	$-1.12579371971295 \times 10^{-16}$	3	7	$1.12112566023581 \times 10^{-14}$	6	3	$-2.85768231341124 \times 10^{-11}$
0	4	$-1.13265016166587 \times 10^{-11}$	2	0	$3.74547734805679 \times 10^{-9}$	4	0	$1.48400265810797 \times 10^{-8}$	6	4	$-2.19531090111075 \times 10^{-12}$
0	5	$2.59326201844053 \times 10^{-12}$	2	1	$-6.83326218348459 \times 10^{-9}$	4	1	$-8.18214743502133 \times 10^{-9}$	7	0	$-6.26595167233416 \times 10^{-8}$
0	6	$-4.01407631594698 \times 10^{-13}$	2	2	$4.50304220343962 \times 10^{-9}$	4	2	$3.81858691213582 \times 10^{-9}$	7	1	$1.18345081383843 \times 10^{-8}$
0	7	$4.20546124661511 \times 10^{-14}$	2	3	$-1.47842817249421 \times 10^{-9}$	4	3	$-1.00814014221601 \times 10^{-9}$	7	2	$-1.95221464285268 \times 10^{-10}$
0	8	$-2.87018830339552 \times 10^{-15}$	2	4	$2.78924412091172 \times 10^{-10}$	4	4	$1.24324450815098 \times 10^{-10}$	7	3	$2.70989222978676 \times 10^{-11}$
0	9	$1.15159946184350 \times 10^{-16}$	2	5	$-3.25532731205188 \times 10^{-11}$	4	5	$-7.02051970613448 \times 10^{-12}$	8	0	$3.22964489272539 \times 10^{-9}$
0	10	$-2.05485407533207 \times 10^{-18}$	2	6	$2.40008362810406 \times 10^{-12}$	4	6	$1.27771307749498 \times 10^{-13}$	8	1	$-5.24025196193952 \times 10^{-9}$
1	0	$-8.27665331374217 \times 10^{-10}$	2	7	$-1.05309962007498 \times 10^{-13}$	5	0	$-3.82128399646057 \times 10^{-8}$	8	2	$-4.14196544462777 \times 10^{-11}$
1	1	$1.55896078845997 \times 10^{-9}$	2	8	$2.11144278824276 \times 10^{-15}$	5	1	$8.61165773602971 \times 10^{-9}$	9	0	$-8.35760085684382 \times 10^{-9}$
1	2	$-1.01231143749898 \times 10^{-9}$	3	0	$-7.12756897329521 \times 10^{-9}$	5	2	$-1.03558713701492 \times 10^{-9}$	9	1	$1.03868339224250 \times 10^{-9}$
1	3	$3.13409590234525 \times 10^{-10}$	3	1	$1.00393010742688 \times 10^{-8}$	5	3	$2.39230607884171 \times 10^{-10}$	10	0	$8.47595203890549 \times 10^{-10}$
1	4	$-4.81050397623846 \times 10^{-11}$	3	2	$-6.02106444139650 \times 10^{-9}$	5	4	$-2.35824243963634 \times 10^{-11}$			
1	5	$2.30261130144263 \times 10^{-12}$	3	3	$1.70643459526364 \times 10^{-9}$	5	5	$1.10391700857033 \times 10^{-12}$			